



PRELIMINARY STUDY OF EMILIA (MAY 29th 2012) EARTHQUAKE GROUND MOTION RECORDS V1.0



Eugenio Chioccarelli, Flavia De Luca, and Iunio Iervolino.

eugenio.chioccarelli@unina.it; flavia.deluca@unina.it; iunio.iervolino@unina.it

Dipartimento di Ingegneria Strutturale, Università degli Studi di Napoli Federico II.

Index

1. Introduction	2
2. Geographic Information	3
3. Signal correction	9
4. Peak and integral parameters of the corrected waveforms	10
5. Comparison of the data with Bindi et al. GMPE predictions, PGA, PGV and Sa(T).....	13
6. Direct spectral comparison of the data registered within 70km.....	22
7. Epsilon values of the data registered within 70km	32
8. Comparison of data with Sabetta and Pugliese (1996) and Iervolino et al. (2010) GMPE predictions, I_A and I_D	41
9. Comparison with Italian hazard data	42
Appendix	54
References	63

1. Introduction

On the 29th of May 2012, at 07:00:03 (UTC), (09:00:03 Italian time), Emilia region (Northern Italy) was struck by a Magnitude, M_L 5.8 (INGV) earthquake, (lat 44.85, long 11.09). The epicentre was located at 12 km WSW-ward with respect to the 20th of May event (M_L 5.9; [Chioccarelli et al., 2012](#)), ([Mirandola Earthquake Working Group, 2012a](#)). The 29th event was followed by three relevant aftershocks characterized by magnitude higher or equal than 5.0, ([Mirandola Earthquake Working Group, 2012b](#)). The 29th event was registered by 135 RAN stations, including temporary stations (see [Table 1](#)). In [Figure 1](#) is shown the trend of the number of daily earthquakes updated at the 27th of June.

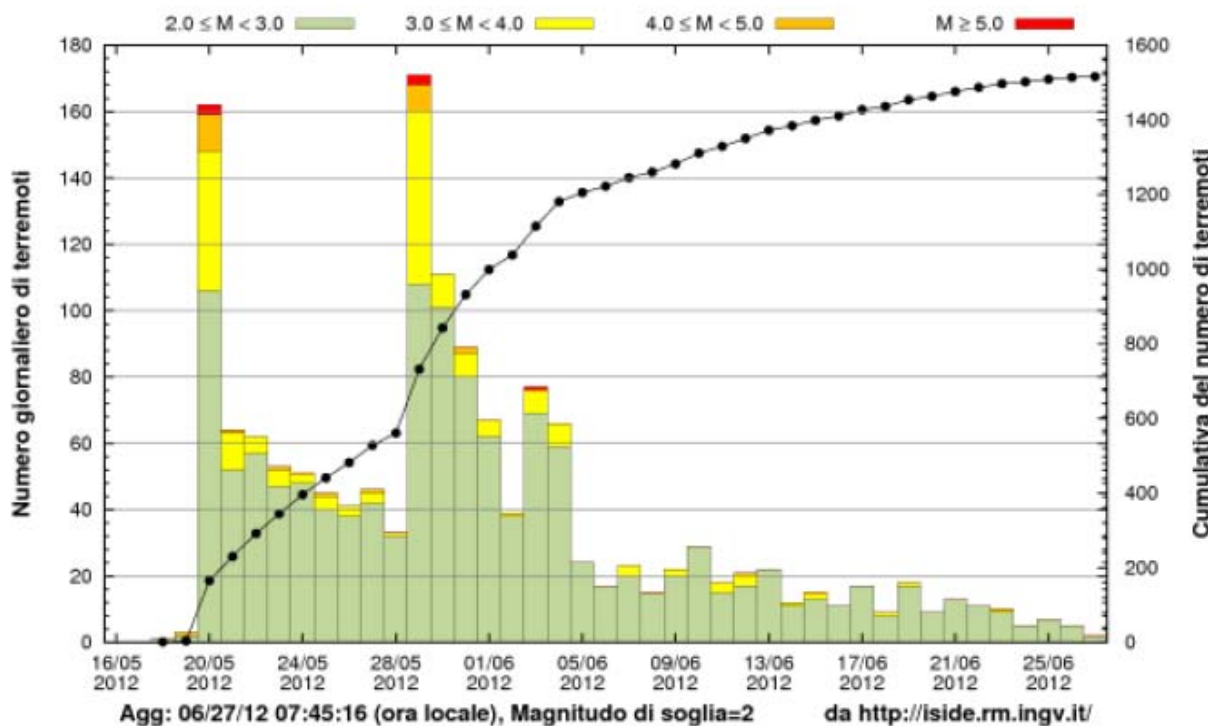


Figure 1. Number of daily earthquakes, update 06/27 (8.00, Italian time), [<http://www.ingv.it/primo-piano/comunicazione/2012/05200508/>].

Waveforms were corrected according to the procedure briefly described in section 3. *Peak Ground Acceleration* (PGA), *Peak Ground Velocity* (PGV), *Peak Ground Displacement* (PGD) were calculated for the two horizontal direction (East-West and North-South, as recorded) and for the vertical one. *Arias Intensity* (I_A), *Cosenza and Manfredi Index* (I_D), evaluated according to Cosenza et al. (1993), and *Housner Intensity* (H_{50}) are the integral parameters computed for each waveform. Housner intensity (H_{50}) is evaluated as the integral of the pseudo-velocity spectrum in the range 0.2- 2.0 seconds. Durations computed for each record are: *Significant Duration* (Sd) and

Bracketed Duration (Bd); the former estimated between 5% and 95% of the I_A, the latter assuming 0.05 PGA as reference value.

The analysis of peak and integral values is made by a comparison with different ground motion attenuation relationships (GMPE). Bindi et al. (2011) GMPE was employed for the comparison in term of PGA, PGV and elastic spectral acceleration at given spectral ordinates, Sa(T). I_A attenuation relationship by Sabetta and Pugliese (1996) and Iervolino et al. (2010a) attenuation law in terms of I_D have been employed. Sabetta and Pugliese (1996) and Iervolino et al. (2010a) GMPEs are based on epicentral distance (R_{epi}) as distance measure, while Bindi et al. (2011) GMPE employs the epicentral distance (R_{epi}), for $M_w < 5.5$ events, and the closest distance to fault projection or *Joyner and Boore distance*, R_{jb} (Joyner and Boore, 1981), for stronger earthquakes. Given the lack of information on the fault, at the moment, an approximate conversion law was employed to switch form the distance data in terms of R_{epi} to that in terms of R_{jb} . Equation (1) shows the expression used for the conversion according to (Gruppo di Lavoro INGV, 2004).

$$R_{jb} = -3.5525 + 0.8845 \cdot R_{epi} \geq 1 \quad (R^2 = 0.95) \quad (1)$$

2. Geographic Information

In Table 1 is possible to relate station IDs, geographic coordinates of the stations, and station names. These data are courtesy of the Department of Civil Protection. Figure 2 shows the map of the stations within 70 km together with epicentre and main cities locations. For the same stations, Figure 3 and Figure 4 show the map of horizontal (geometrical mean of two direction) and vertical PGA (PGA_h and PGA_v) and PGV (PGV_h and PGV_v), respectively.

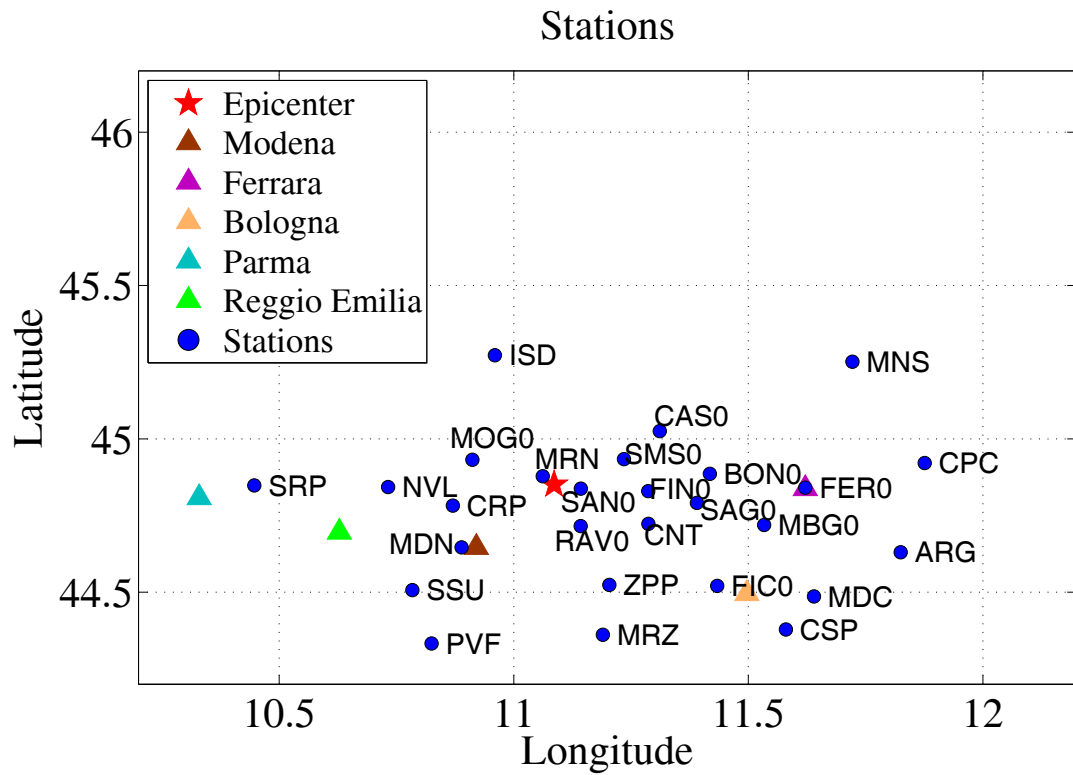
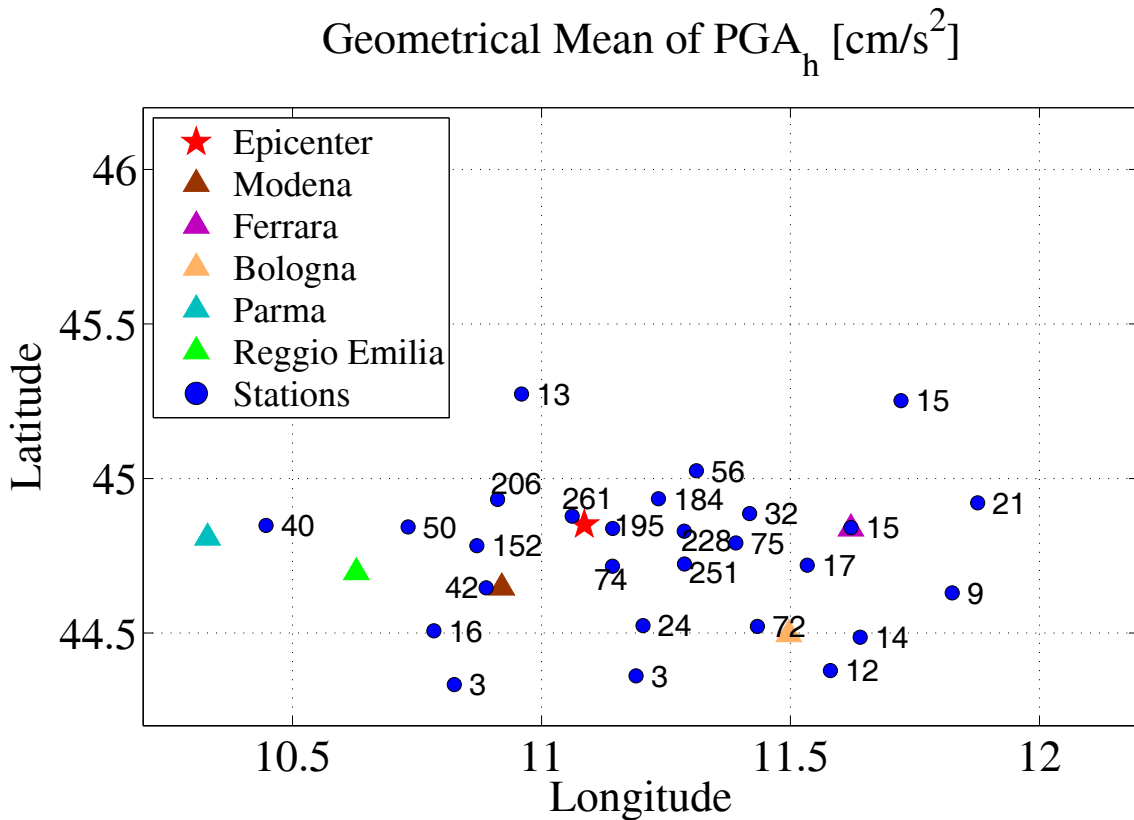


Figure 2. Map of the stations within 70 km from the epicentre.



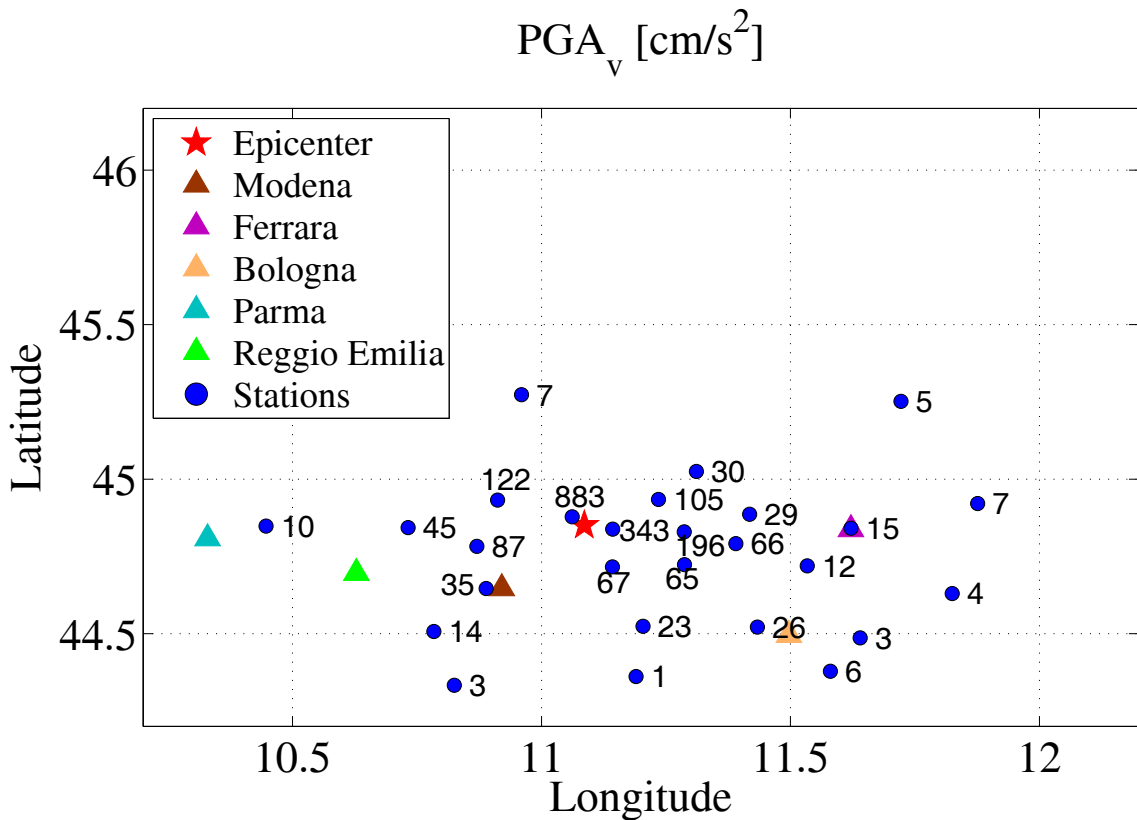
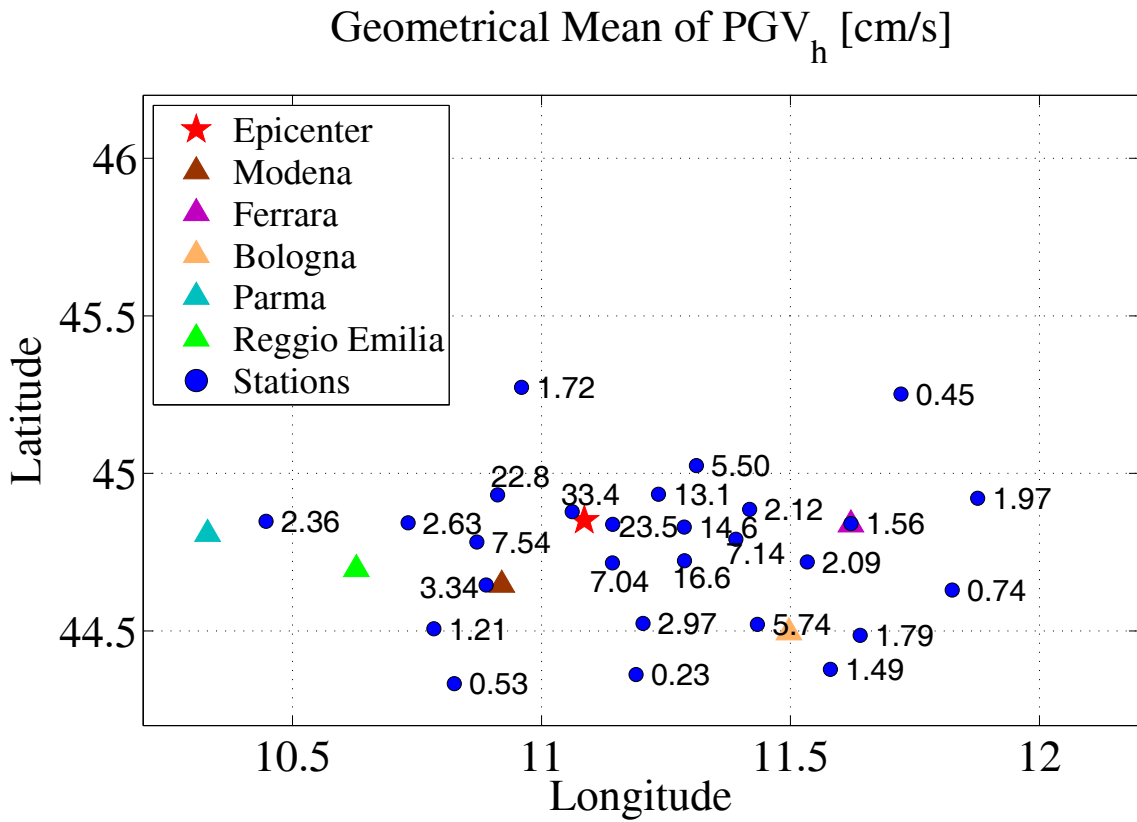


Figure 3. Peak Ground Acceleration (PGA) maps at the stations within 70 km. PGA_h is the geometrical mean of the registered horizontal components, PGA_v is the vertical component.



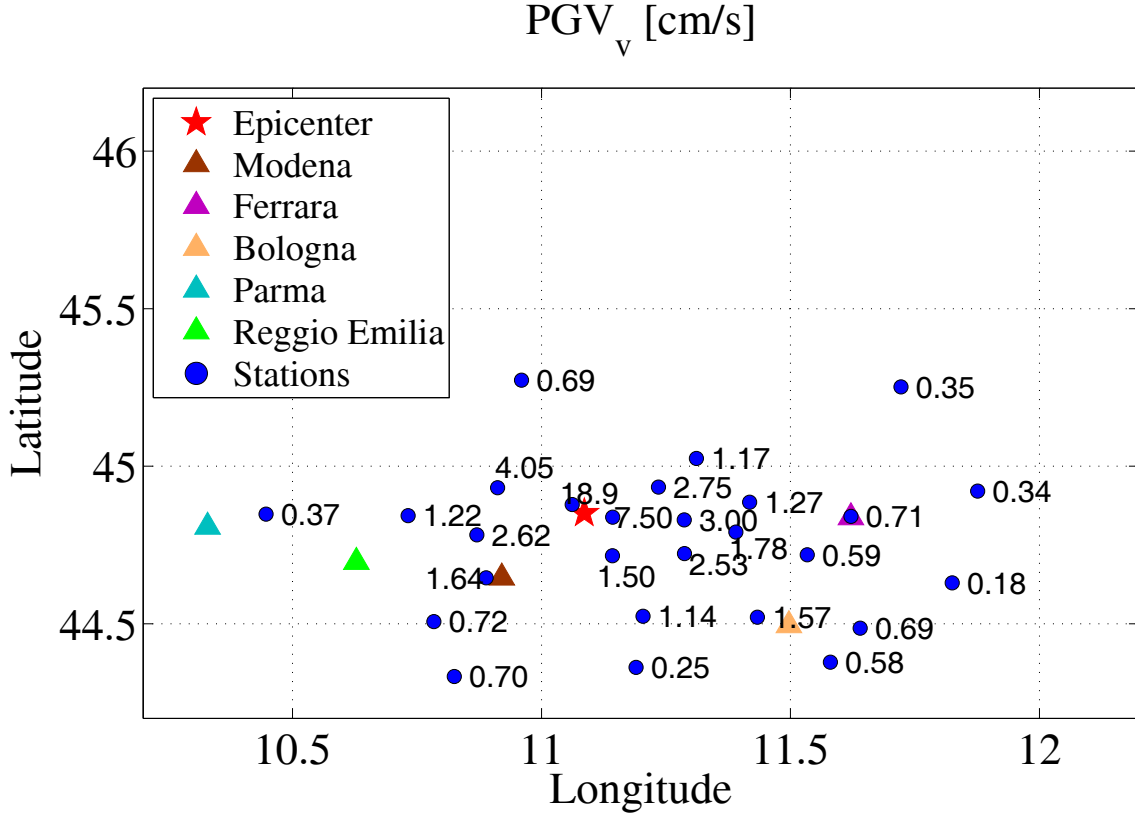


Figure 4. Peak Ground Velocity (PGV) maps at the stations within 70 km. PGV_h is the geometrical mean of the registered horizontal components, PGV_v is the vertical component.

Table 1. Station ID, geographic coordinates, and station names.

Station ID	Lat	Lon	elevation (km)	R _{epi} (km)	Station Name
MRN	44.878	11.062	0.015	3.58	Mirandola
SAN0	44.838	11.143	0.071	4.73	San_Felice_sul_Panaro_temporanea
SMS0	44.934	11.235	0.055	14.95	San_Martino_Spino_temporanea
RAV0	44.716	11.143	0.087	15.69	Ravarino_temporanea
FIN0	44.830	11.287	0.061	16.04	Finale_Emilia_temporanea
MOG0	44.932	10.912	0.079	16.43	Moglia_temporanea
CRP	44.782	10.870	0.089	18.69	Carpi
CNT	44.723	11.287	0.071	21.34	Cento
SAG0	44.791	11.390	0.066	24.98	Sant_Agostino_temporanea
CAS0	45.025	11.311	0.065	26.25	Castelmassa_temporanea
BON0	44.886	11.418	0.065	26.52	Bondeno_temporanea
MDN	44.646	10.889	0.080	27.61	Modena
NVL	44.843	10.732	0.022	28.00	Novellara
ZPP	44.524	11.204	0.069	37.52	Zola_Pedrosa_Piana
MBG0	44.719	11.534	0.055	38.37	Malalbergo_temporanea
FER0	44.841	11.622	0.056	42.36	Ferrara_temporanea
SSU	44.507	10.784	0.448	45.10	Sassuolo
FIC0	44.952	11.434	0.061	45.88	Ficarolo_temporanea
ISD	45.273	10.960	0.400	47.93	Isola_Della_Scala

SRP	44.848	10.447	0.032	50.51	Sorbolo
MRZ	44.361	11.190	0.456	55.03	Marzabotto
MDC	44.486	11.640	0.026	59.79	Medicina
PVF	44.333	10.825	0.743	61.17	Pavullo_del_Frignano
CPC	44.921	11.876	0.008	62.90	Copparo_Coccanile
ARG	44.630	11.825	0.045	63.48	Argenta
CSP	44.378	11.580	0.088	65.55	CastelSanPietroTerme
MNS	45.252	11.722	0.014	67.04	Monselice
VLM	44.365	10.466	0.677	73.06	Villa_Minazzo
PRT	44.149	10.926	0.862	79.03	Porretta_Terme
TGG	45.562	11.183	0.762	79.39	Tregnago
BRM	44.129	11.118	0.851	80.27	Brasimone
ALF	44.502	12.033	0.006	84.60	Alfonsine
FRE1	44.118	11.382	0.461	84.79	Firenzuola
BRH	44.208	11.764	0.149	89.53	Brisighella
SMP	44.064	10.803	1.022	90.30	San_Marcello_Pistoiese
PTV	45.274	10.088	0.055	91.57	Pontevico
MDG	44.159	11.789	0.187	95.08	Modigliana
BSZ	44.031	11.467	0.685	96.04	Borgo_San_Lorenzo
PIT	43.989	10.944	0.537	96.44	Pistoia
MRR	44.064	11.603	0.369	96.65	Marradi
GAI	45.659	10.616	0.400	97.07	Gaino
PZS	44.188	10.288	0.659	97.21	Piazza_al_Serchio
SNZ1	45.074	9.894	0.042	97.21	S_Nazzaro1
CNF	44.110	10.411	0.323	98.29	Castelnuovo_di_Garfagnana
MDT	44.135	11.830	0.571	99.15	Modigliana
BRB	43.954	11.212	0.426	100.18	Barberino_Mugello
FVZ	44.238	10.131	0.428	101.96	Fivizzano
BGL	43.995	10.576	0.447	103.41	Bagni_Di_Lucca
VGL	44.111	10.290	0.613	103.77	Vagli_Paese
BGN	44.322	9.992	0.304	104.87	Bagnone
Station ID	Lat	Lon	elevation (km)	R _{epi} (km)	Station Name
MLC	45.808	10.849	0.098	107.96	Malcesine
PNM	44.379	9.881	0.339	109.06	Pontremoli
CST	45.660	11.902	0.487	110.40	Castelfranco_Veneto
PRM	43.979	11.781	0.450	111.60	Premilcuore
DCM	43.891	11.518	0.200	112.10	Dicomano
MLD	44.118	12.071	0.116	113.32	Meldola
AUL	44.208	9.973	0.177	113.70	Aulla
CVT	44.006	11.937	0.228	115.80	Civitella_Di_Romagna
RNC	43.870	11.607	0.534	116.66	Rincine_Londa
RVR	44.904	9.598	0.237	117.68	Rivergaro
STS	43.942	11.905	0.640	120.26	Santa_Sofia
BDG	44.507	9.623	0.537	122.10	Bedonia_Gallareto
VRL	44.392	9.633	0.804	126.06	Varese_Ligure
CES	44.210	12.386	0.049	126.76	Cesenatico
LSP	44.096	9.807	0.107	131.86	La_Spezia
SLS	44.632	9.406	0.381	135.23	Salsominore_Centrale
BBN	43.747	11.821	0.471	135.98	Bibbiena
FLP	46.027	11.923	0.294	146.20	Feltre_Pasquer
SEL	44.265	9.403	0.076	148.69	Sestri_Levante
SNM	43.934	12.449	0.742	150.68	San_Marino

BDT	43.706	12.188	0.795	155.58	Badia_Tebalda
TGL	44.533	9.165	1.035	156.27	Torriglia
MCR	43.800	12.448	0.303	161.40	Macerata_Feltria
APR	46.156	10.158	1.203	162.13	Aprica
BRA	46.004	9.762	0.815	164.75	Branzi
SNS	43.567	12.143	0.377	166.53	San_Sepolcro
CTL	43.955	12.735	0.062	167.37	Cattolica
POR	45.952	12.681	0.022	172.01	Pordenone
LEC	45.861	9.412	0.231	172.59	Lecco
RNS	44.595	8.936	0.437	172.64	Ronco_Scrivia
GNV	44.431	8.932	0.419	177.09	Genova
MOV	46.155	12.655	0.373	186.89	Montereale_Valcellina
PSR	45.949	13.014	0.080	190.35	Passariano Villa Manin
CLA	46.271	12.514	0.680	190.79	Claut
PTL	43.427	12.449	0.688	194.32	Pietralunga
OVD	44.636	8.642	0.235	194.96	Ovada
SPI	46.108	12.905	0.180	195.60	Spilimbergo
UMB	43.254	12.256	0.628	202.02	Umbertide
PRAD	46.248	12.889	0.520	205.70	Pradis
GBB	43.357	12.597	0.754	208.20	Gubbio
FDS	46.451	12.562	1.795	209.03	ForniDiSopra
MAJ	46.182	13.069	0.176	209.86	Majano casa di riposo
SAS	44.483	8.486	0.415	210.13	Sassello
GBP	43.314	12.589	0.426	211.74	Gubbio_Piana
AVS	46.295	13.050	0.256	217.41	Avasinis
GEDE	46.254	13.124	0.232	218.16	Gemona Depuratore
GEPF	46.275	13.139	0.250	220.49	Gemona Piazza del Ferro
TLM2	46.381	12.984	0.519	221.11	Tolmezzo2
GESC	46.282	13.140	0.320	221.12	Gemona Scugelars
CESC	46.357	13.057	0.355	222.66	Cesclans
CVF	46.092	13.429	0.135	224.22	Cividale del Friuli
Station ID	Lat	Lon	elevation (km)	R _{epi} (km)	Station Name
VINO	46.256	13.281	0.608	226.75	Villanova station
DST2	45.659	13.801	0.080	227.09	DST Trieste station
SDV	45.628	13.897	0.488	232.87	San_Dorligo_Della_Valle
MOGG	46.406	13.189	0.387	233.13	Moggio
RST	46.362	13.353	0.673	238.37	Resia
STOL	46.361	13.355	0.570	238.45	Stolvizza
DRN	46.166	13.641	0.784	241.68	Drenchia
AUP	46.506	13.256	0.905	244.42	Aupa
CLF	43.037	12.920	0.701	253.91	Colfiorito_Casone
MCT	43.292	13.418	0.349	260.32	Macerata
TNS	45.030	7.684	0.408	269.15	Torino_Superga
SPM	42.723	12.751	0.778	275.58	Spoleto_Monteluco
RQT	42.813	13.311	1.188	294.57	Arquata_Del_Tronto
PCB	42.558	13.338	1.315	319.13	Poggio_Cancelli
MSC	42.527	13.351	1.335	322.65	Mascioni
PLS	42.084	12.763	0.278	340.12	Palombara_Sabina_S_S_636
SPD	42.515	13.710	1.338	342.51	Sella_Pedicate
CDM	42.003	14.199	0.809	414.49	Colle_di_Macine
MND	41.640	15.891	0.067	543.83	Manfredonia
SSB3	41.079	15.229	0.724	552.94	San_Sossio_Baronia

RSF3	40.964	15.176	0.865	560.40	Rocca_San_Felice
MNT3	40.837	15.007	0.866	563.26	Montella
LIO3	40.897	15.180	0.737	566.77	Lioni
NSC3	40.847	15.122	1.300	568.31	Nusco
AND3	40.930	15.333	0.905	571.93	Andretta
CLT3	40.903	15.404	0.525	578.20	Calitri
SNR3	40.736	15.193	1.009	582.22	Senerchia
CMP3	40.652	15.080	0.958	584.26	Campagna
RDM3	40.876	15.536	0.784	587.86	Ruvo_Del_Monte
CSG3	40.818	15.463	1.253	589.03	Toppo di Castelgrande (Osservatorio Astronomico)
COL3	40.687	15.330	1.026	593.87	Colliano
VDS3	40.741	15.427	1.154	594.07	Muro_Lucano_(Varco_Staccarino)
SFL3	40.789	15.578	1.062	597.90	San_Fele
PST3	40.561	15.243	0.762	601.03	Postiglione
SCL3	40.695	15.511	0.744	602.74	Muro_Lucano_(Serra_Campolungo)
BEL3	40.715	15.637	0.758	607.70	Bella
AVG3	40.762	15.725	1.213	608.39	Avgigliano
VDP3	40.605	15.572	0.959	614.14	Vietri_di_Potenza
CGG3	40.542	15.523	1.067	617.27	Caggiano
SRN3	40.486	15.458	1.067	619.03	Sant_Arsenio
STN3	40.530	15.652	0.832	625.22	Satriano
PGN3	40.572	15.797	0.882	629.26	Pignola
MRN3	40.426	15.730	0.772	638.89	Marsico_Nuovo_(PZ)
VGG3	40.336	15.901	0.882	656.23	Viggiano_(Prot.Civ.Gr.Lucano)

3. Signal correction

Each component of the waveforms registered at the stations in [Table 1](#) was corrected. The correction approach is different from that described in ([Mirandola Earthquake Working Group, 2012b](#)). The correction applied to all the waveforms, and employed to obtain all the results shown in the next sections, is a linear baseline correction and an order 4 bandpass Butterworth filter with a frequency range of 0.25-25 Hz. Such a correction is the same employed in the European Strong Motion database, it was employed in Chioccarelli et al. (2009) and it does not differ significantly with respect to the processing employed in the ITalian Accelerometric Archive ([Pacor et al., 2011](#); [Massa et al., 2011](#)).

An example of the effect of the correction is shown in for the East-West components at the two closest stations; MRN and SAN0, respectively at 3.58 and 4.73 km. MRN (Figure 5) is a permanent station and it was the closest to the epicentre of both the May 20th and the 29th events. SAN0 (Figure 6) is a temporary station placed after the event of the 20th of May.

Notwithstanding the fact that MRN station shows an atypical trend in the acceleration waveform, probably caused by problems in data acquisition; it can be observed that the bandpass

filter applied in the frequency range 0.25-25 Hz allows to overpass this kind of problem and to obtain velocity and displacement time history which appear, at least visually, usable (see [Figure 5](#)).

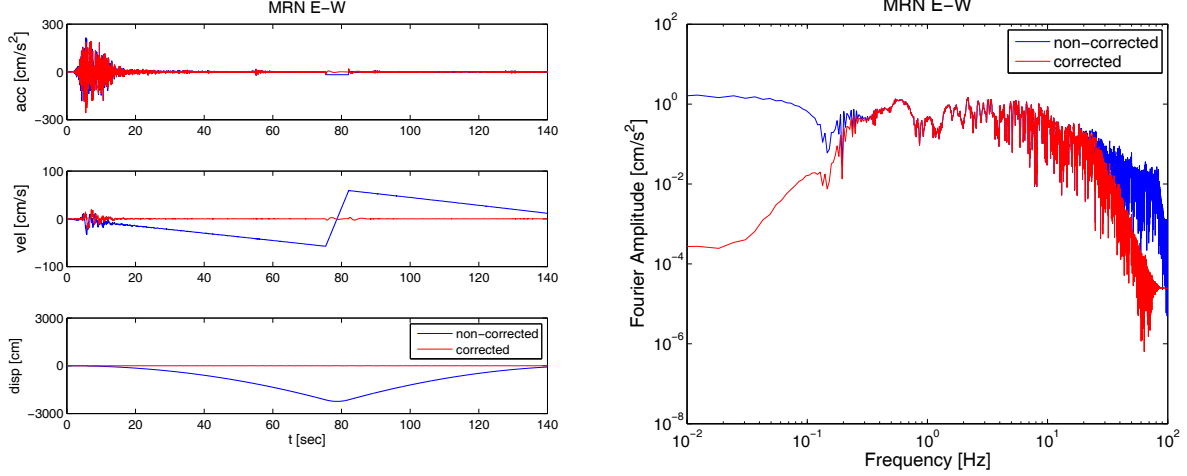


[Figure 5](#). Acceleration, velocity and displacement time histories (a), and Fourier amplitude spectra (b) of the non-corrected and corrected waveforms of the E-W component of the signal registered at MRN station.

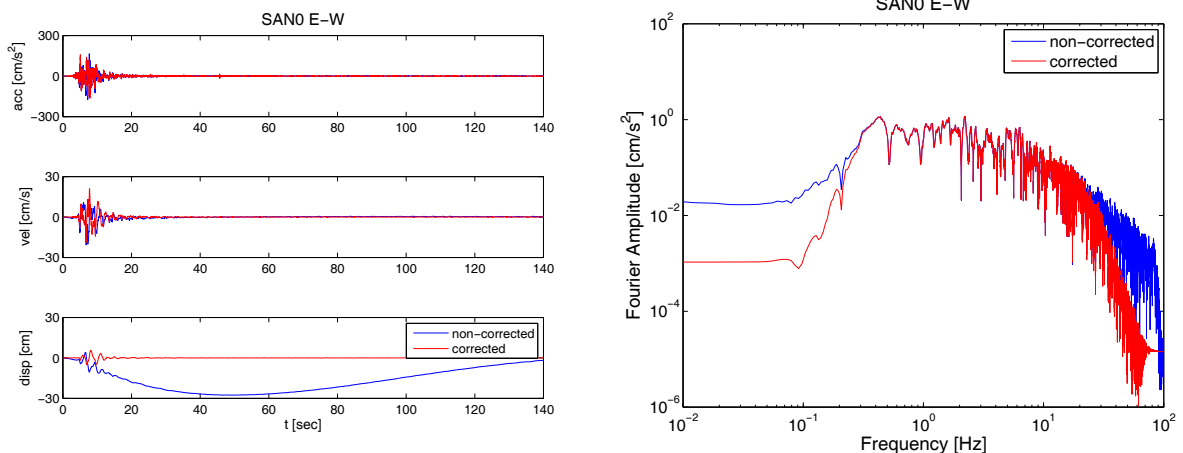


[Figure 6](#). Acceleration, velocity and displacement time histories (a), and Fourier amplitude spectra (b) of the non-corrected and corrected waveforms of the E-W component of the signal registered at SAN0 station.

4. Peak and integral parameters of the corrected waveforms

Peak and integral parameters defined in Section 1 are computed for the corrected waveforms for the two horizontal components (N-S, E-W) and for the vertical component (Z). The result are shown in [Table A1](#), [A2](#), and [A3](#) in the Appendix.

From [Figure 7](#) to [Figure 14](#) several intensity measures (IMs) computed from the geometrical mean of the horizontal components and the vertical components are shown as function of the epicentral distance (R_{epi}). Peak ground acceleration (PGA), peak ground velocity (PGV), Arias intensity (I_A), and Housner intensity (H_{50}) are characterized by a strict attenuation after 20km.

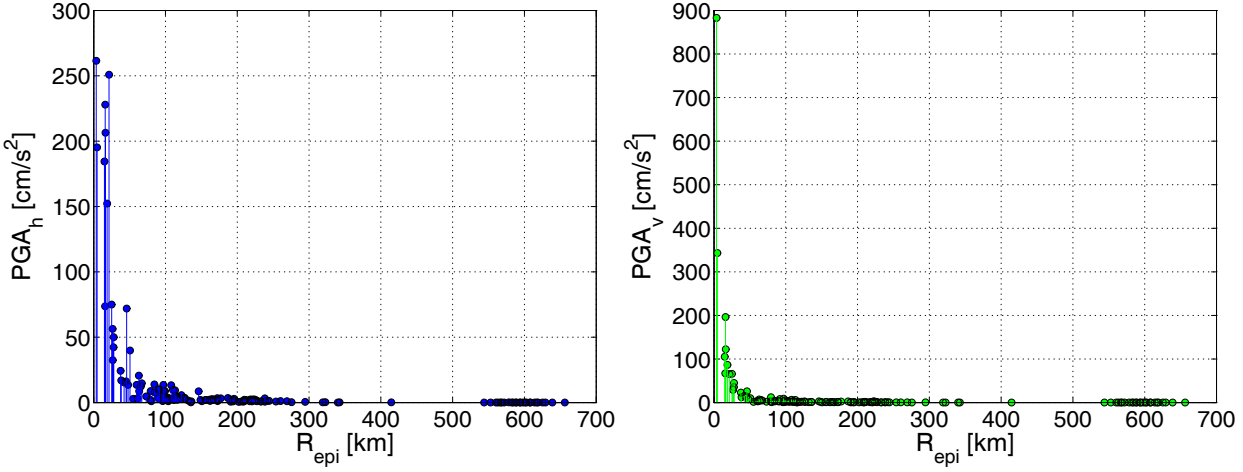


Figure 7. PGA values: geometrical mean of the horizontal components, PGA_h (on the left), and vertical component PGA_v (on the right).

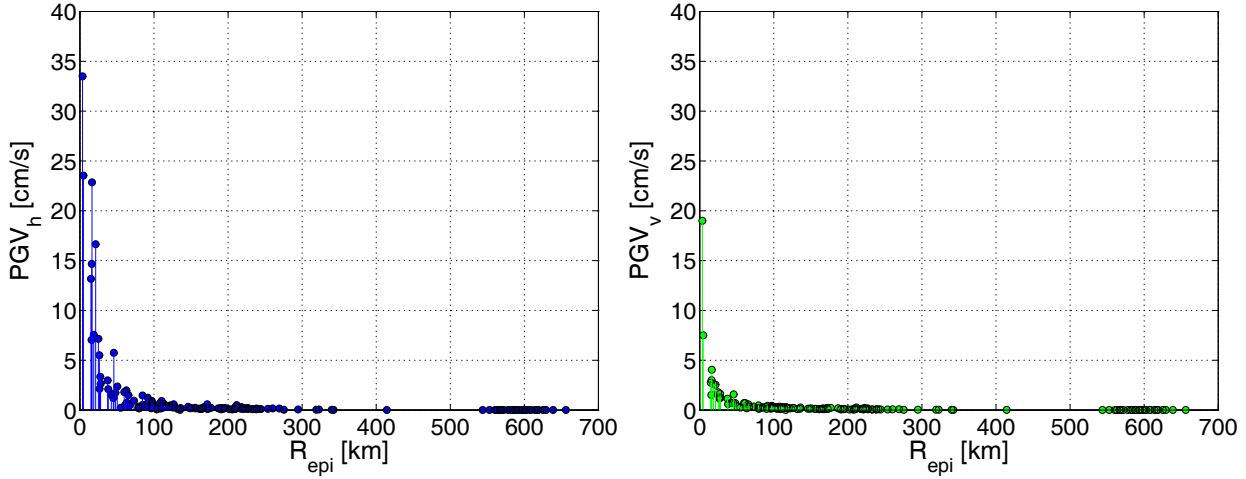


Figure 8. PGV values: geometrical mean of the horizontal components, PGV_h (on the left), and vertical component PGV_v (on the right).

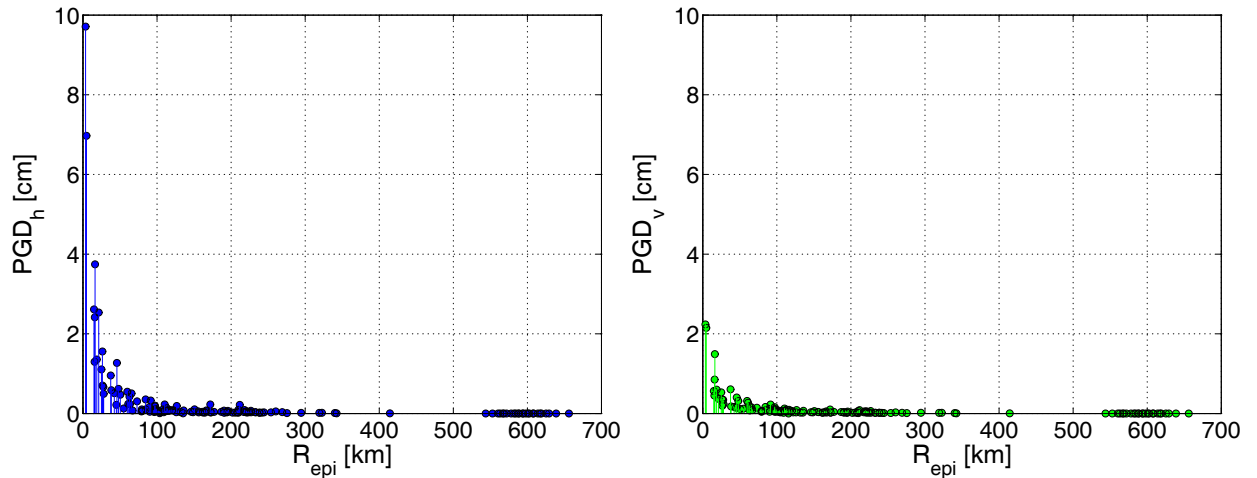


Figure 9. PGD values: geometrical mean of the horizontal components, PGD_h (on the left), and vertical component PGD_v (on the right).

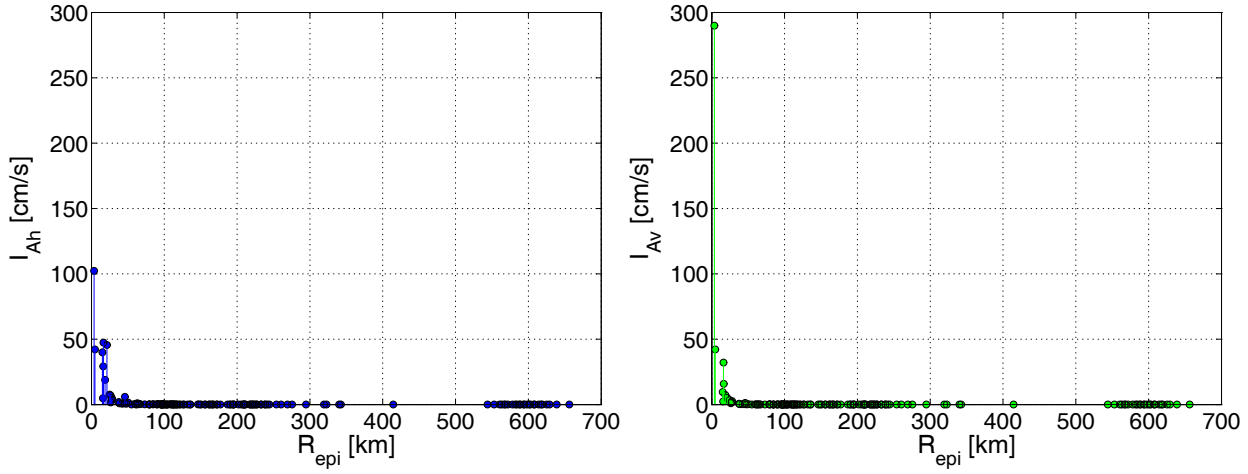


Figure 10. I_A values: geometrical mean of the horizontal components, I_{Ah} (on the left), and vertical component I_{Av} (on the right).

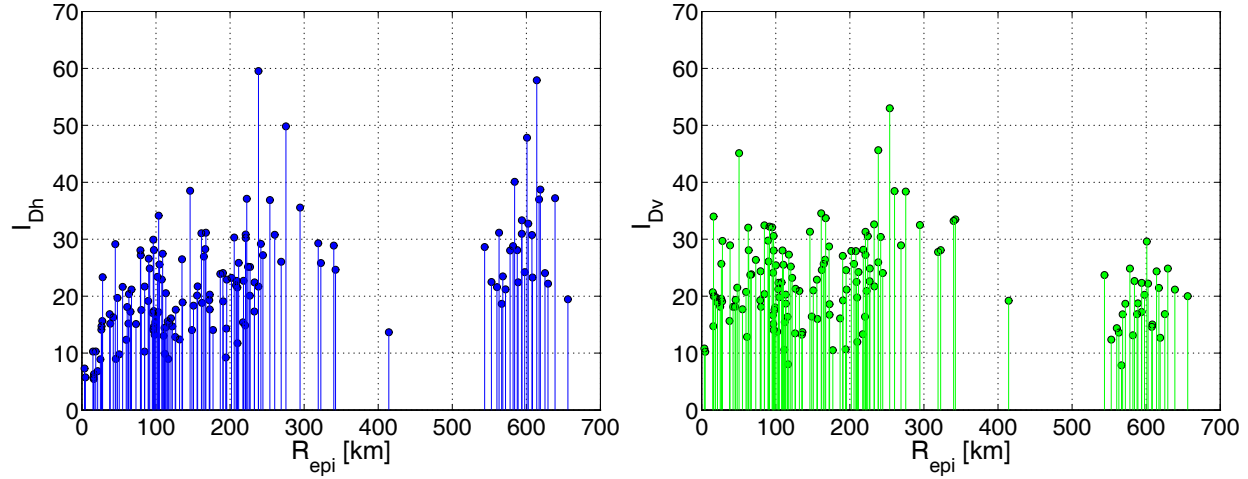


Figure 11. I_D values: geometrical mean of the horizontal components, I_{Dh} (on the left), and vertical component I_{Dv} (on the right).

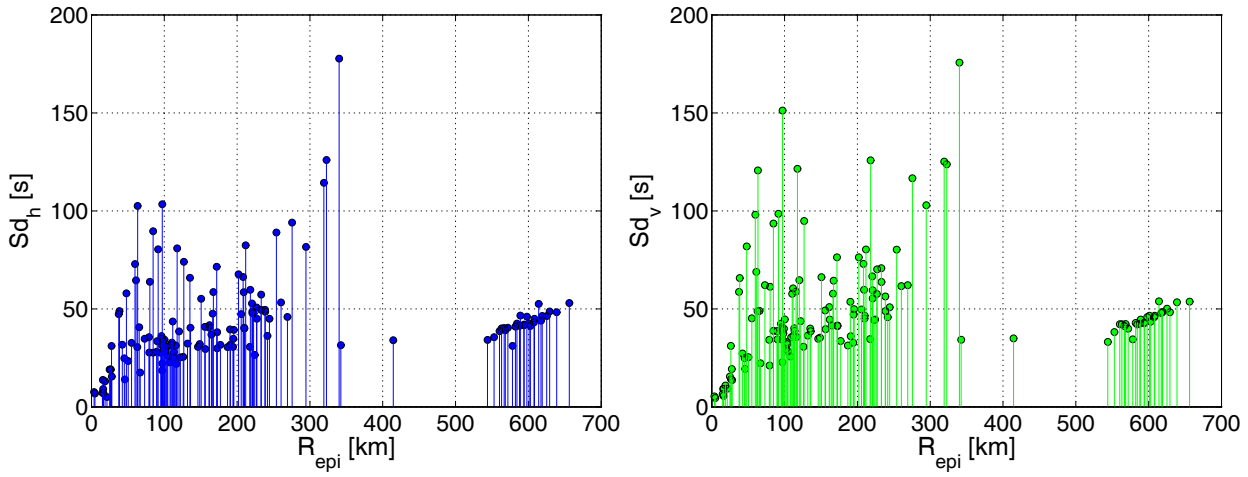


Figure 12. Sd values: geometrical mean of the horizontal components, Sd_h (on the left), and vertical component Sd_v (on the right).

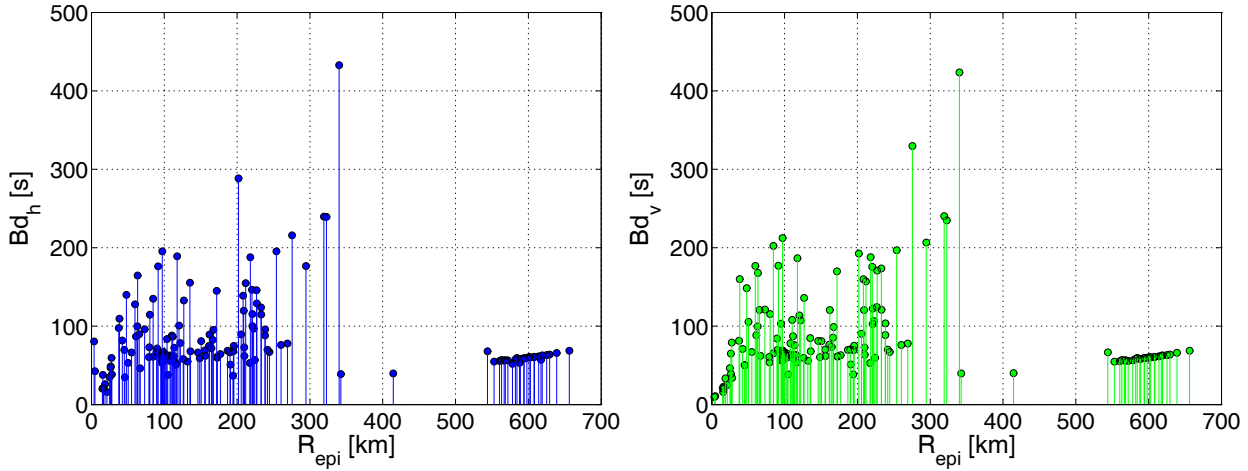


Figure 13. Bd values: geometrical mean of the horizontal components, Bd_h (on the left), and vertical component Bd_v (on the right).

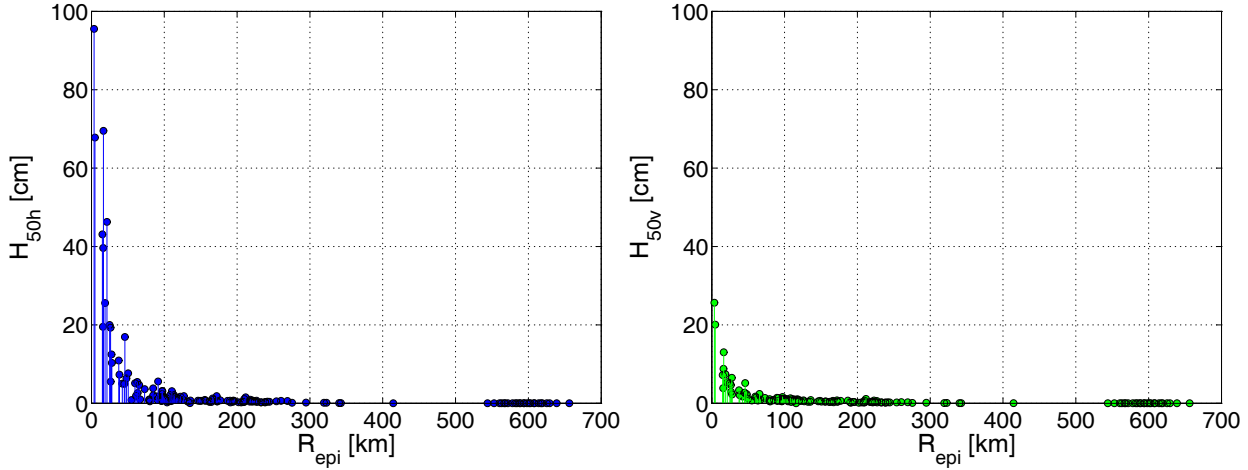


Figure 14. H_{50} values: geometrical mean of the horizontal components, H_{50h} (on the left), and vertical component H_{50v} (on the right).

5. Comparison of the data with Bindi et al. GMPE predictions, PGA, PGV and Sa(T).

In the following, preliminary comparisons of the registered data with Bindi et al. (2011) GMPE median predictions and their uncertainties bands (represented by the median plus and median minus one total standard deviation, $Median + \sigma$ and $Median - \sigma$, respectively) in terms of PGA, PGV, Sa(T) are provided. It is worth to note that the range of validity of such GMPE is within 0km up to 200km, thus hereafter the extrapolation of the prediction outside this range is represented by dotted lines. The predictions are made, preliminarily, for A soil class according to Eurocode 8 or EC8, (CEN, 2004), notwithstanding the fact that each station is located on different soil classes and their classification is provided by the Italian Accelerometric Archive (ITACA), <http://itaca.mi.ingv.it>. A soil class is defined as “*rock or other rock-like geological formation, including at most 5 m of*

weaker material at the surface", characterized by an average value of shear wave velocity in the first 30 m, V_{s30} , higher than 800 m/s. Soil class A is characterized by the least soil amplification factor respect to other, softer soil classes (B, C, D, E) and is the richest soil class in Bindi et al. (2011) dataset, with more than 300 waveforms.

Figure 15 show the comparison of the geometrical mean of the registered horizontal components data and the median predictions in term of PGA and PGV. Same plot is shown in Figure 16 for the case of the vertical component. It can be observed that registered data are, in most cases, within the $\pm\sigma$ bands. Figure 17 to Figure 38 show the same comparison in terms of Sa(T) at different periods, for geometrical mean of the horizontal and vertical components, respectively. Data are generally in good accordance with the $\pm\sigma$ range. In fact it should also be remembered the that soil amplification was not considered in this case (hypothesis of A soil class).

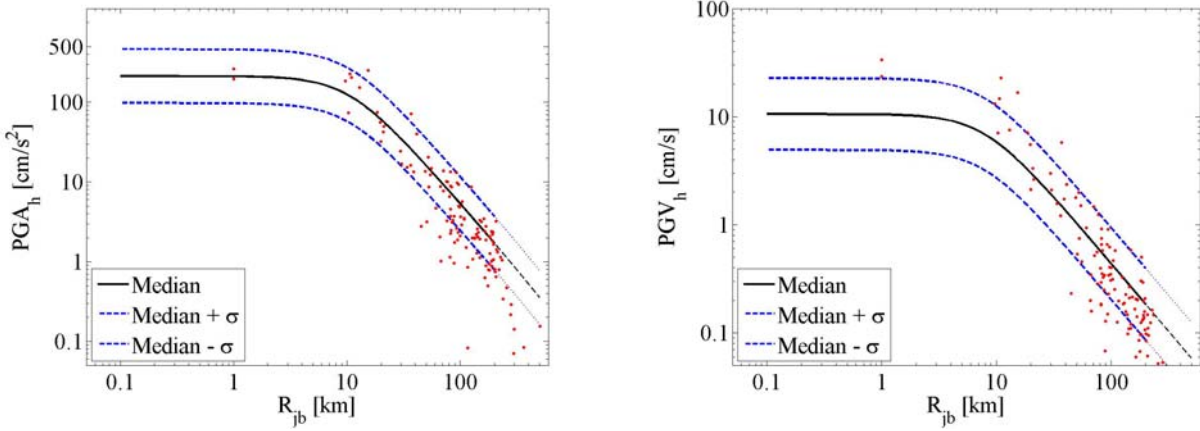


Figure 15. PGA_h and PGV_h comparison of the geometrical mean of the horizontal components of the registered data with the median and $\pm\sigma$ predictions according to Bindi et al. (2011).

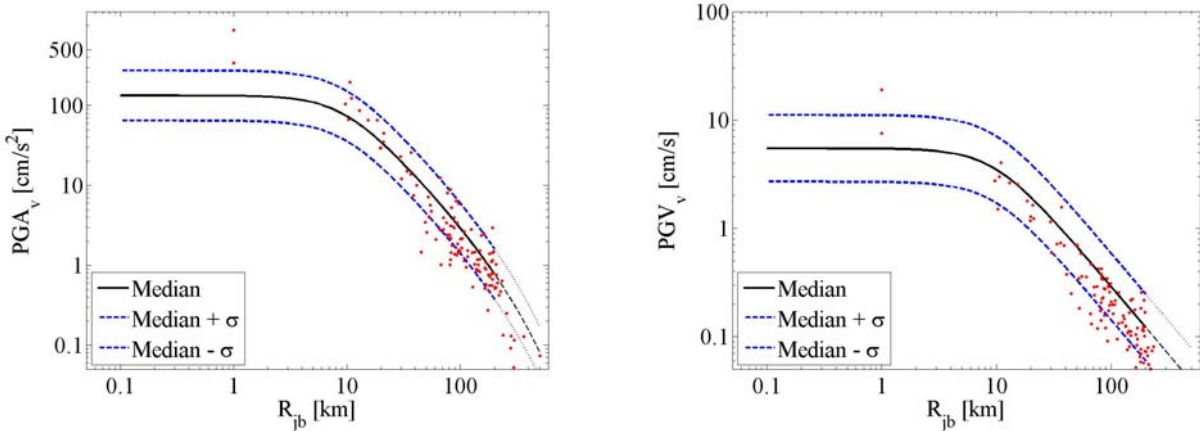


Figure 16. PGA_v and PGV_v comparison of the vertical component of the registered data with the median and $\pm\sigma$ predictions according to Bindi et al. (2011).

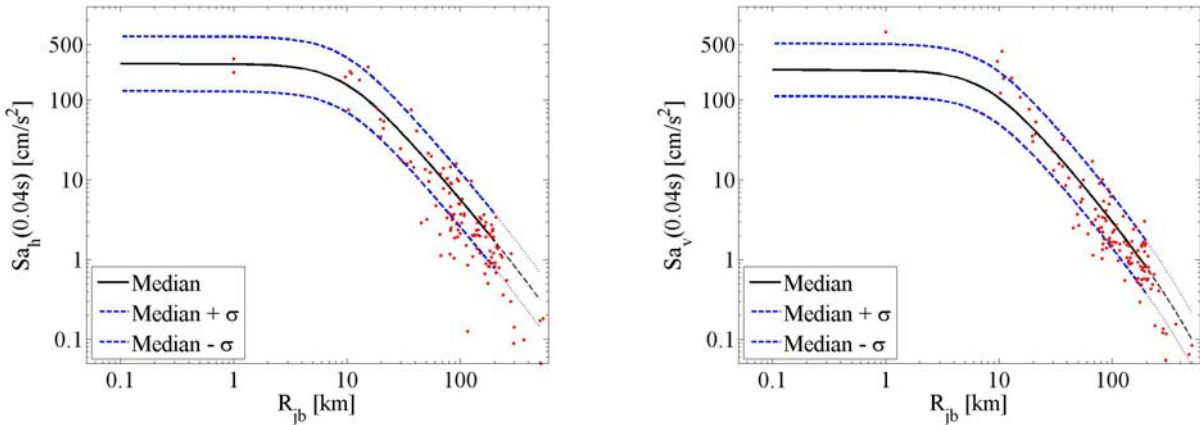


Figure 17. Spectral acceleration comparison of the geometrical mean of the horizontal components $Sa_h(T)$, on the right, and the vertical component $Sa_v(T)$, on the left, of the registered data with the median and $\pm\sigma$ predictions according to Bindi et al. (2011) for $T=0.04s$.

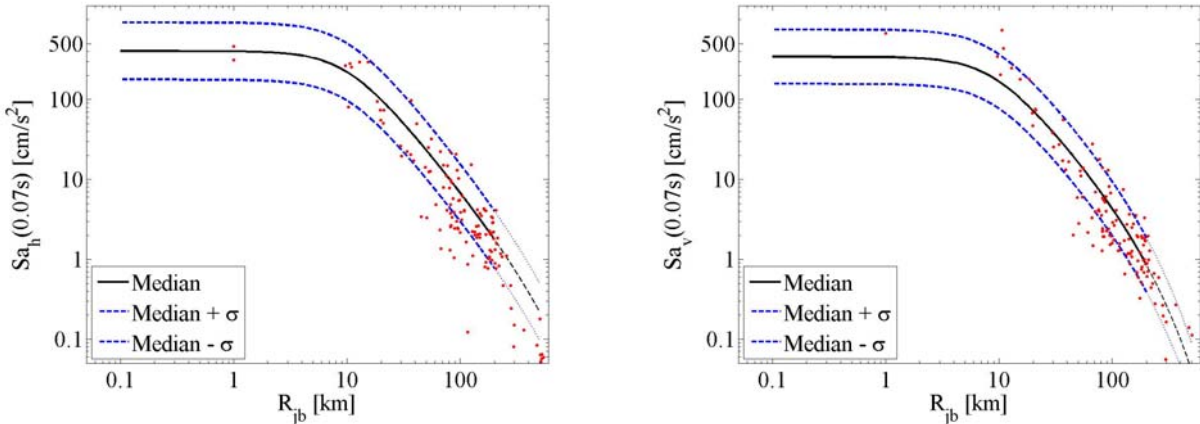


Figure 18. Spectral acceleration comparison of the geometrical mean of the horizontal components $Sa_h(T)$, on the right, and the vertical component $Sa_v(T)$, on the left, of the registered data with the median and $\pm\sigma$ predictions according to Bindi et al. (2011) for $T=0.07s$.

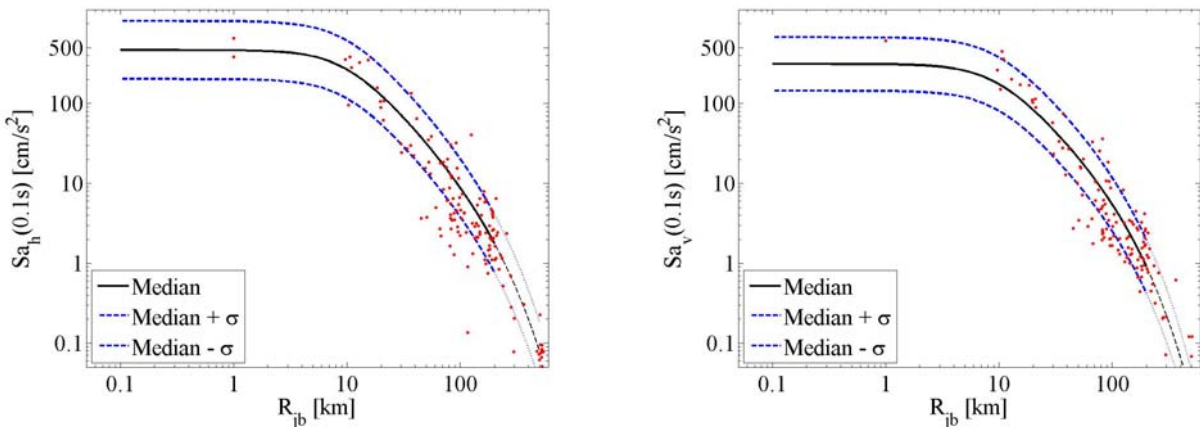


Figure 19. Spectral acceleration comparison of the geometrical mean of the horizontal components $Sa_h(T)$, on the right, and the vertical component $Sa_v(T)$, on the left, of the registered data with the median and $\pm\sigma$ predictions according to Bindi et al. (2011) for $T=0.1s$.

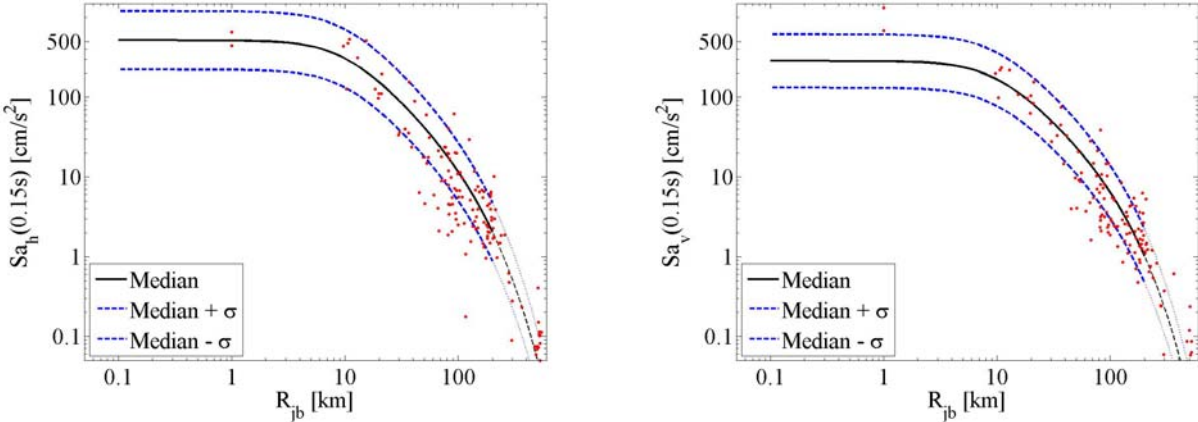


Figure 20. Spectral acceleration comparison of the geometrical mean of the horizontal components $Sa_h(T)$, on the right, and the vertical component $Sa_v(T)$, on the left, of the registered data with the median and $\pm\sigma$ predictions according to Bindi et al. (2011) for $T=0.15s$.

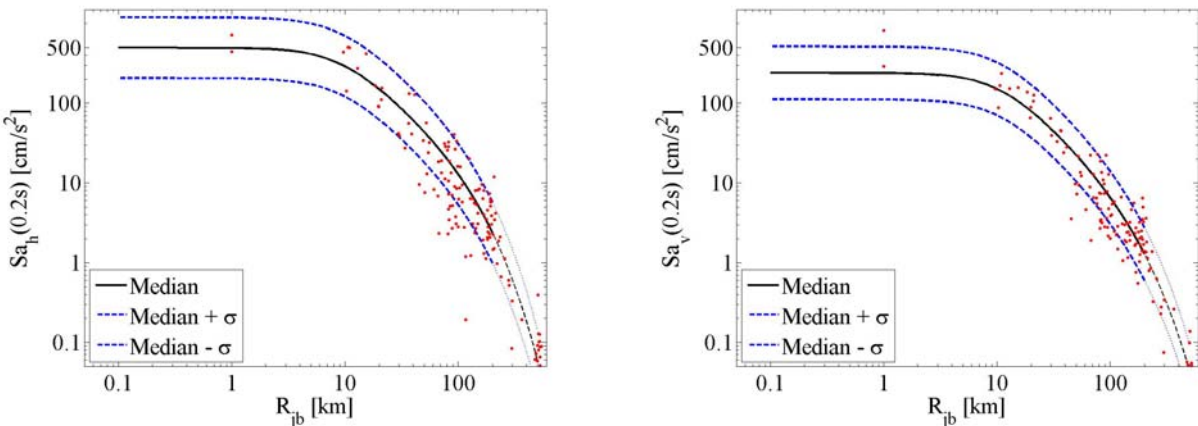


Figure 21. Spectral acceleration comparison of the geometrical mean of the horizontal components $Sa_h(T)$, on the right, and the vertical component $Sa_v(T)$, on the left, of the registered data with the median and $\pm\sigma$ predictions according to Bindi et al. (2011) for $T=0.20s$.

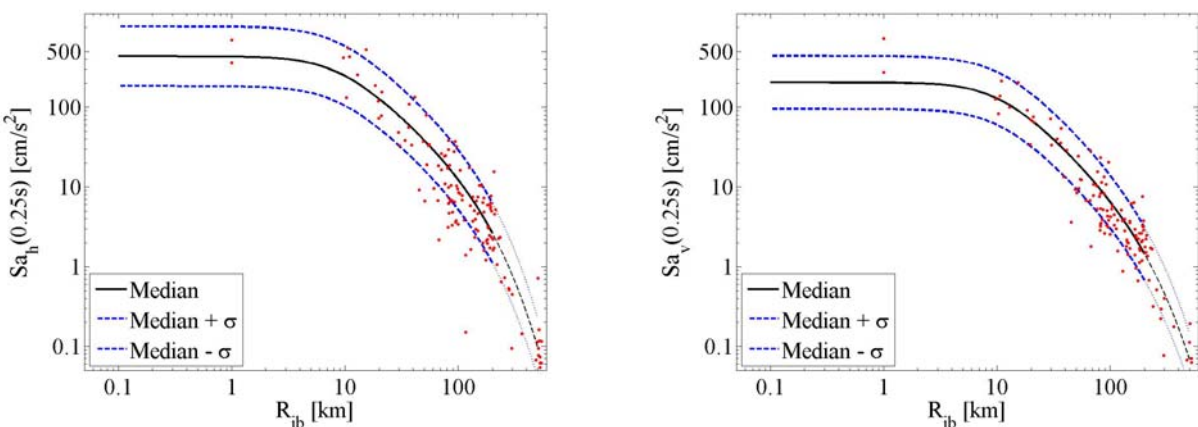


Figure 22. Spectral acceleration comparison of the geometrical mean of the horizontal components $Sa_h(T)$, on the right, and the vertical component $Sa_v(T)$, on the left, of the registered data with the median and $\pm\sigma$ predictions according to Bindi et al. (2011) for $T=0.25s$.

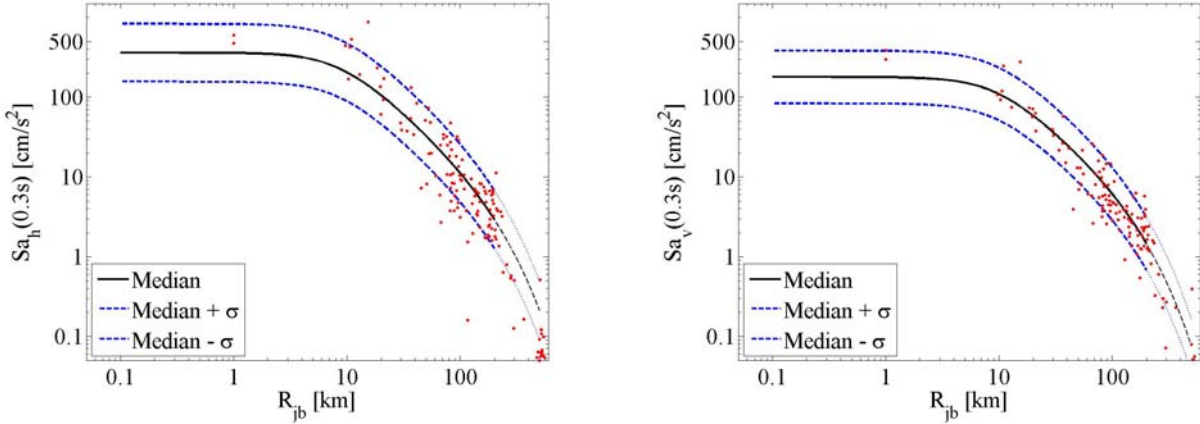


Figure 23. Spectral acceleration comparison of the geometrical mean of the horizontal components $Sa_h(T)$, on the right, and the vertical component $Sa_v(T)$, on the left, of the registered data with the median and $\pm\sigma$ predictions according to Bindi et al. (2011) for $T=0.30s$.

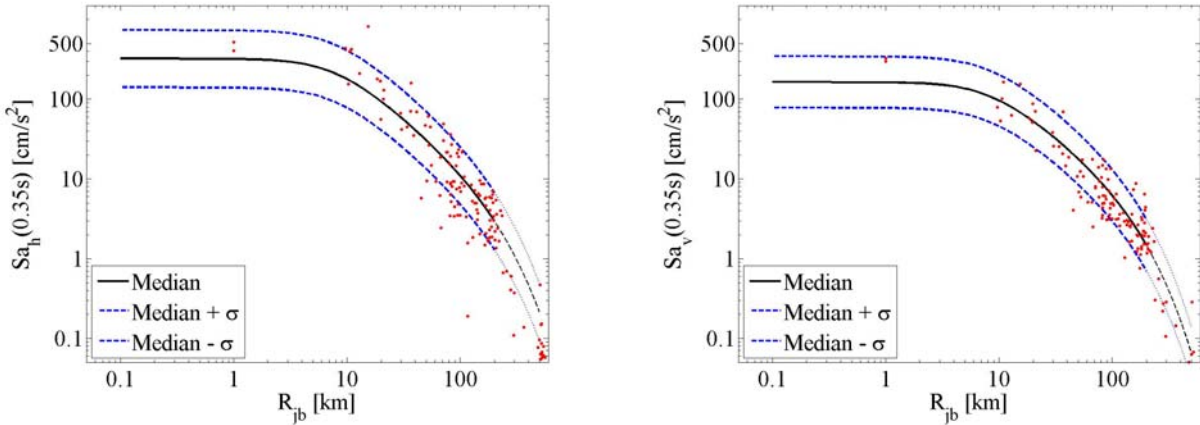


Figure 24. Spectral acceleration comparison of the geometrical mean of the horizontal components $Sa_h(T)$, on the right, and the vertical component $Sa_v(T)$, on the left, of the registered data with the median and $\pm\sigma$ predictions according to Bindi et al. (2011) for $T=0.35s$.

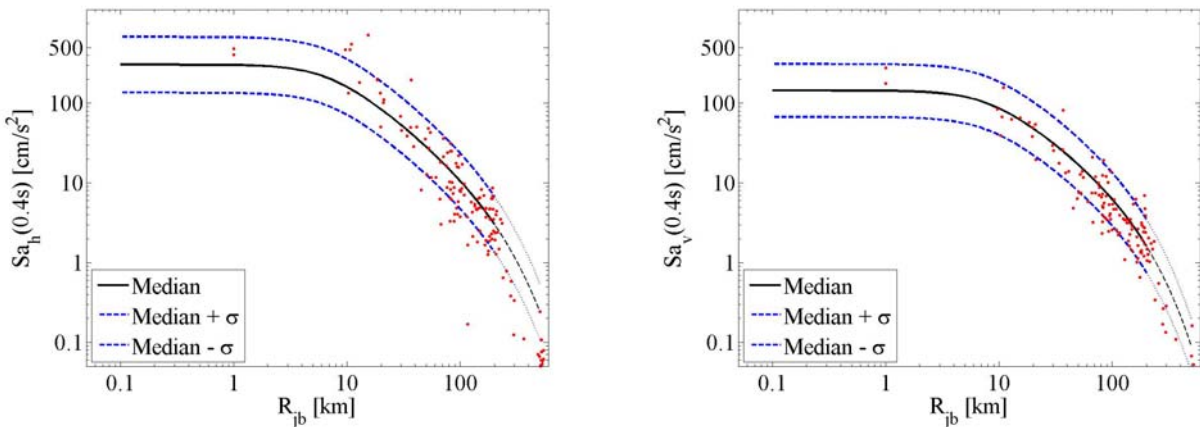


Figure 25. Spectral acceleration comparison of the geometrical mean of the horizontal components $Sa_h(T)$, on the right, and the vertical component $Sa_v(T)$, on the left, of the registered data with the median and $\pm\sigma$ predictions according to Bindi et al. (2011) for $T=0.40s$.

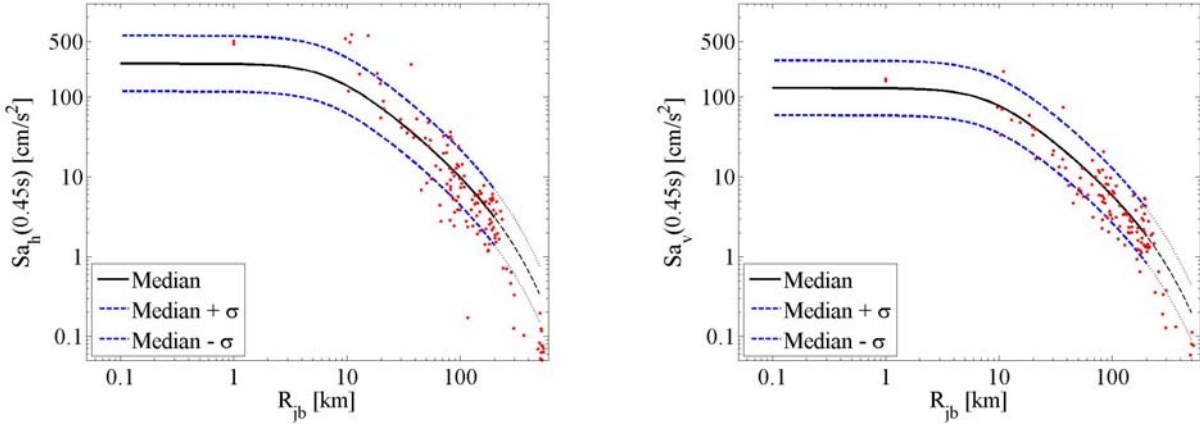


Figure 26. Spectral acceleration comparison of the geometrical mean of the horizontal components $Sa_h(T)$, on the right, and the vertical component $Sa_v(T)$, on the left, of the registered data with the median and $\pm\sigma$ predictions according to Bindi et al. (2011) for $T=0.45s$.

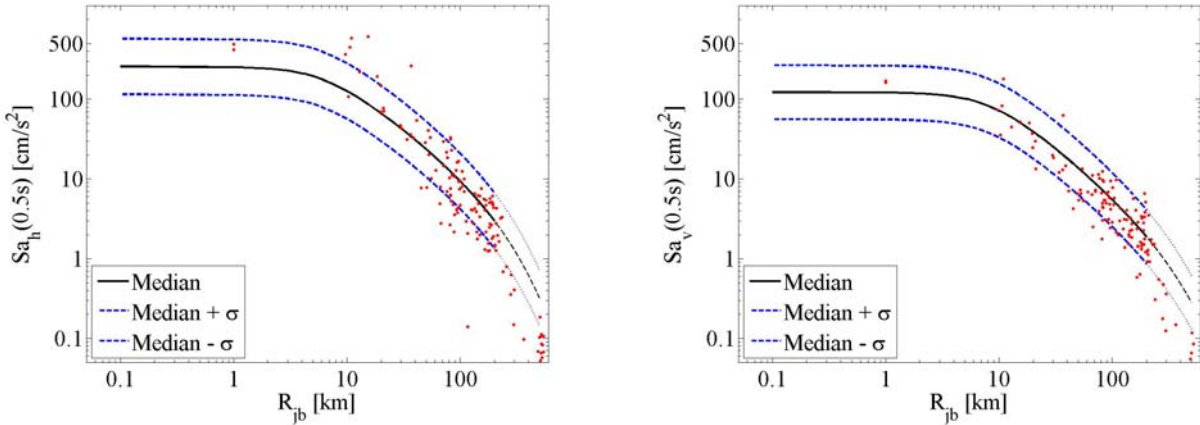


Figure 27. Spectral acceleration comparison of the geometrical mean of the horizontal components $Sa_h(T)$, on the right, and the vertical component $Sa_v(T)$, on the left, of the registered data with the median and $\pm\sigma$ predictions according to Bindi et al. (2011) for $T=0.50s$.

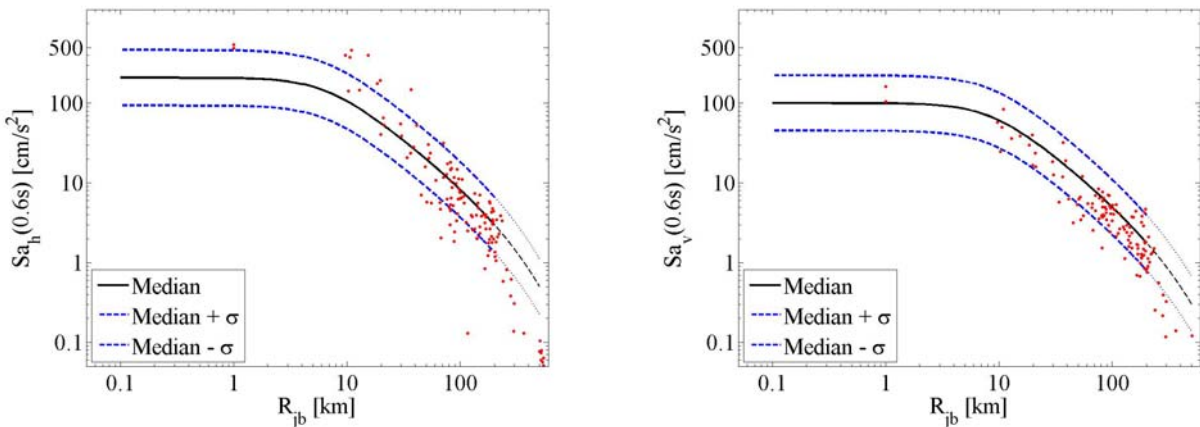


Figure 28. Spectral acceleration comparison of the geometrical mean of the horizontal components $Sa_h(T)$, on the right, and the vertical component $Sa_v(T)$, on the left, of the registered data with the median and $\pm\sigma$ predictions according to Bindi et al. (2011) for $T=0.60s$.

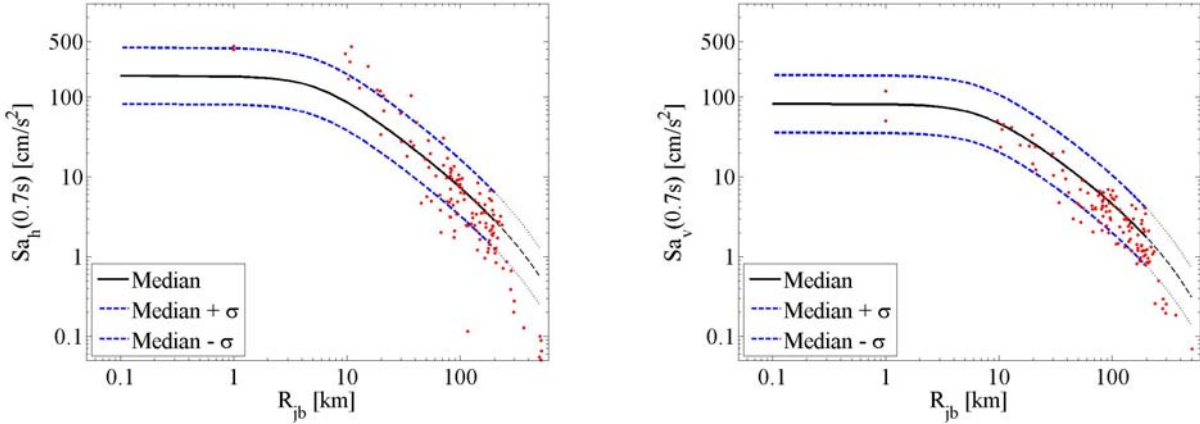


Figure 29. Spectral acceleration comparison of the geometrical mean of the horizontal components $Sa_h(T)$, on the right, and the vertical component $Sa_v(T)$, on the left, of the registered data with the median and $\pm\sigma$ predictions according to Bindi et al. (2011) for $T=0.70s$.

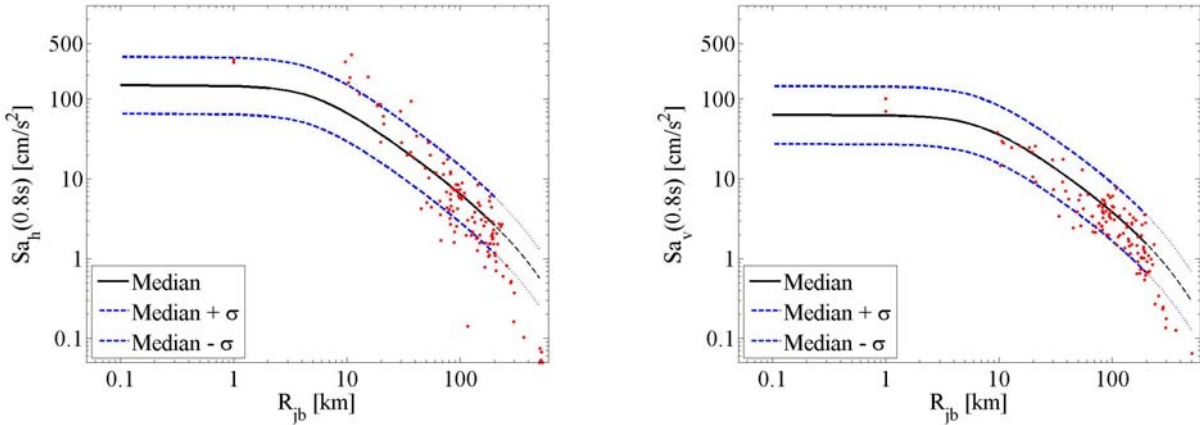


Figure 30. Spectral acceleration comparison of the geometrical mean of the horizontal components $Sa_h(T)$, on the right, and the vertical component $Sa_v(T)$, on the left, of the registered data with the median and $\pm\sigma$ predictions according to Bindi et al. (2011) for $T=0.80s$.

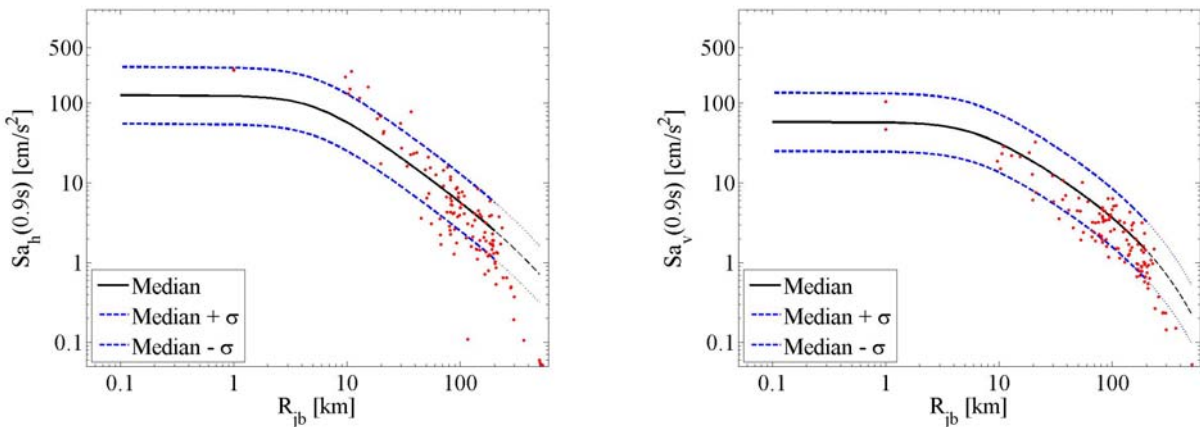


Figure 31. Spectral acceleration comparison of the geometrical mean of the horizontal components $Sa_h(T)$, on the right, and the vertical component $Sa_v(T)$, on the left, of the registered data with the median and $\pm\sigma$ predictions according to Bindi et al. (2011) for $T=0.90s$.

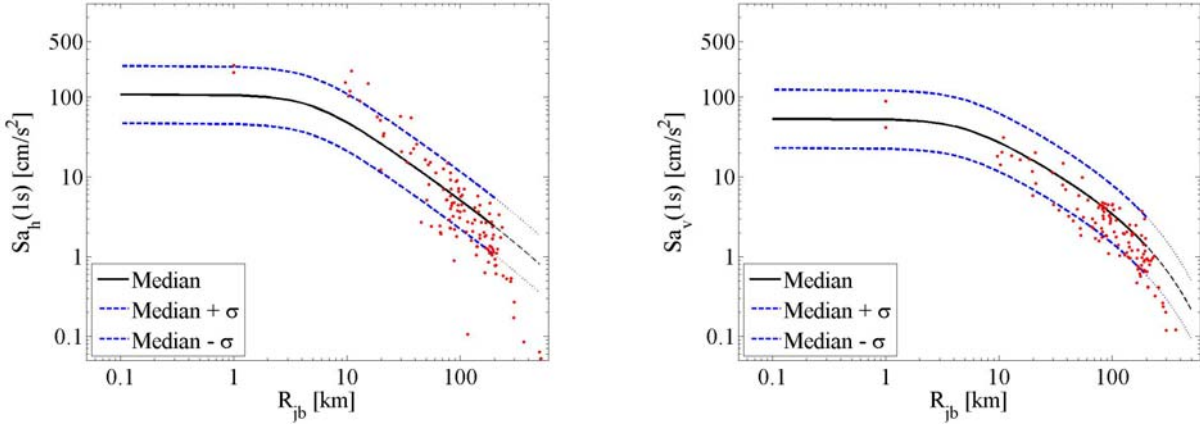


Figure 32. Spectral acceleration comparison of the geometrical mean of the horizontal components $Sa_h(T)$, on the right, and the vertical component $Sa_v(T)$, on the left, of the registered data with the median and $\pm\sigma$ predictions according to Bindi et al. (2011) for $T=1.00s$.

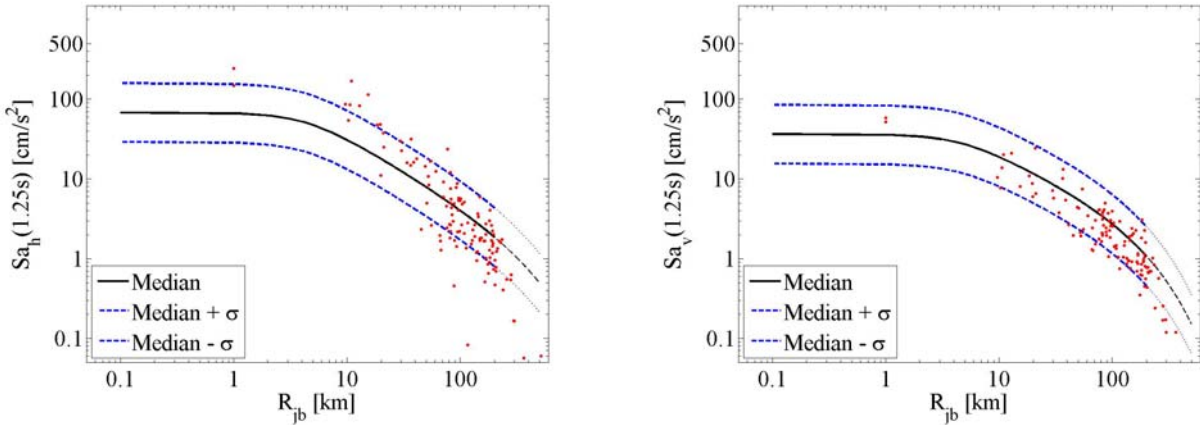


Figure 33. Spectral acceleration comparison of the geometrical mean of the horizontal components $Sa_h(T)$, on the right, and the vertical component $Sa_v(T)$, on the left, of the registered data with the median and $\pm\sigma$ predictions according to Bindi et al. (2011) for $T=1.25s$.

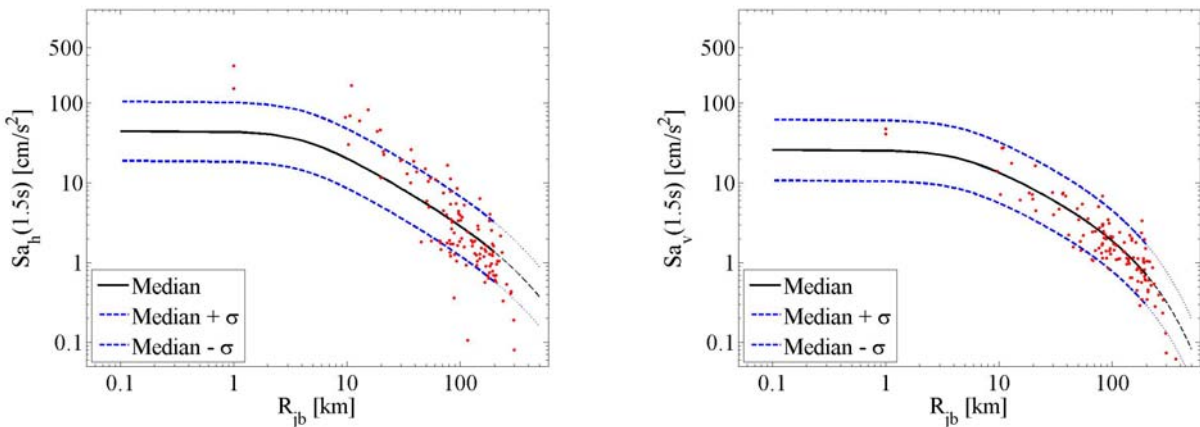


Figure 34. Spectral acceleration comparison of the geometrical mean of the horizontal components $Sa_h(T)$, on the right, and the vertical component $Sa_v(T)$, on the left, of the registered data with the median and $\pm\sigma$ predictions according to Bindi et al. (2011) for $T=1.50s$.

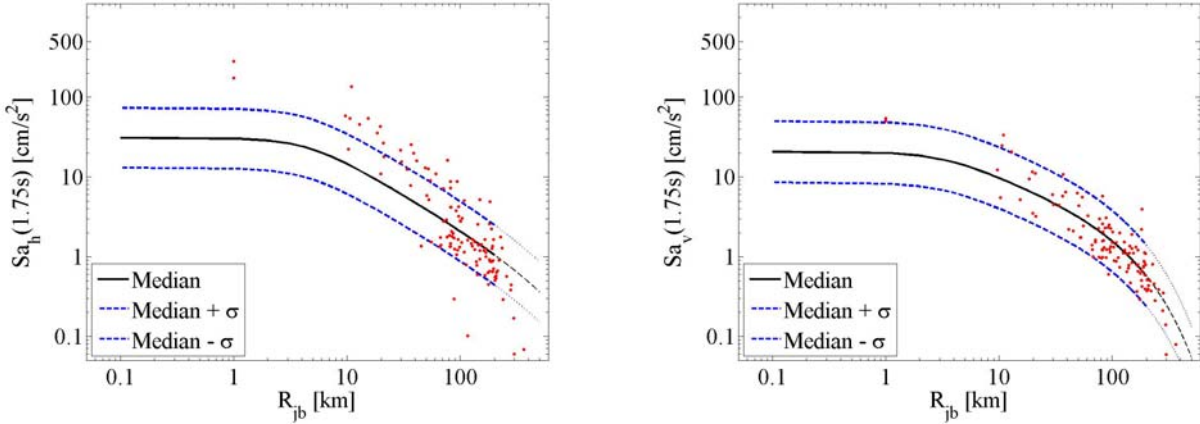


Figure 35. Spectral acceleration comparison of the geometrical mean of the horizontal components $Sa_h(T)$, on the right, and the vertical component $Sa_v(T)$, on the left, of the registered data with the median and $\pm\sigma$ predictions according to Bindi et al. (2011) for $T=1.75s$.

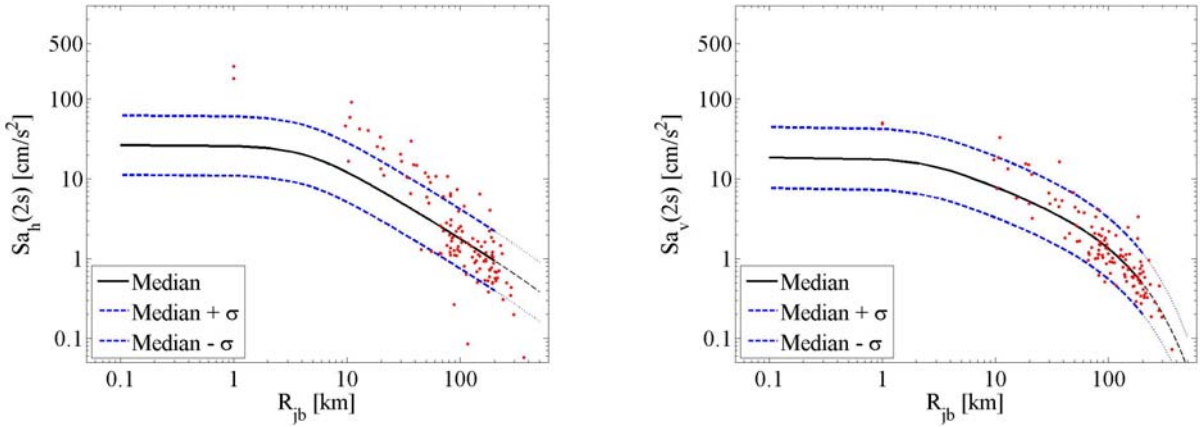


Figure 36. Spectral acceleration comparison of the geometrical mean of the horizontal components $Sa_h(T)$, on the right, and the vertical component $Sa_v(T)$, on the left, of the registered data with the median and $\pm\sigma$ predictions according to Bindi et al. (2011) for $T=2.00s$.

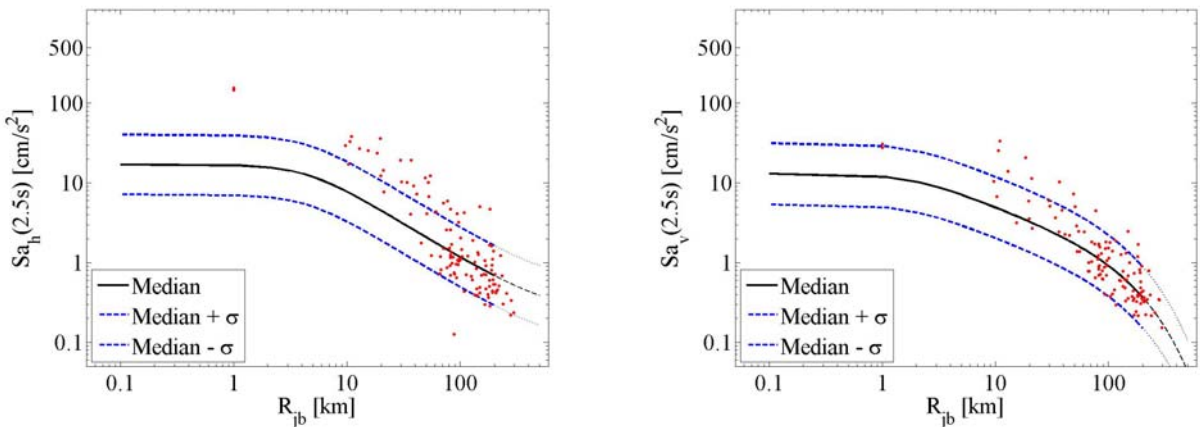


Figure 37. Spectral acceleration comparison of the geometrical mean of the horizontal components $Sa_h(T)$, on the right, and the vertical component $Sa_v(T)$, on the left, of the registered data with the median and $\pm\sigma$ predictions according to Bindi et al. (2011) for $T=2.50s$.

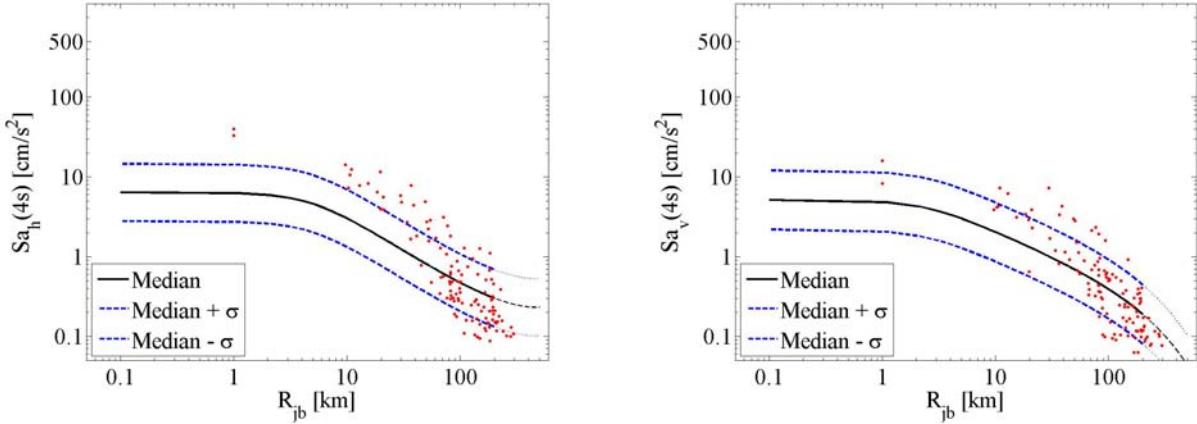


Figure 38. Spectral acceleration comparison of the geometrical mean of the horizontal components $Sa_h(T)$, on the right, and the vertical component $Sa_v(T)$, on the left, of the registered data with the median and $\pm\sigma$ predictions according to Bindi et al. (2011) for $T=4.0s$.

6. Direct spectral comparison of the data registered within 70km

A direct spectral comparison is made for the signals registered within 70km from the epicenter. For such stations the classification according to the Italian Accelerometric Archive (ITACA) is provided in [Table 2](#). Soil type marked with a star (*) means that the identification is carried out from Italian geological maps (1:100.000 scale). Two stations, ZPP and MRZ were *not found* in ITACA; thus, in [Table 2](#) they are indicated as “nf”, and for the following direct spectral comparison such stations are considered on soil class A (even if it is unlikely the stations are on this soil class) in analogy with the hypothesis made in the previous section. Same assumption is accepted for all the temporary stations (*temp* in the Table 2) which are clearly not available in ITACA website.

In [Figure 39](#) to [Figure 65](#) the direct comparison of the horizontal and vertical component registered spectra with median and $\pm\sigma$ bands of Bindi et al. (2011) GMPE is provided. Joyner and Boore distance is evaluated according to the approximate expression in Equation (1).

Table 2. Soil classification of the stations within 70 km from the epicentre.

Station ID	R_{epi} (km)	Soil Class	Soil ID
MRN	3.58	C*	3
SAN0	4.73	temp	1
SMS0	14.95	temp	1
RAV0	15.69	temp	1
FIN0	16.04	temp	1
MOG0	16.43	temp	1
CRP	18.69	temp	1

CNT	21.34	temp	1
SAG0	24.98	temp	1
CAS0	26.25	temp	1
BON0	26.52	temp	1
MDN	27.61	C*	3
NVL	28.00	C*	3
ZPP	37.52	nf	1
MBG0	38.37	temp	1
FER0	42.36	temp	1
SSU	45.10	A*	1
FIC0	45.88	temp	1
ISD	47.93	B*	2
SRP	50.51	C*	3
MRZ	55.03	nf	1
MDC	59.79	C*	3
PVF	61.17	A*	1
CPC	62.90	C*	3
ARG	63.48	D	4
CSP	65.55	B*	2
MNS	67.04	C*	3

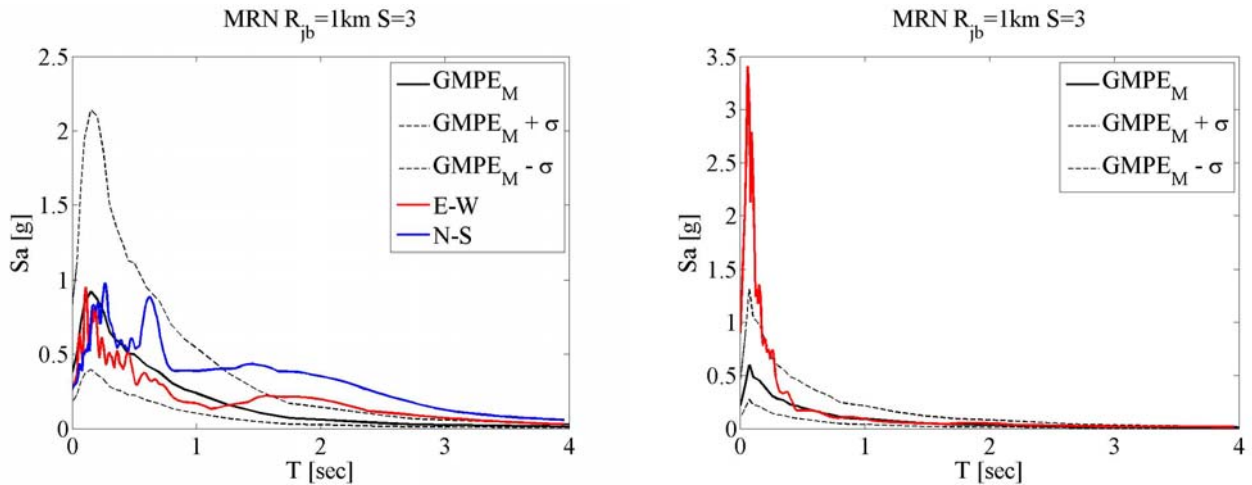


Figure 39. Comparison of the registered spectra at MRN station for E-W and N-S components (on the left) and vertical component (on the right) with the mean $\pm\sigma$ predictions according to Bindi et al. (2011).

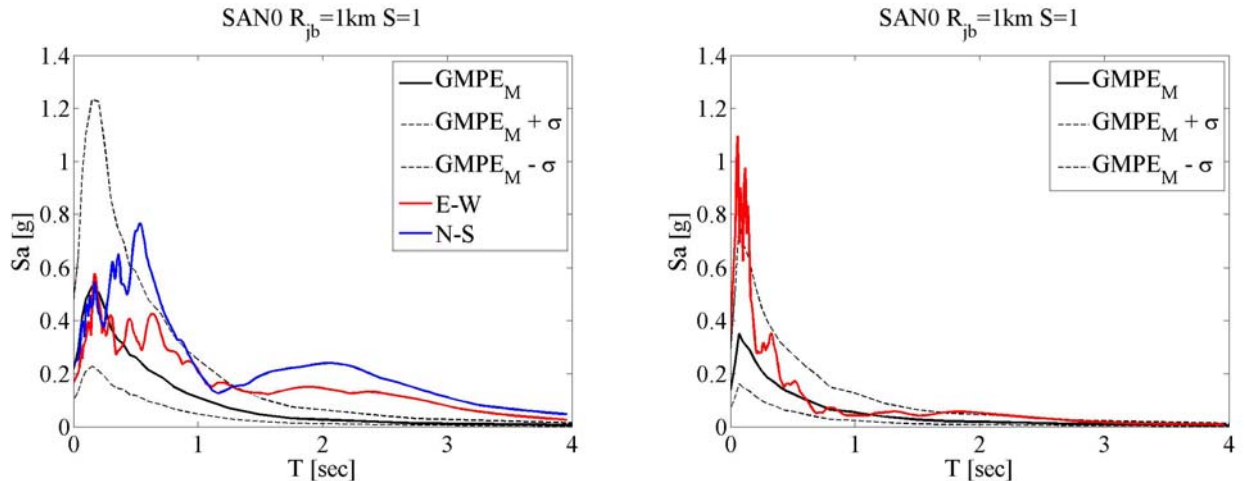


Figure 40. Comparison of the registered spectra at SAN0 station for E-W and N-S components (on the left) and vertical component (on the right) with the mean $\pm\sigma$ predictions according to Bindi et al. (2011).

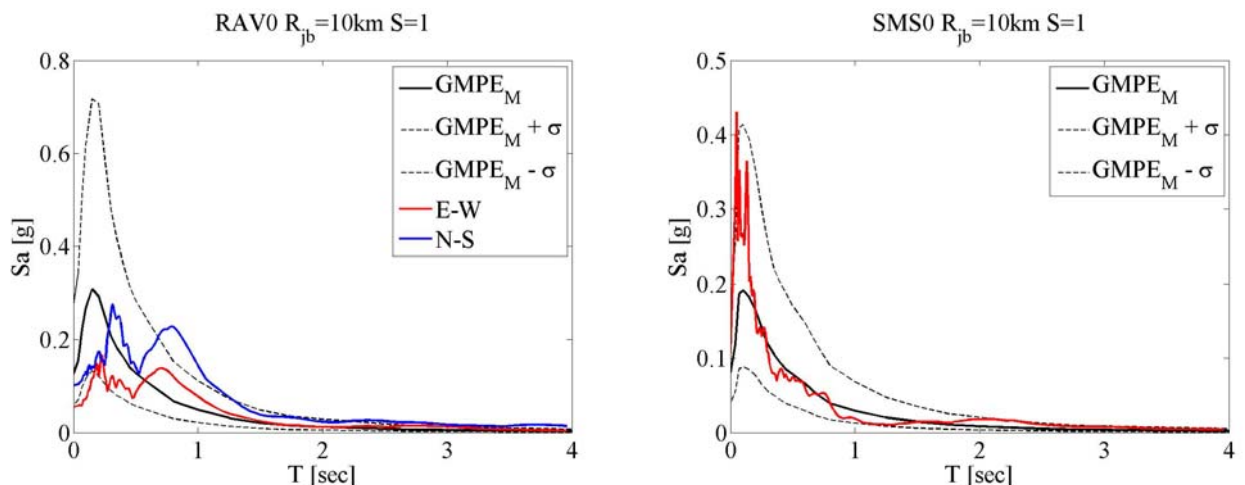


Figure 41. Comparison of the registered spectra at RAV0 station for E-W and N-S components (on the left) and vertical component (on the right) with the mean $\pm\sigma$ predictions according to Bindi et al. (2011).

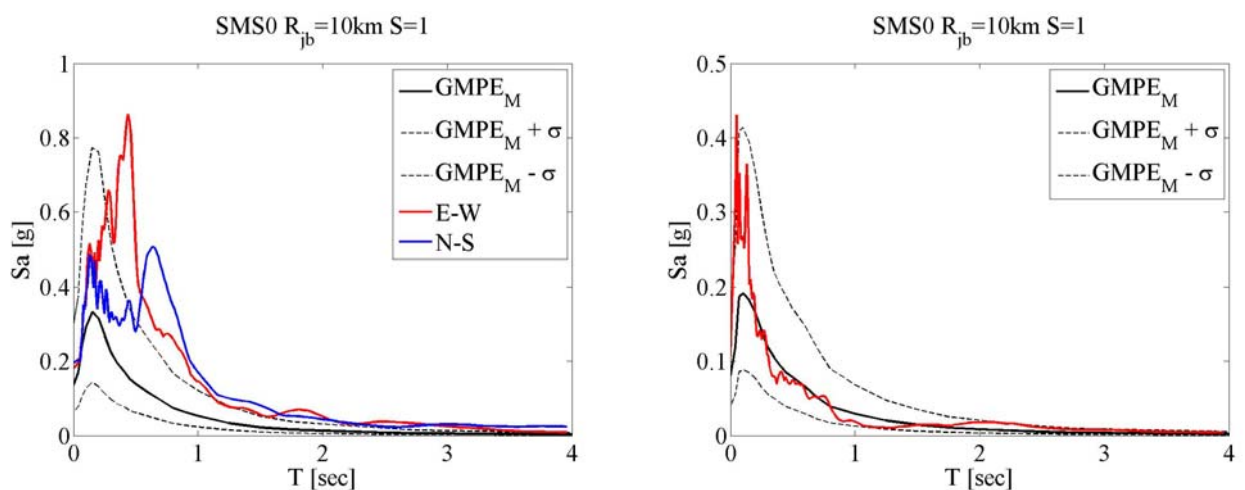


Figure 42. Comparison of the registered spectra at SMS0 station for E-W and N-S components (on the left) and vertical component (on the right) with the mean $\pm\sigma$ predictions according to Bindi et al. (2011).

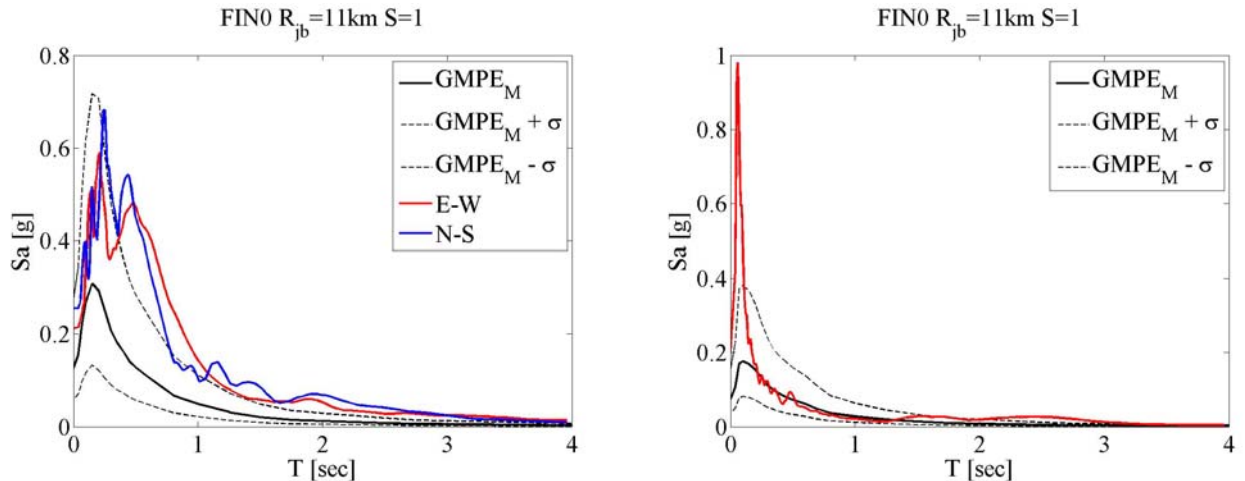


Figure 43. Comparison of the registered spectra at FIN0 station for E-W and N-S components (on the left) and vertical component (on the right) with the mean $\pm\sigma$ predictions according to Bindi et al. (2011).

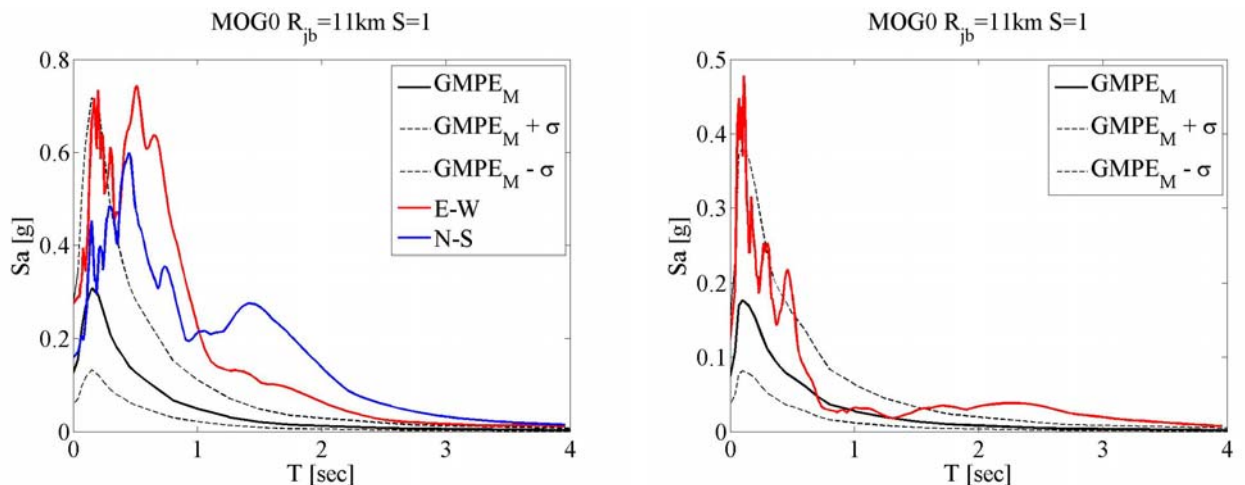


Figure 44. Comparison of the registered spectra at MOG0 station for E-W and N-S components (on the left) and vertical component (on the right) with the mean $\pm\sigma$ predictions according to Bindi et al. (2011).

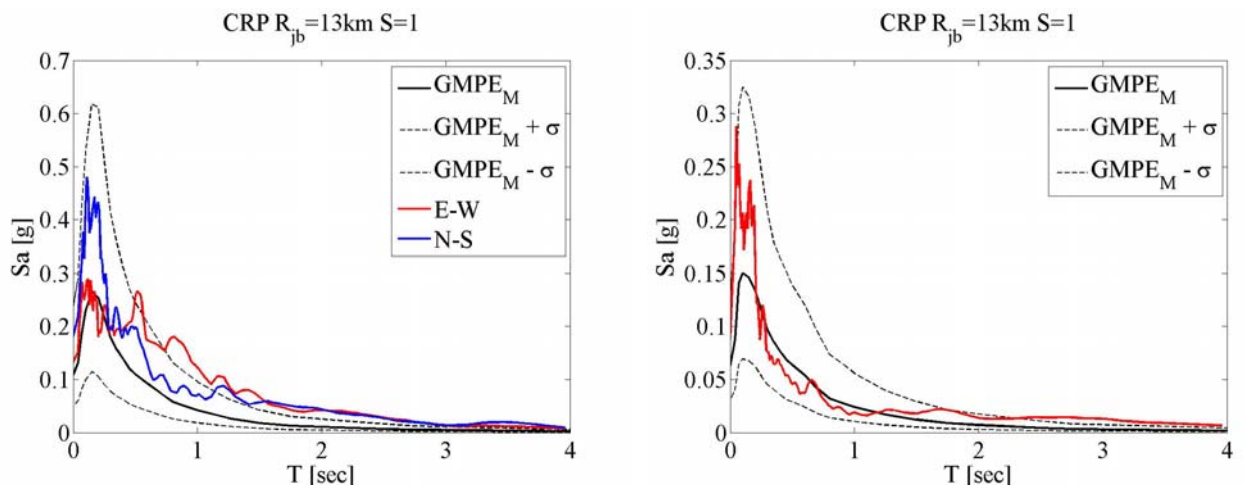


Figure 45. Comparison of the registered spectra at CRP station for E-W and N-S components (on the left) and vertical component (on the right) with the mean $\pm\sigma$ predictions according to Bindi et al. (2011).

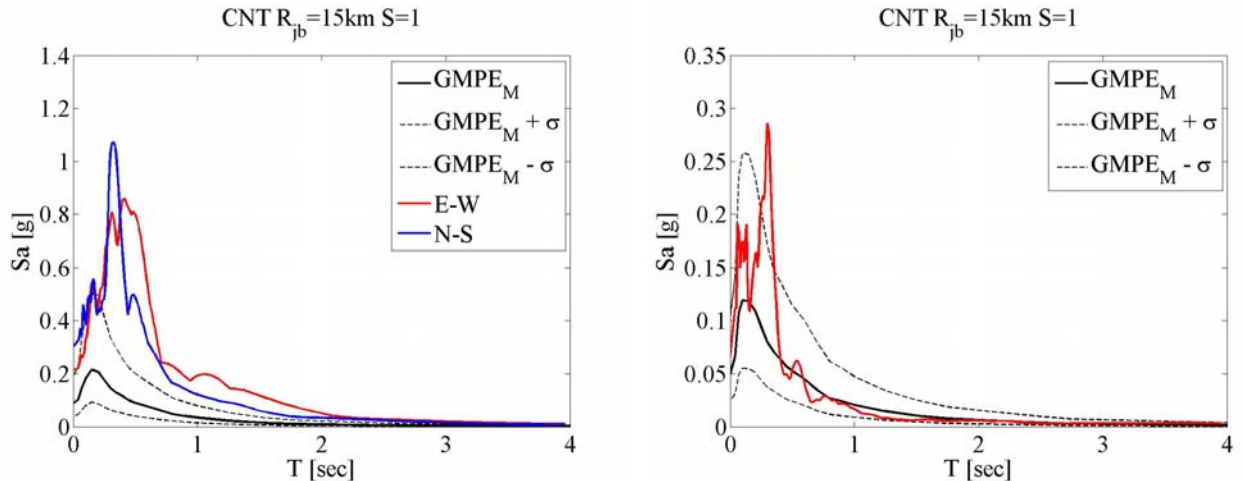


Figure 46. Comparison of the registered spectra at CNT station for E-W and N-S components (on the left) and vertical component (on the right) with the mean $\pm\sigma$ predictions according to Bindi et al. (2011).

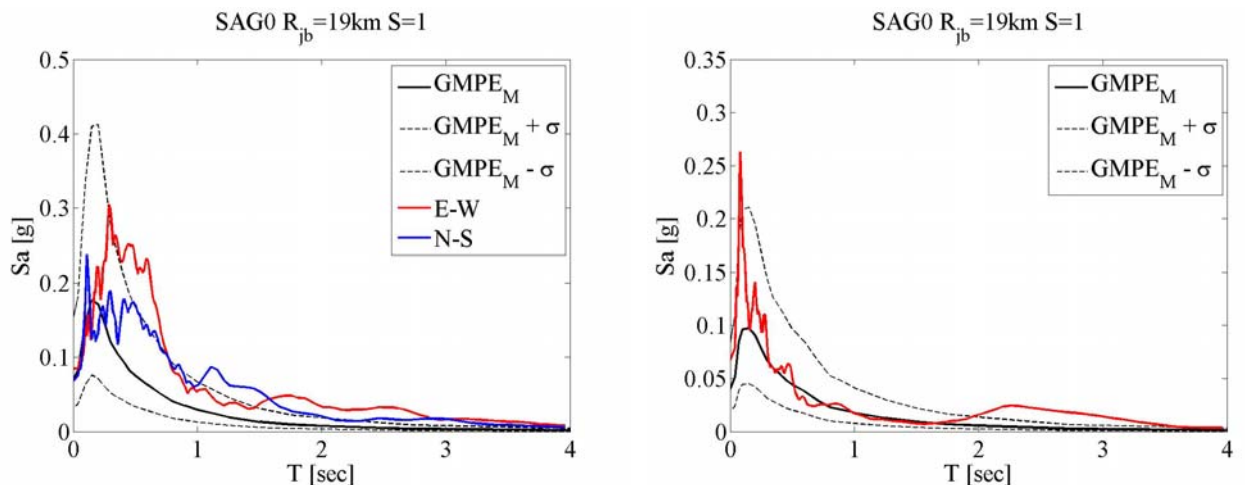


Figure 47. Comparison of the registered spectra at SAG0 station for E-W and N-S components (on the left) and vertical component (on the right) with the mean $\pm\sigma$ predictions according to Bindi et al. (2011).

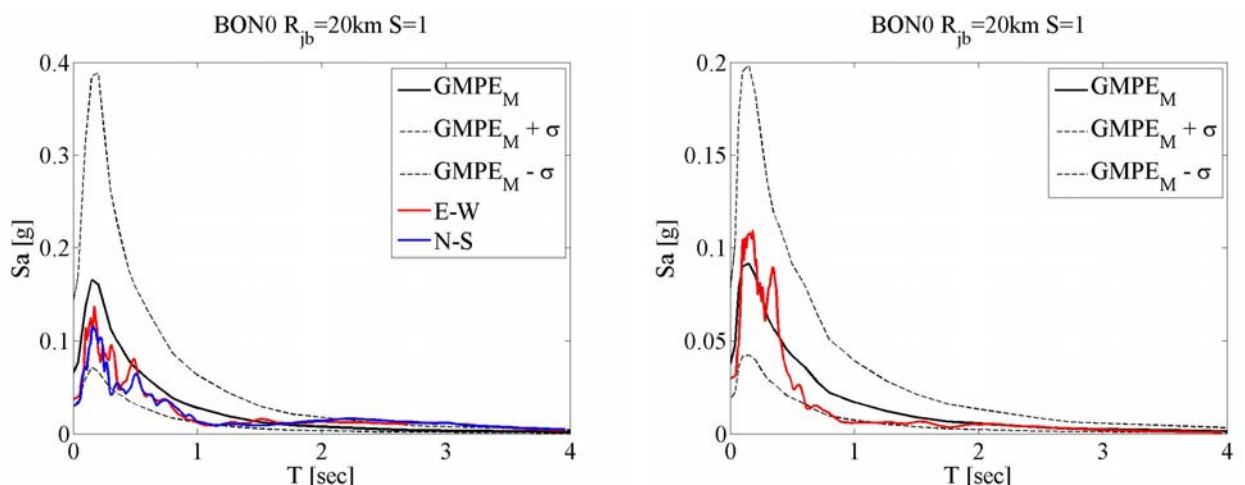


Figure 48. Comparison of the registered spectra at BON0 station for E-W and N-S components (on the left) and vertical component (on the right) with the mean $\pm\sigma$ predictions according to Bindi et al. (2011).

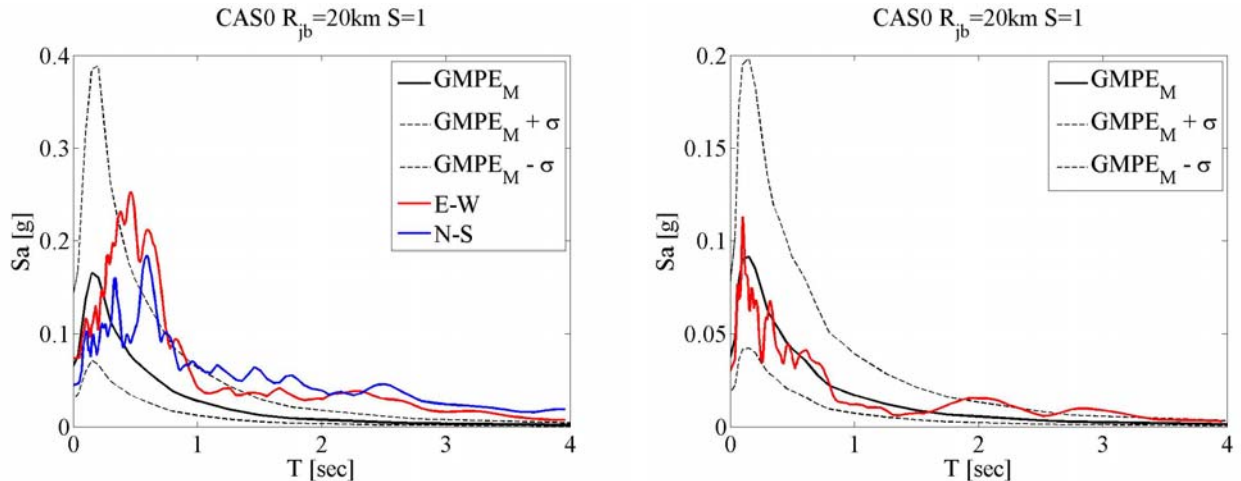


Figure 49. Comparison of the registered spectra at CAS0 station for E-W and N-S components (on the left) and vertical component (on the right) with the mean $\pm\sigma$ predictions according to Bindi et al. (2011).

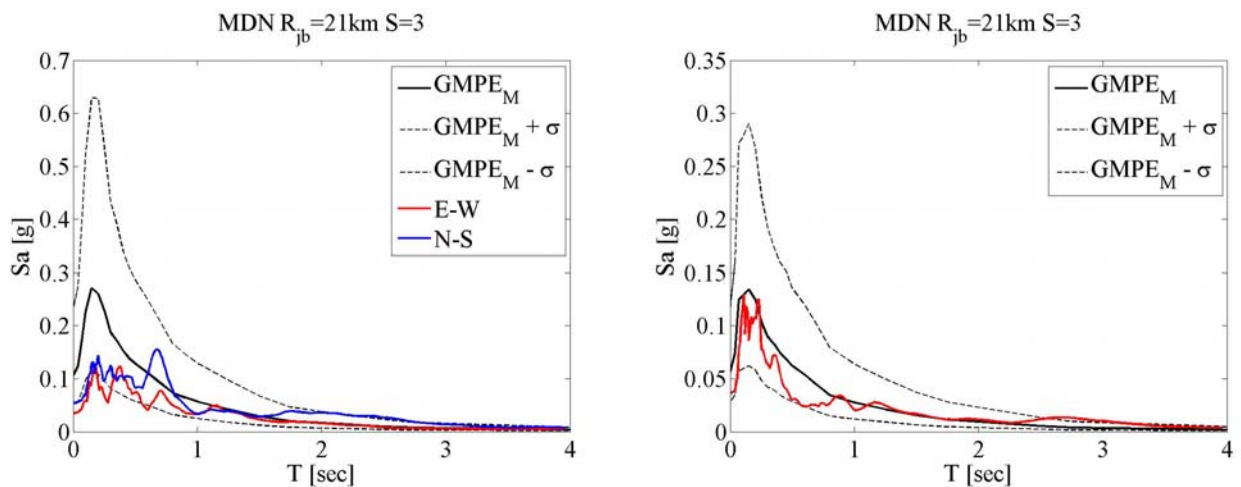


Figure 50. Comparison of the registered spectra at MDN station for E-W and N-S components (on the left) and vertical component (on the right) with the mean $\pm\sigma$ predictions according to Bindi et al. (2011).

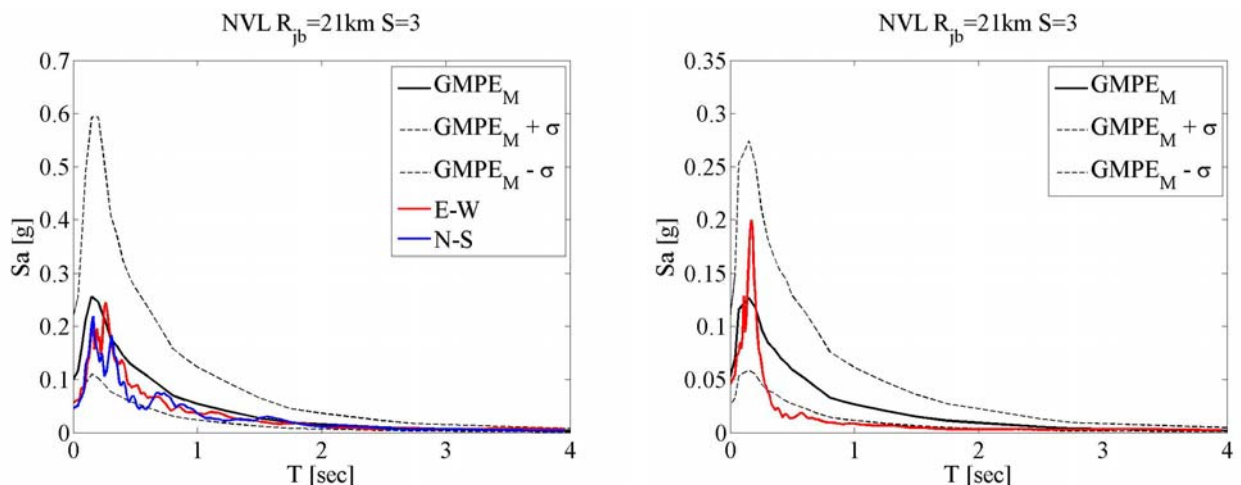


Figure 51. Comparison of the registered spectra at NVL station for E-W and N-S components (on the left) and vertical component (on the right) with the mean $\pm\sigma$ predictions according to Bindi et al. (2011).

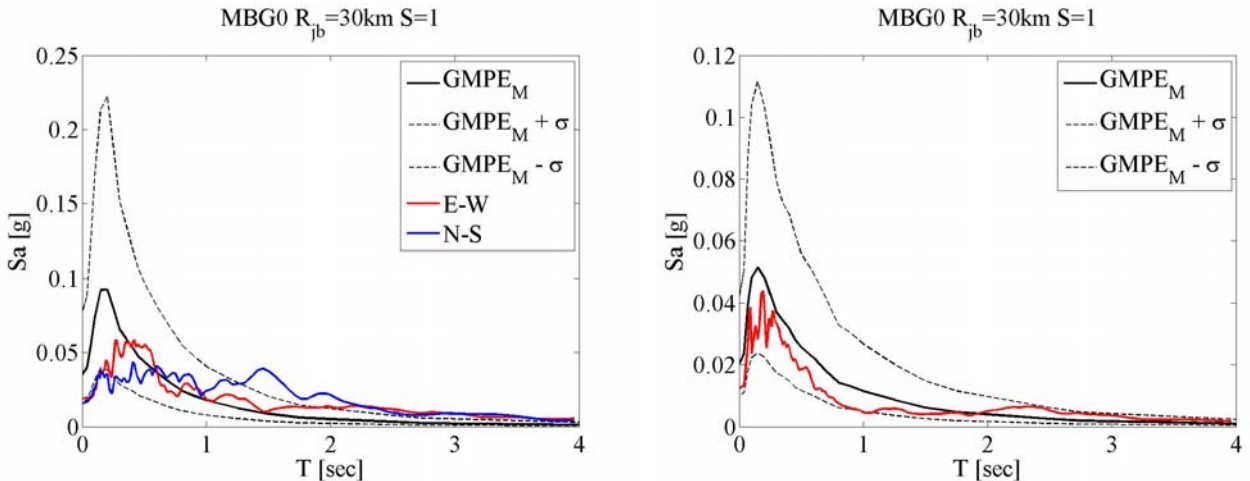


Figure 52. Comparison of the registered spectra at MBG0 station for E-W and N-S components (on the left) and vertical component (on the right) with the mean $\pm\sigma$ predictions according to Bindi et al. (2011).

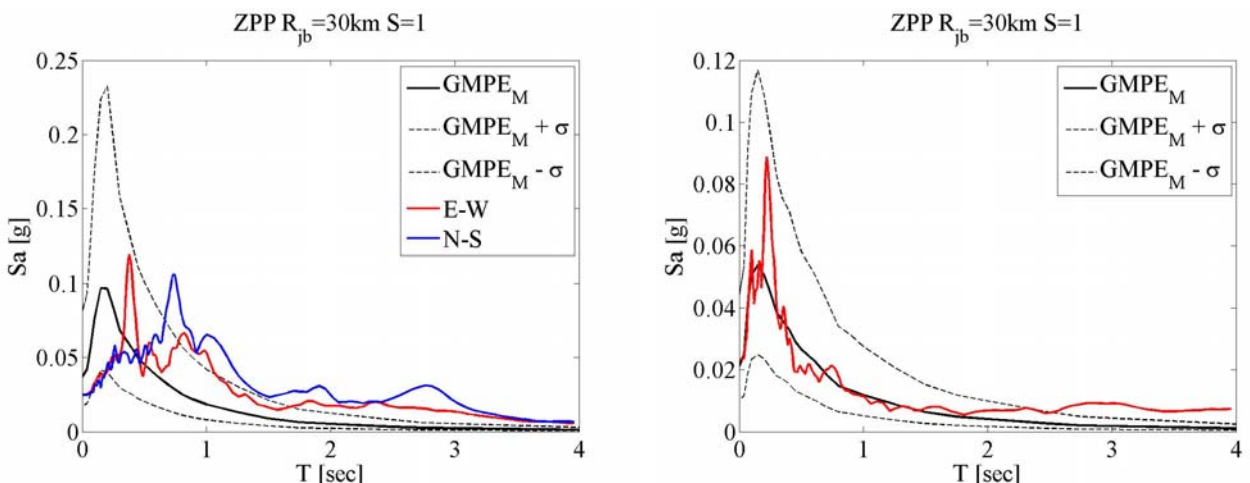


Figure 53. Comparison of the registered spectra at ZPP station for E-W and N-S components (on the left) and vertical component (on the right) with the mean $\pm\sigma$ predictions according to Bindi et al. (2011).

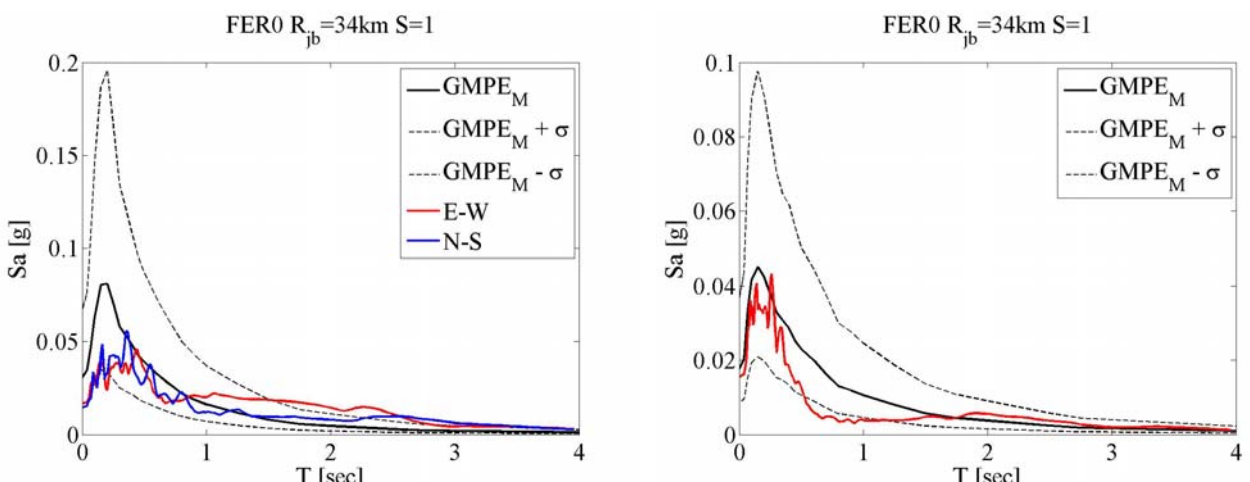


Figure 54. Comparison of the registered spectra at FER0 station for E-W and N-S components (on the left) and vertical component (on the right) with the mean $\pm\sigma$ predictions according to Bindi et al. (2011).

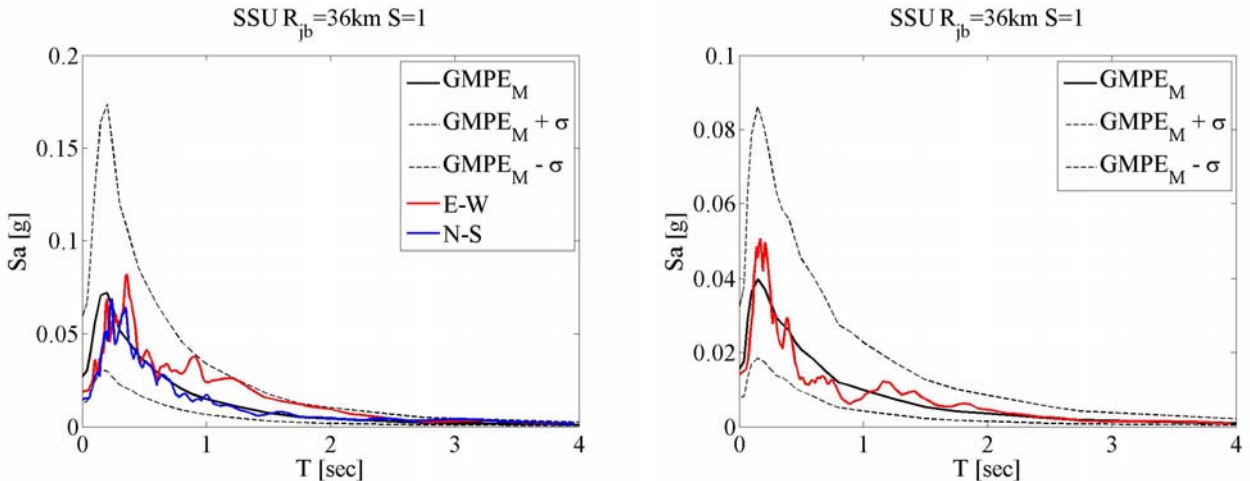


Figure 55. Comparison of the registered spectra at SSU station for E-W and N-S components (on the left) and vertical component (on the right) with the mean $\pm\sigma$ predictions according to Bindi et al. (2011).

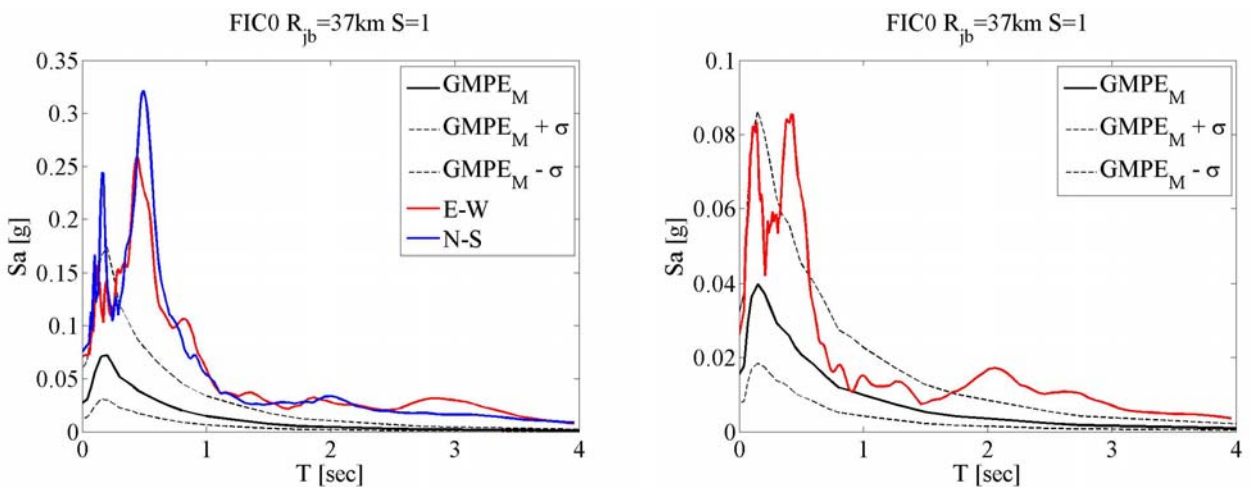


Figure 56. Comparison of the registered spectra at FIC0 station for E-W and N-S components (on the left) and vertical component (on the right) with the mean $\pm\sigma$ predictions according to Bindi et al. (2011).

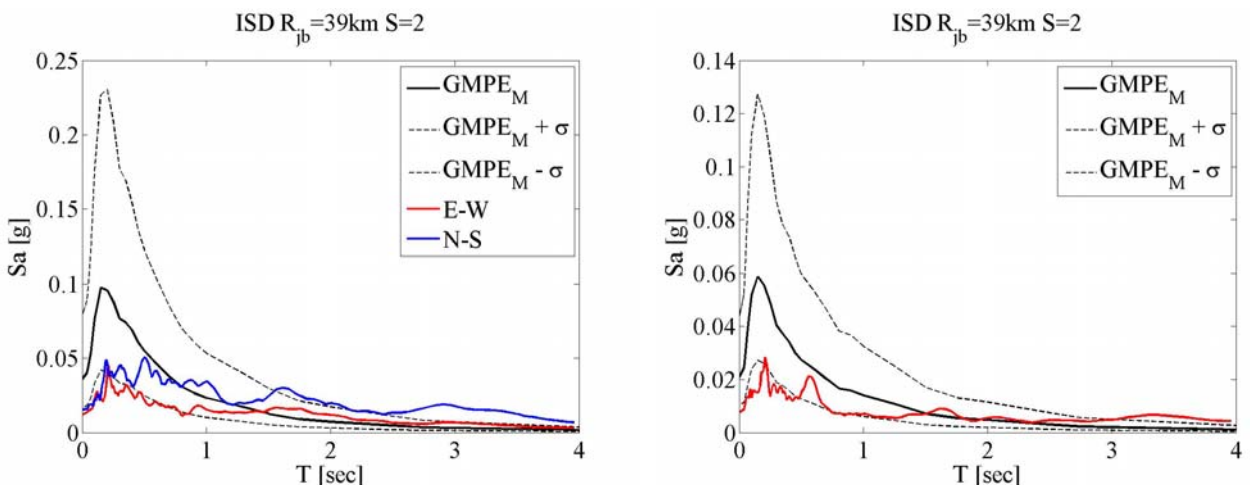


Figure 57. Comparison of the registered spectra at ISD station for E-W and N-S components (on the left) and vertical component (on the right) with the mean $\pm\sigma$ predictions according to Bindi et al. (2011).

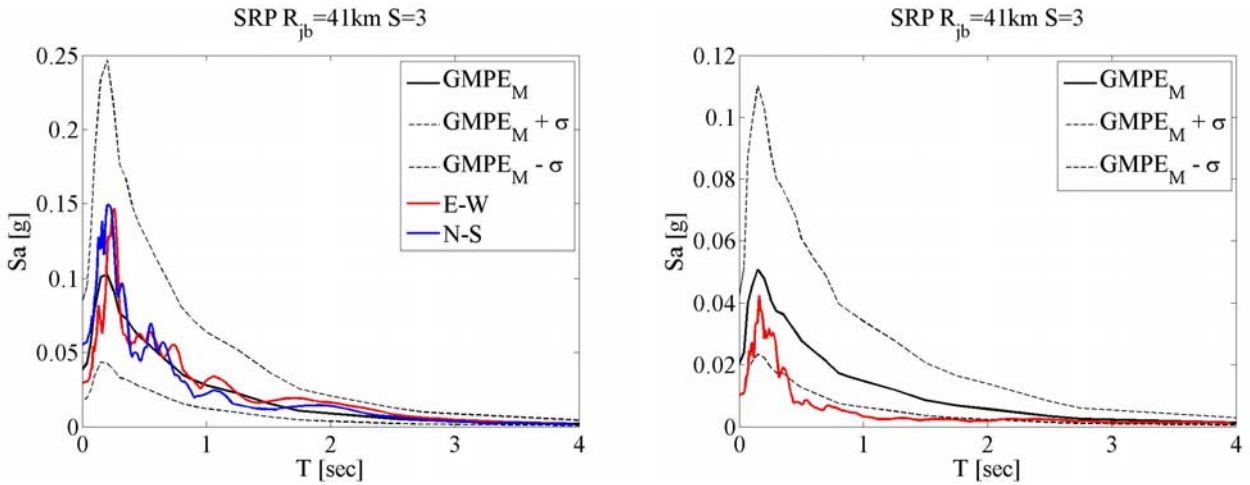


Figure 58. Comparison of the registered spectra at SRP station for E-W and N-S components (on the left) and vertical component (on the right) with the mean $\pm\sigma$ predictions according to Bindi et al. (2011).

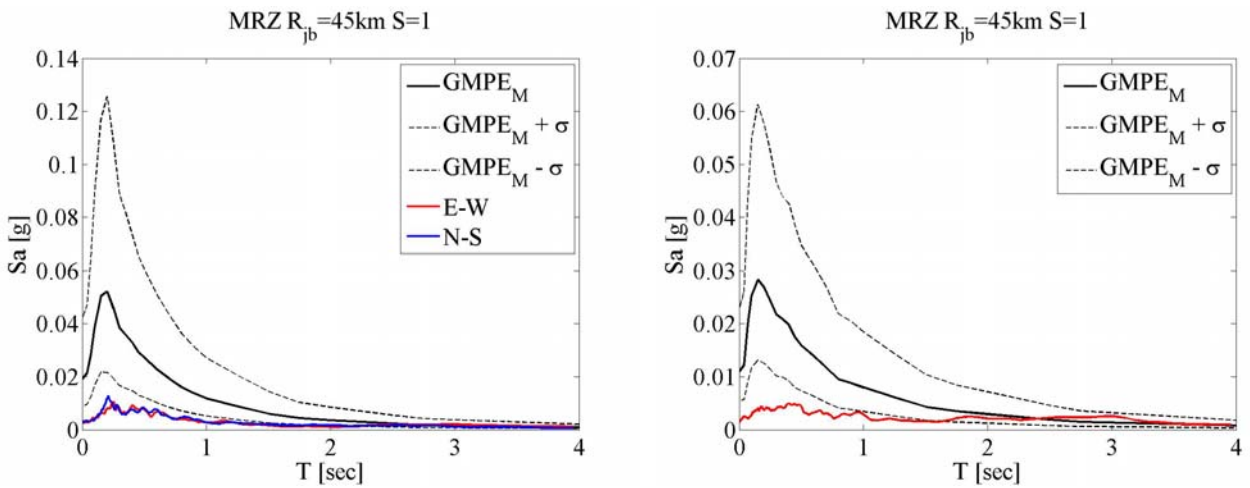


Figure 59. Comparison of the registered spectra at MRZ station for E-W and N-S components (on the left) and vertical component (on the right) with the mean $\pm\sigma$ predictions according to Bindi et al. (2011).

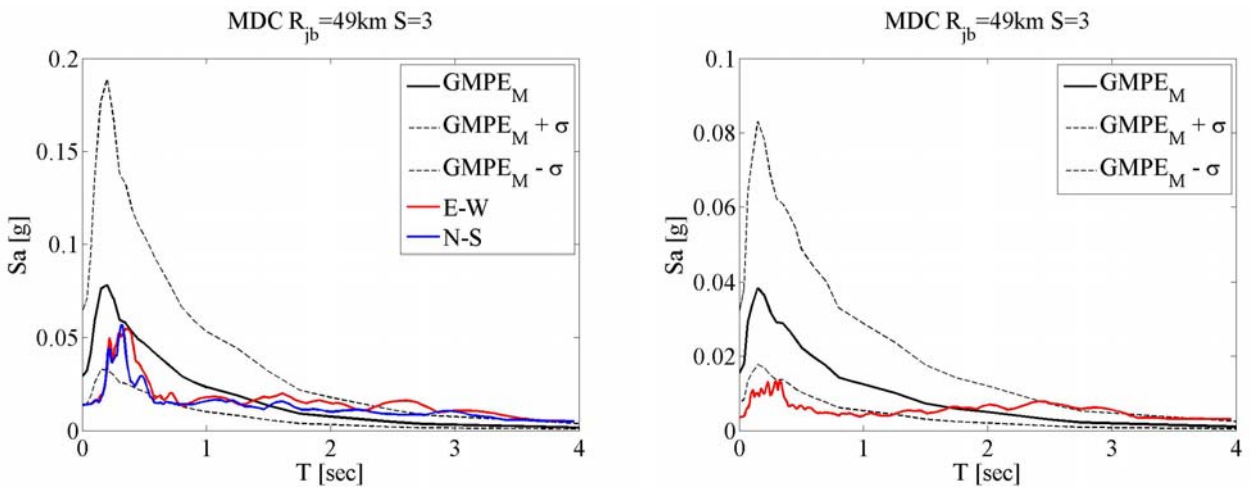


Figure 60. Comparison of the registered spectra at MDC station for E-W and N-S components (on the left) and vertical component (on the right) with the mean $\pm\sigma$ predictions according to Bindi et al. (2011).

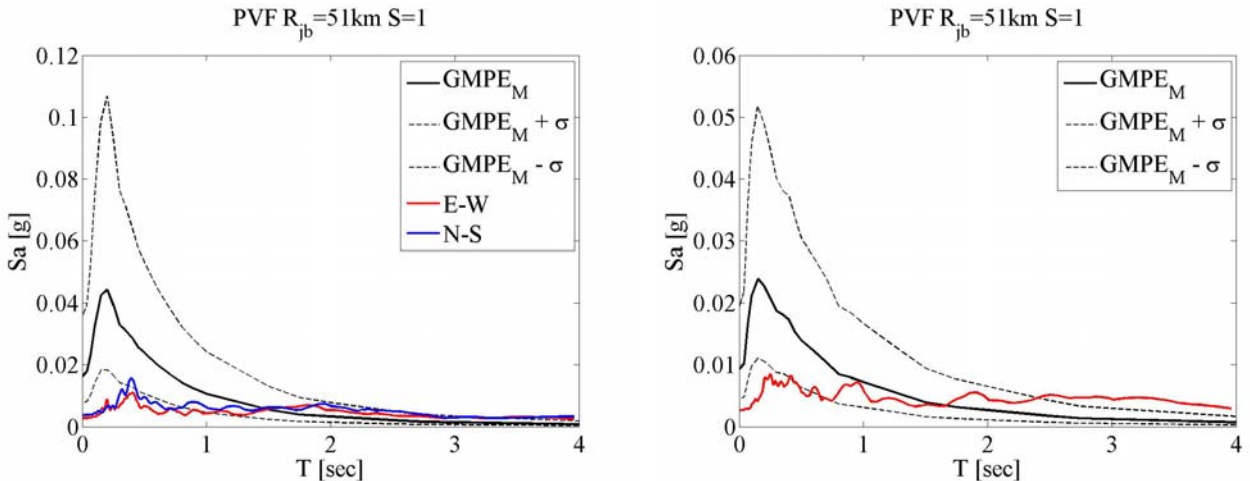


Figure 61. Comparison of the registered spectra at PVF station for E-W and N-S components (on the left) and vertical component (on the right) with the mean $\pm\sigma$ predictions according to Bindi et al. (2011).

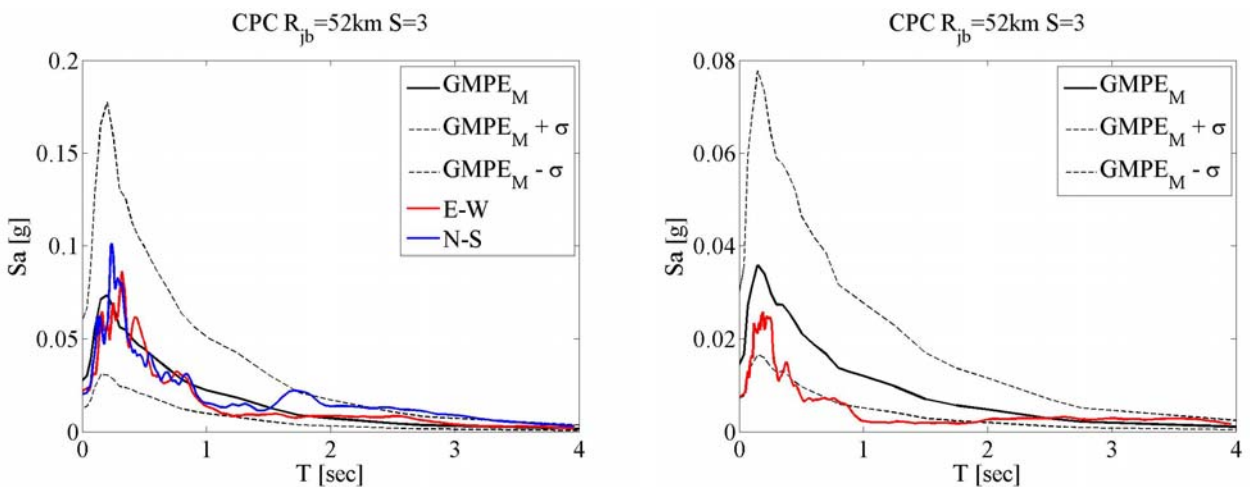


Figure 62. Comparison of the registered spectra at CPC station for E-W and N-S components (on the left) and vertical component (on the right) with the mean $\pm\sigma$ predictions according to Bindi et al. (2011).

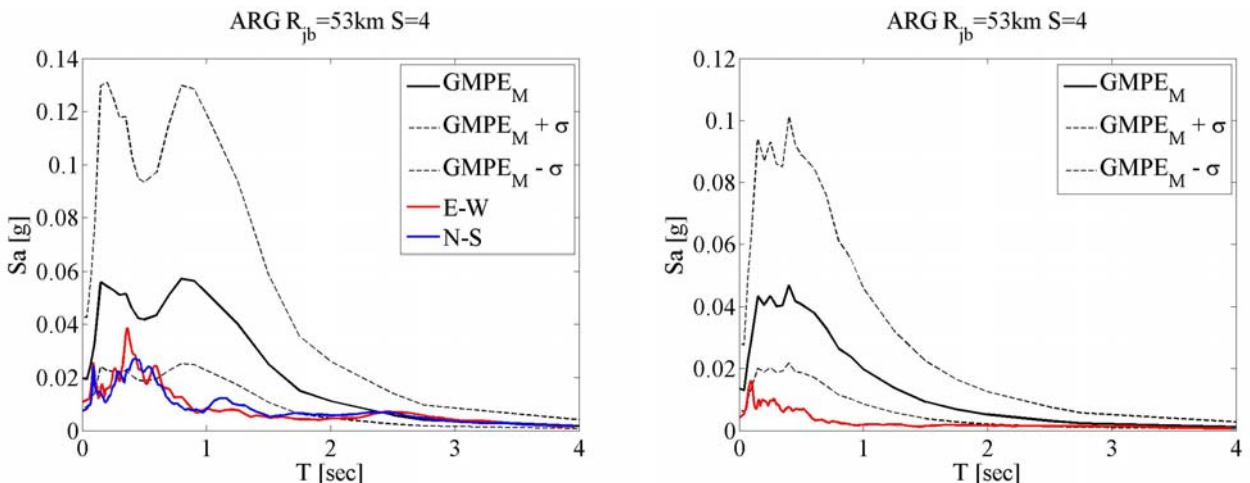


Figure 63. Comparison of the registered spectra at ARG station for E-W and N-S components (on the left) and vertical component (on the right) with the mean $\pm\sigma$ predictions according to Bindi et al. (2011).

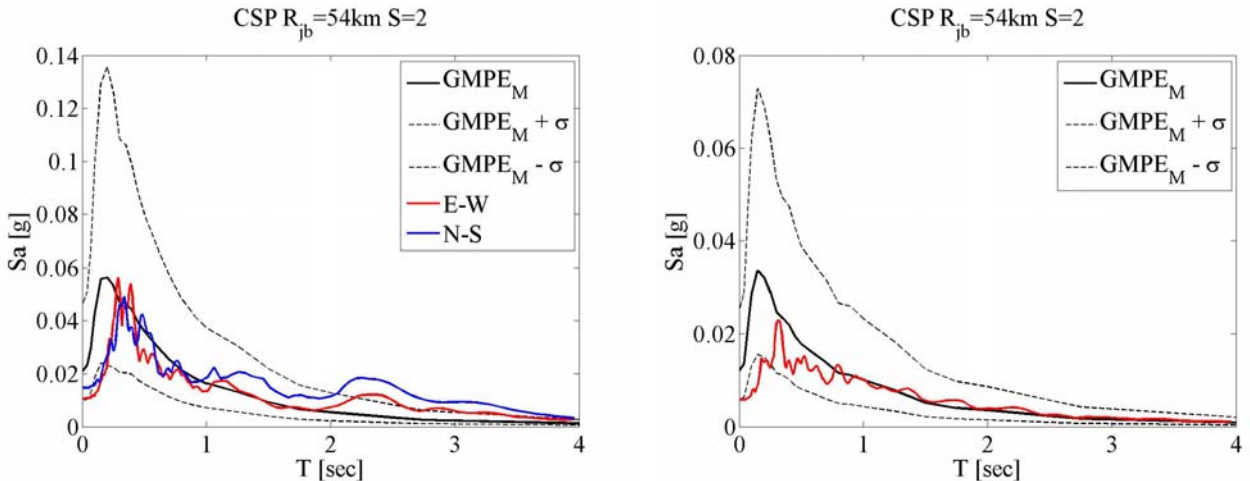


Figure 64. Comparison of the registered spectra at CSP station for E-W and N-S components (on the left) and vertical component (on the right) with the mean $\pm\sigma$ predictions according to Bindi et al. (2011).

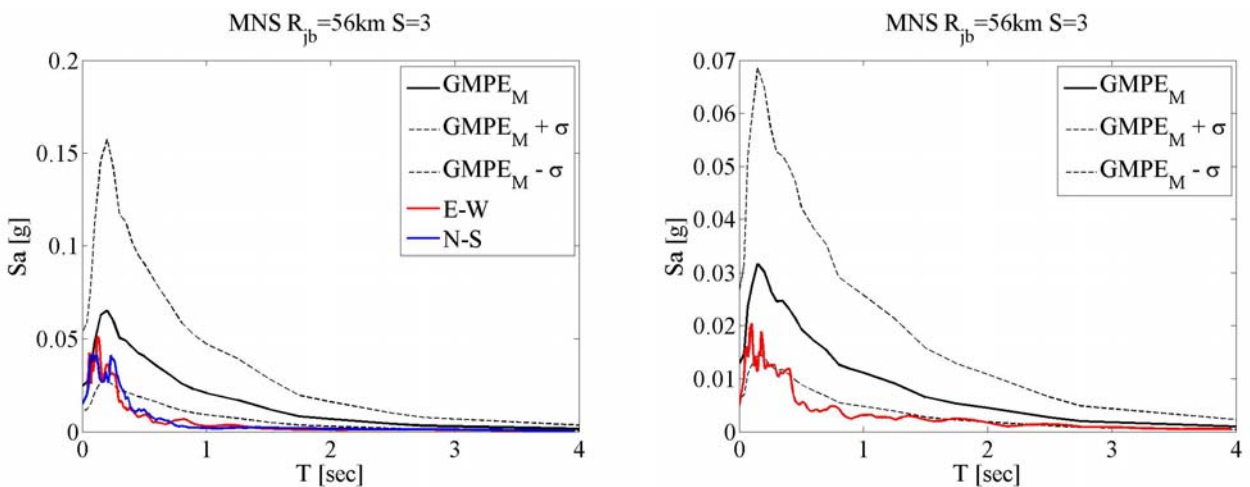


Figure 65. Comparison of the registered spectra at MNS station for E-W and N-S components (on the left) and vertical component (on the right) with the mean $\pm\sigma$ predictions according to Bindi et al. (2011).

7. Epsilon values of the data registered within 70km

In this section, according to the previous one, signals registered within 70km form the epicentre are compared with Bindi et al. (2011) GMPE. Results are reported in terms of epsilon values (ε) which measures the number of total standard deviations ($\sigma_{\log IM}$) by which logarithms of observed intensity measures ($\log IM$) differs from its predicted mean ($\mu_{\log IM}$):

$$\varepsilon = \frac{\log IM - \mu_{\log IM}}{\sigma_{\log IM}} \quad (2)$$

Joyner Boore distance is evaluated according to the approximate expression in Equation (1).

In Figure 66 epsilon values of PGA are shown for geometrical mean of horizontal components (in accordance with estimated variable of used GMPE) and for the vertical components. In Figure 67 epsilon values of PGV are shown for geometrical mean of horizontal components and for the vertical components. Figures 68 to 89 show epsilon values of spectral acceleration at a fixed vibration period ($\varepsilon_{Sa(T)} = \varepsilon(T)$) of the geometrical mean of horizontal components and the vertical components.

Epsilon values referred to temporary stations (for which the hypothesis of soil class A was accepted) are circled in red.

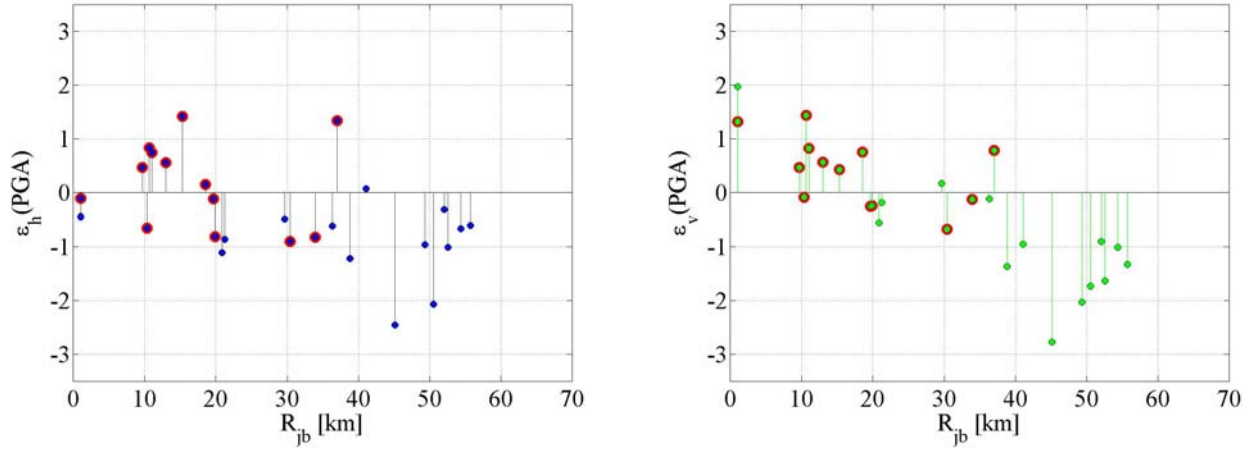


Figure 66. Epsilon values of PGA for geometrical mean of the horizontal components (ε_h) and vertical components (ε_v): left and right, respectively.

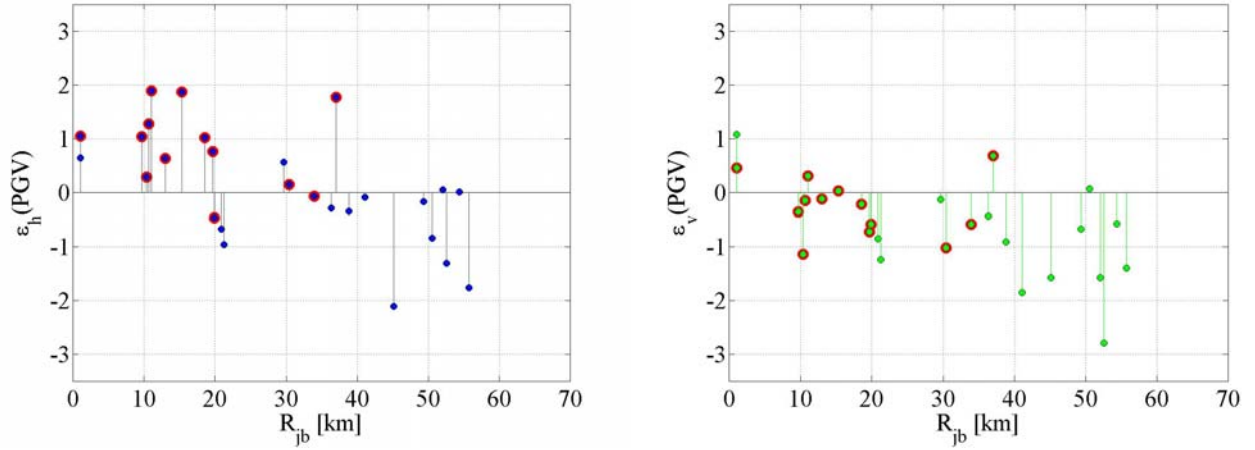


Figure 67. Epsilon values of PGV for geometrical mean of the horizontal components (ε_h) and vertical components (ε_v): left and right, respectively.

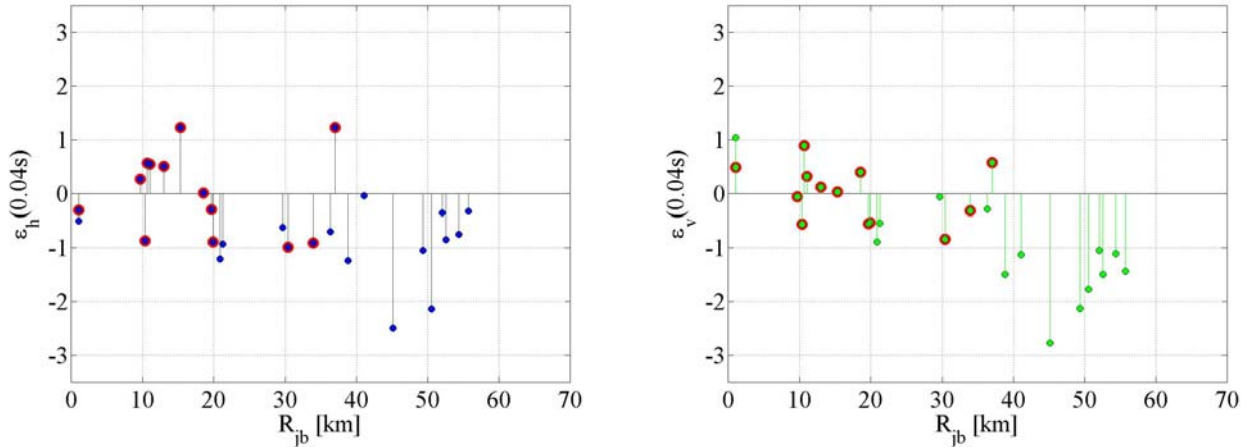


Figure 68. Epsilon values of $Sa(T)$ for geometrical mean of the horizontal components (ϵ_h) and vertical components (ϵ_v): left and right, respectively for T equal to 0.04s.

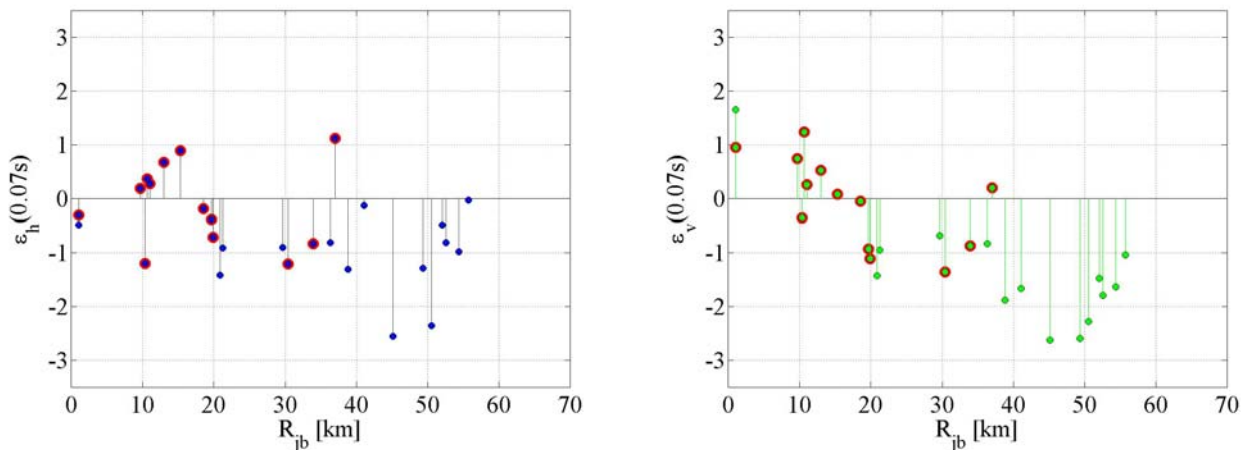


Figure 69. Epsilon values of $Sa(T)$ for geometrical mean of the horizontal components (ϵ_h) and vertical components (ϵ_v): left and right, respectively for T equal to 0.07s.

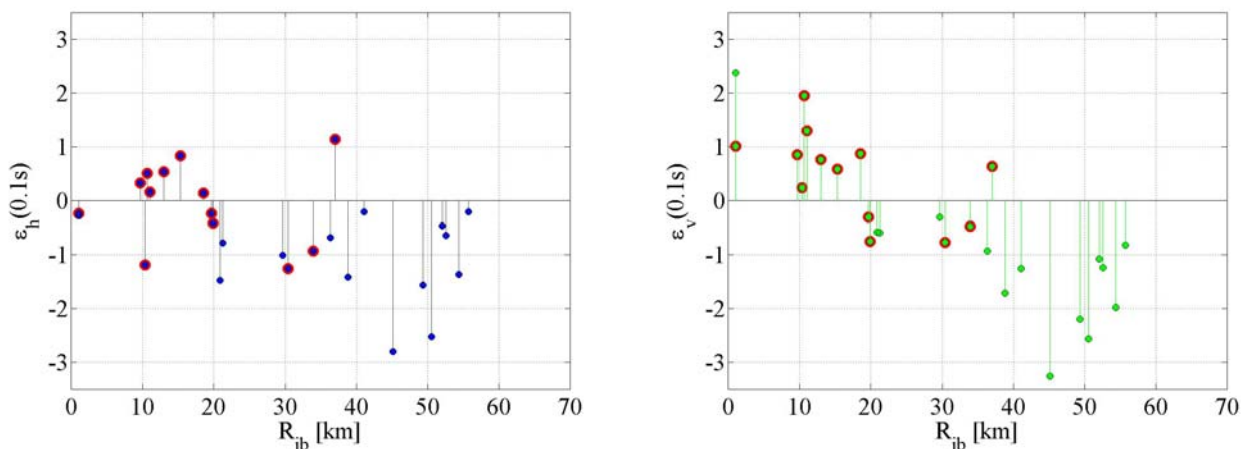


Figure 70. Epsilon values of $Sa(T)$ for geometrical mean of the horizontal components (ϵ_h) and vertical components (ϵ_v): left and right, respectively for T equal to 0.1s.

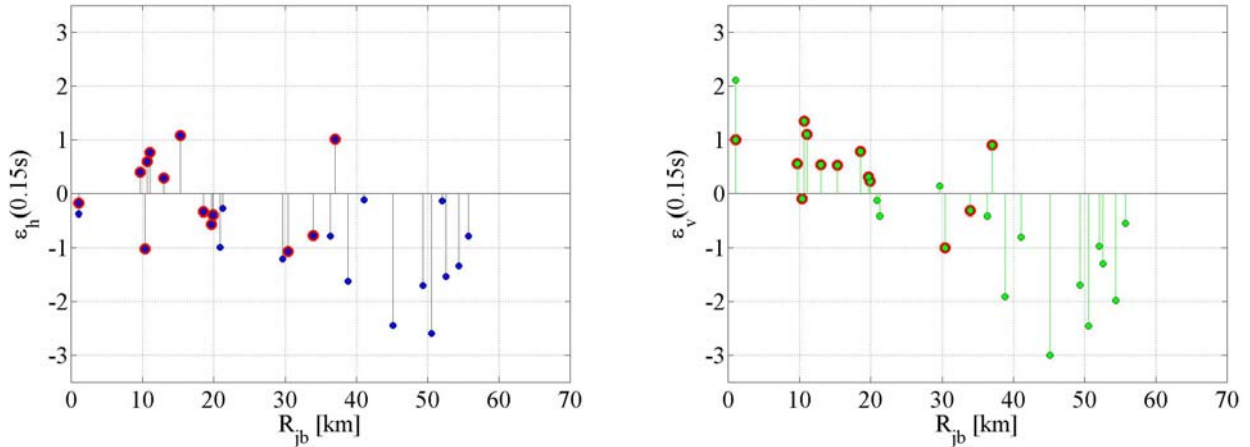


Figure 71. Epsilon values of $Sa(T)$ for geometrical mean of the horizontal components (ϵ_h) and vertical components (ϵ_v): left and right, respectively for T equal to 0.15s.

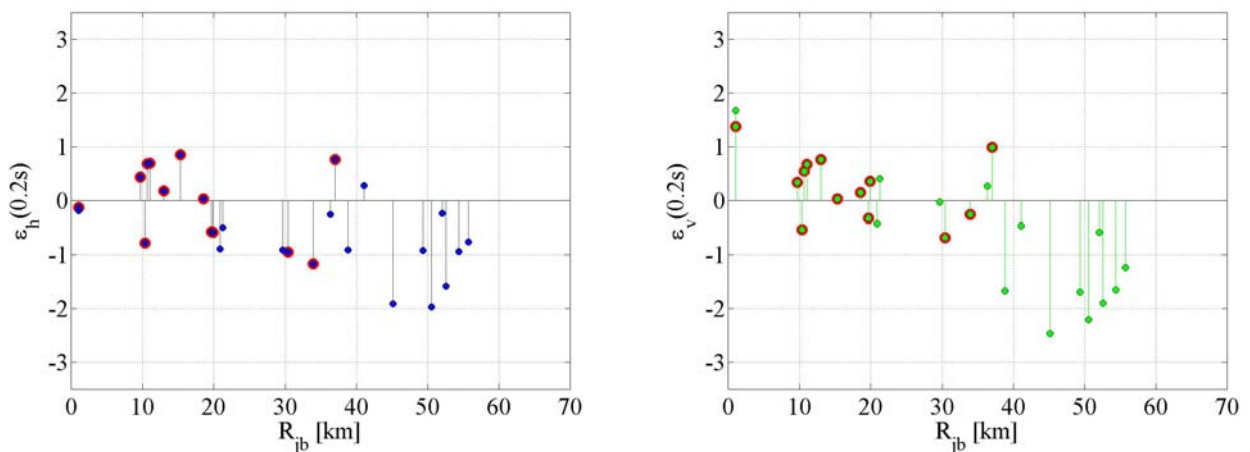


Figure 72. Epsilon values of $Sa(T)$ for geometrical mean of the horizontal components (ϵ_h) and vertical components (ϵ_v): left and right, respectively for T equal to 0.20s.

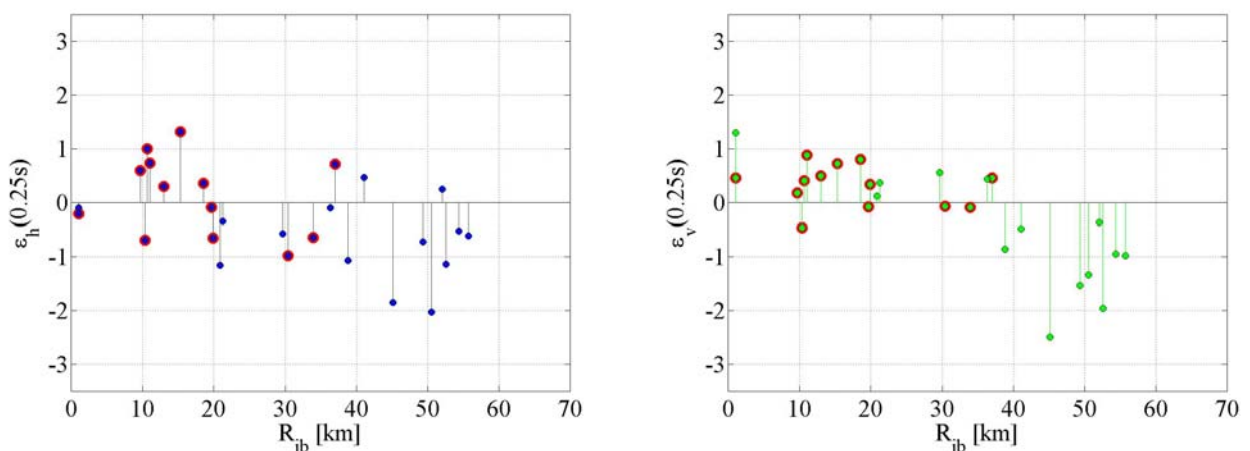


Figure 73. Epsilon values of $Sa(T)$ for geometrical mean of the horizontal components (ϵ_h) and vertical components (ϵ_v): left and right, respectively for T equal to 0.25s.

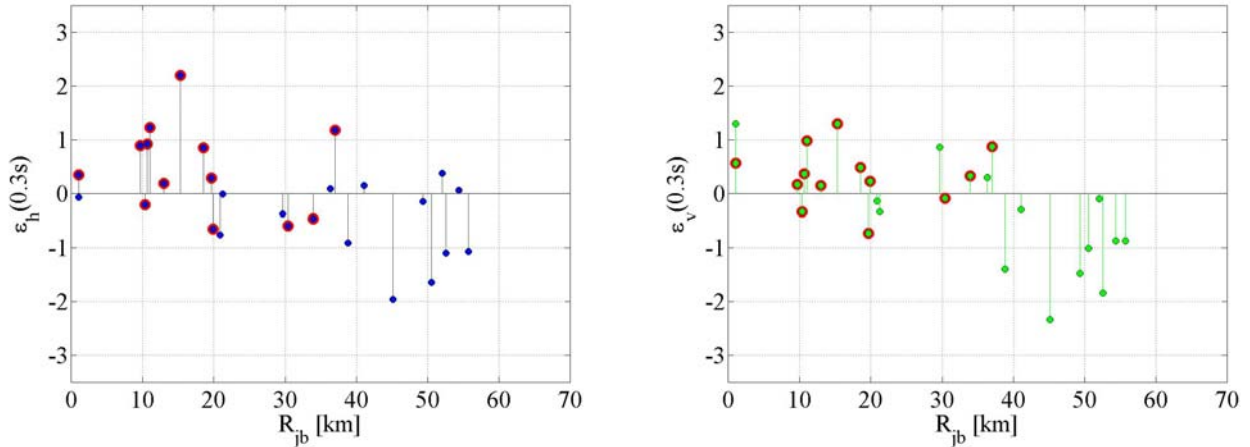


Figure 74. Epsilon values of $Sa(T)$ for geometrical mean of the horizontal components (ε_h) and vertical components (ε_v): left and right, respectively for T equal to 0.30s.

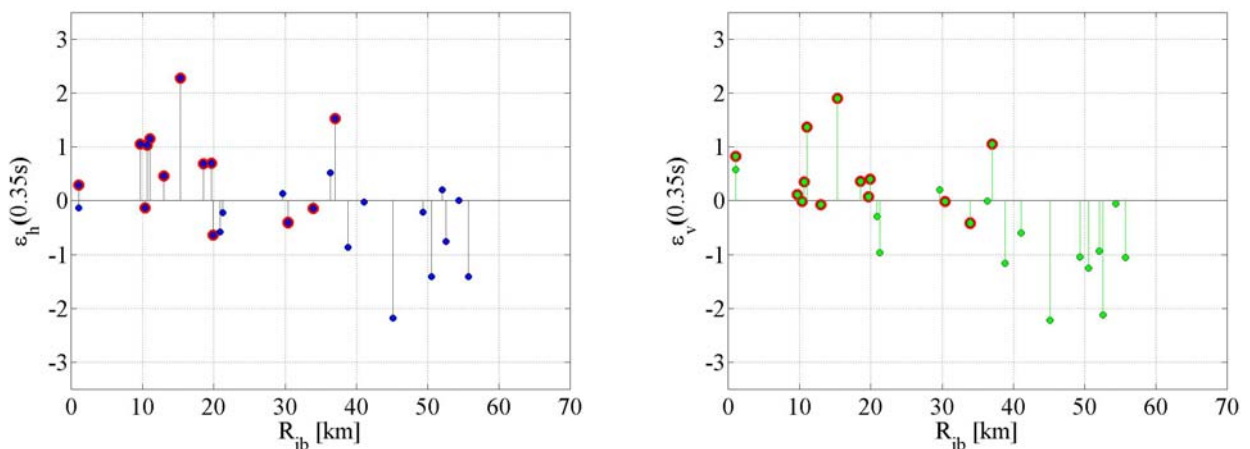


Figure 75. Epsilon values of $Sa(T)$ for geometrical mean of the horizontal components (ε_h) and vertical components (ε_v): left and right, respectively for T equal to 0.35s.

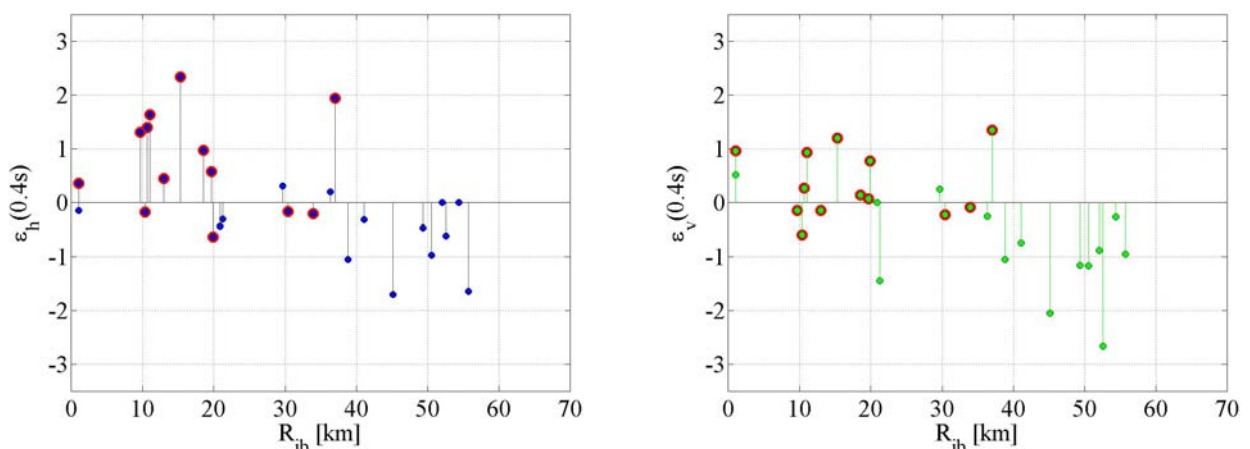


Figure 76. Epsilon values of $Sa(T)$ for geometrical mean of the horizontal components (ε_h) and vertical components (ε_v): left and right, respectively for T equal to 0.40s.

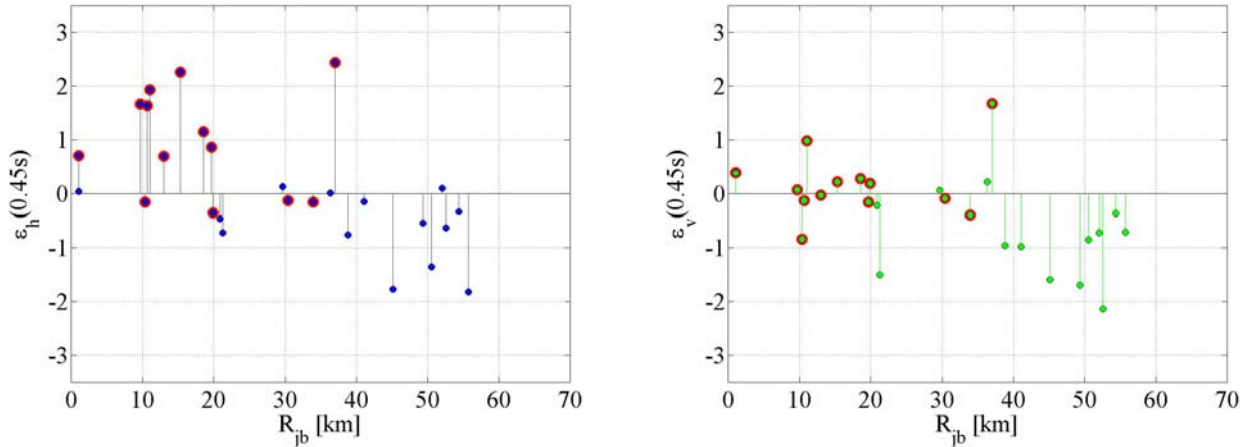


Figure 77. Epsilon values of $Sa(T)$ for geometrical mean of the horizontal components (ϵ_h) and vertical components (ϵ_v): left and right, respectively for T equal to 0.45s.

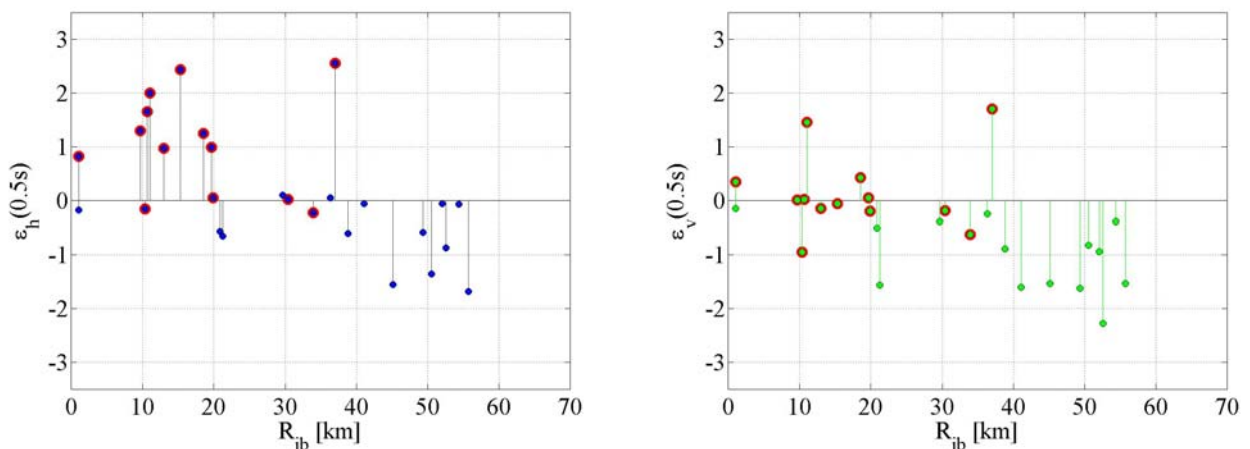


Figure 78. Epsilon values of $Sa(T)$ for geometrical mean of the horizontal components (ϵ_h) and vertical components (ϵ_v): left and right, respectively for T equal to 0.50s.

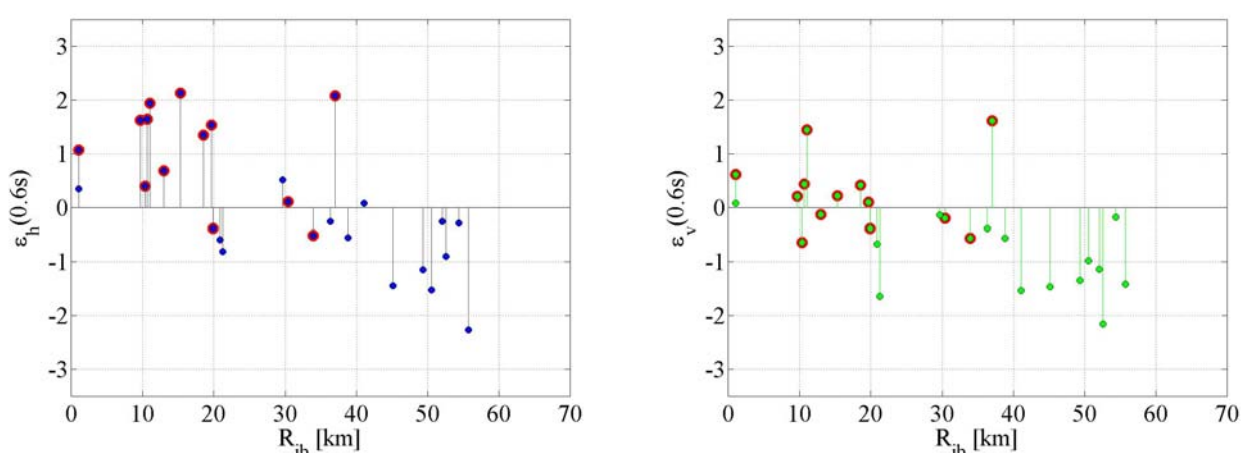


Figure 79. Epsilon values of $Sa(T)$ for geometrical mean of the horizontal components (ϵ_h) and vertical components (ϵ_v): left and right, respectively for T equal to 0.60s.

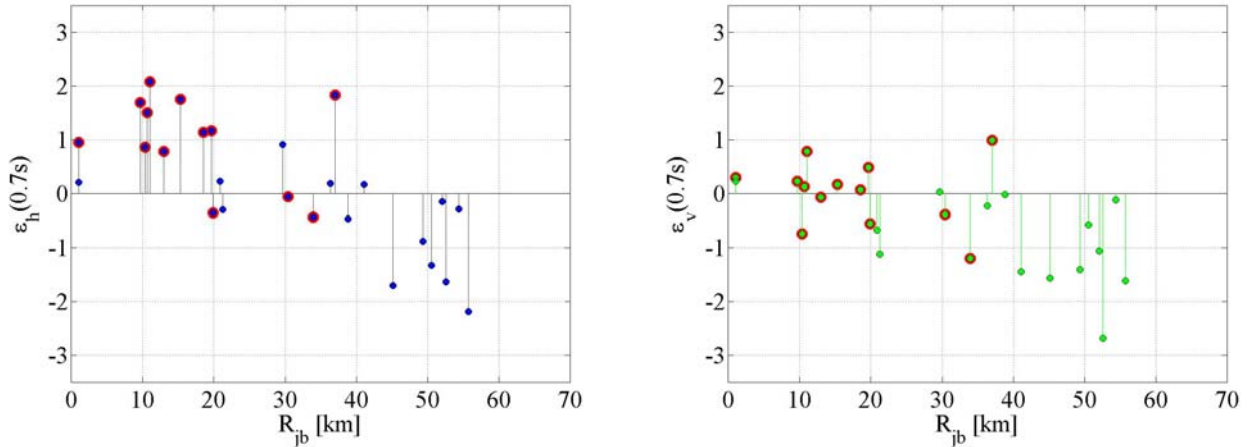


Figure 80. Epsilon values of $Sa(T)$ for geometrical mean of the horizontal components (ε_h) and vertical components (ε_v): left and right, respectively for T equal to 0.70s.

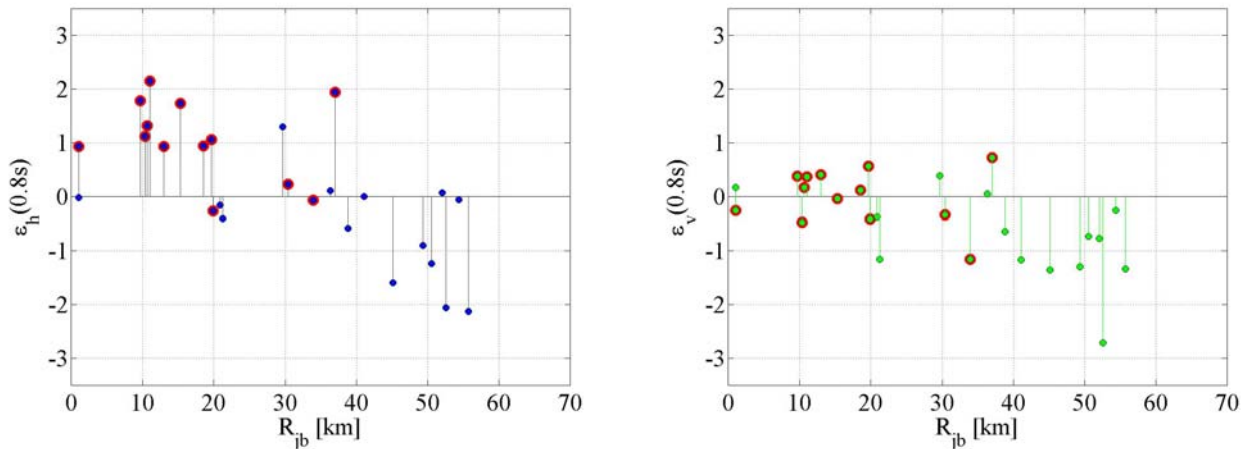


Figure 81. Epsilon values of $Sa(T)$ for geometrical mean of the horizontal components (ε_h) and vertical components (ε_v): left and right, respectively for T equal to 0.80s.

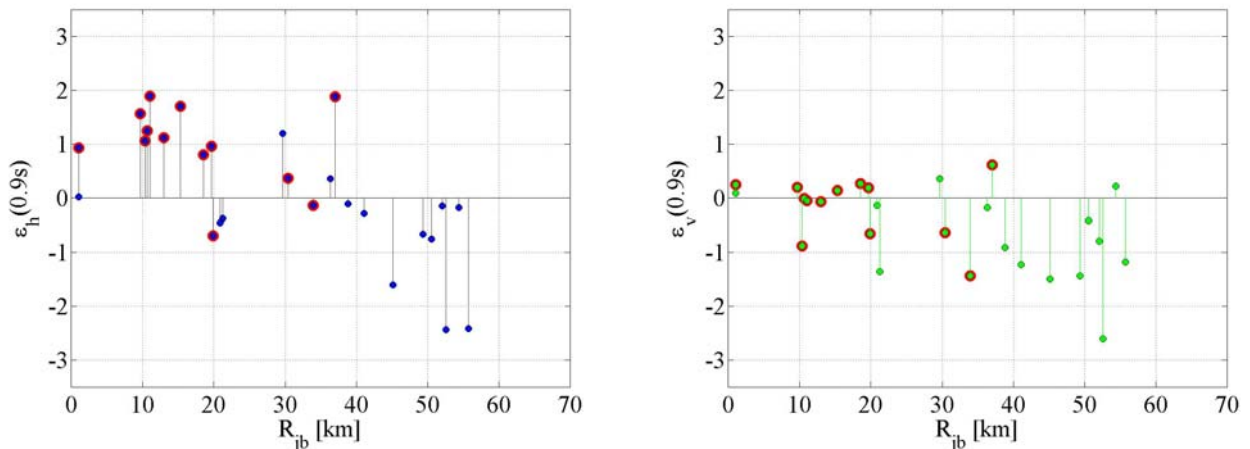


Figure 82. Epsilon values of $Sa(T)$ for geometrical mean of the horizontal components (ε_h) and vertical components (ε_v): left and right, respectively for T equal to 0.90s.

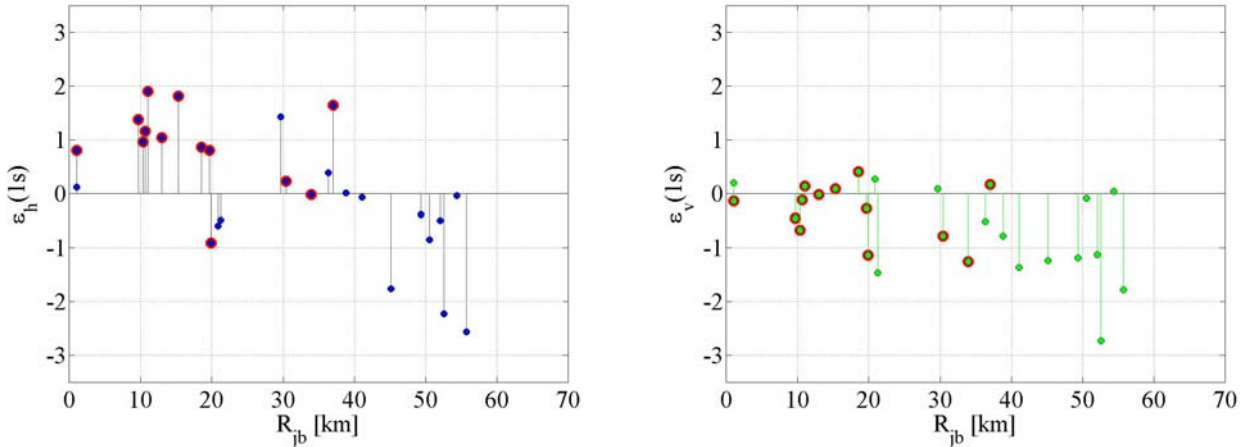


Figure 83. Epsilon values of $Sa(T)$ for geometrical mean of the horizontal components (ε_h) and vertical components (ε_v): left and right, respectively for T equal to 1.00s.

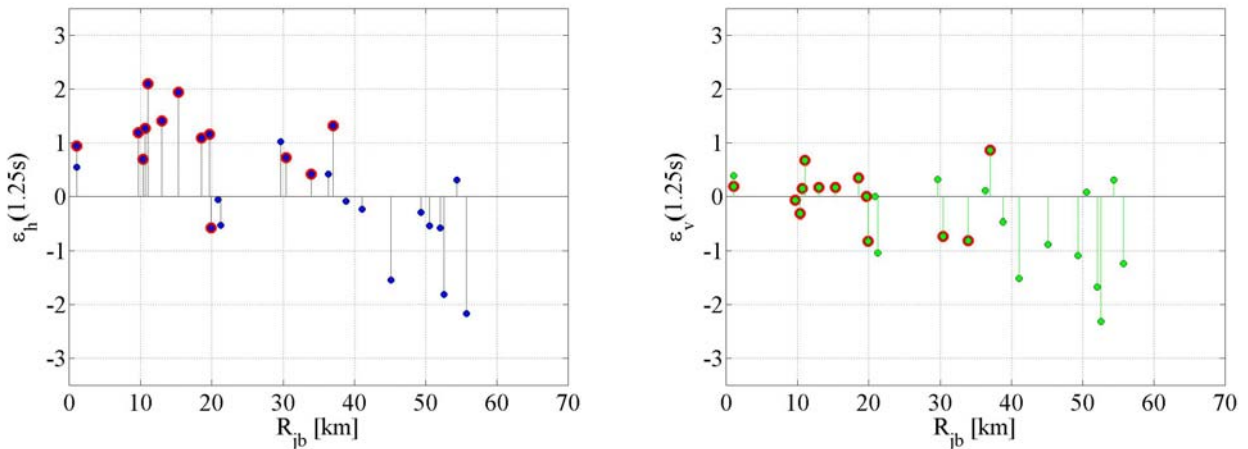


Figure 84. Epsilon values of $Sa(T)$ for geometrical mean of the horizontal components (ε_h) and vertical components (ε_v): left and right, respectively for T equal to 1.25s.

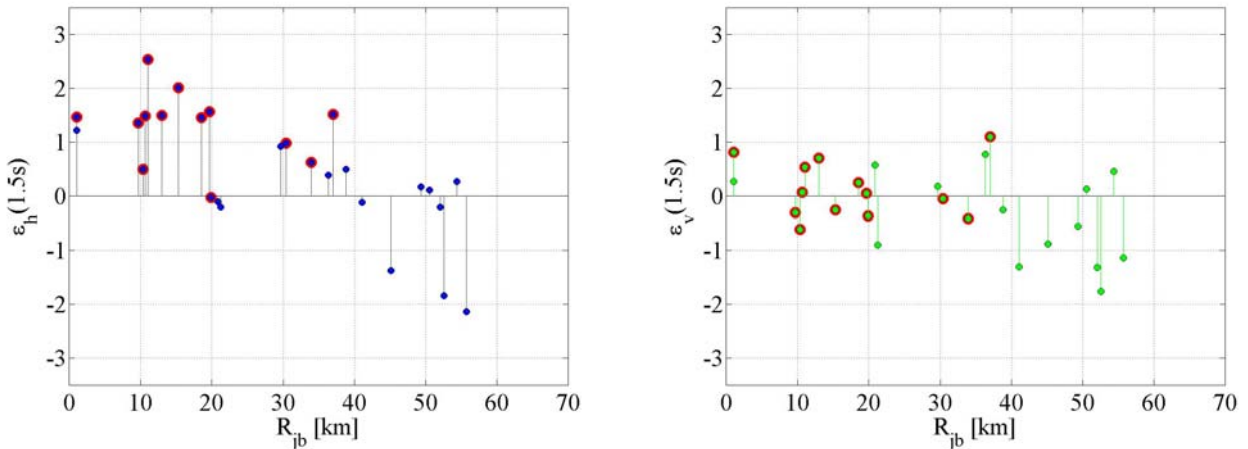


Figure 85. Epsilon values of $Sa(T)$ for geometrical mean of the horizontal components (ε_h) and vertical components (ε_v): left and right, respectively for T equal to 1.50s.

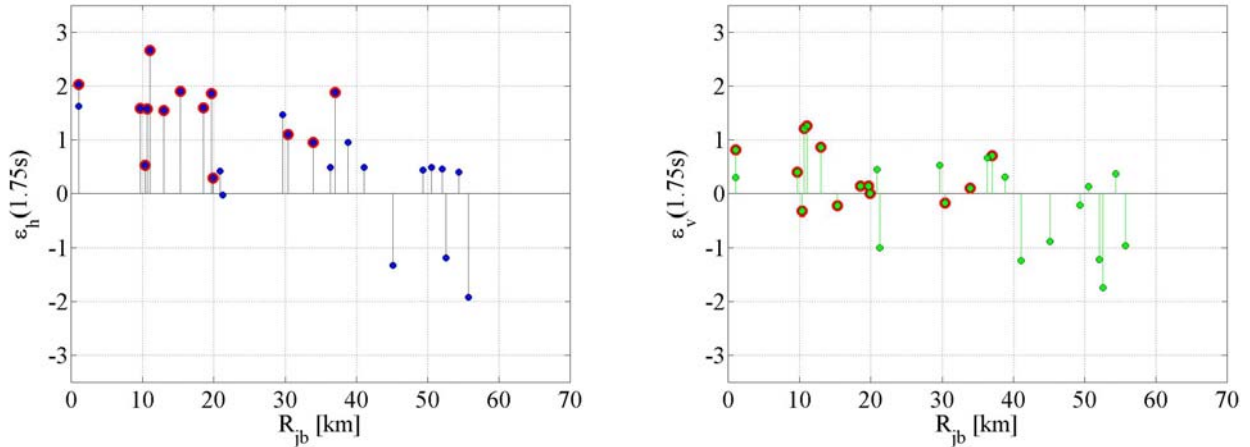


Figure 86. Epsilon values of $Sa(T)$ for geometrical mean of the horizontal components (ε_h) and vertical components (ε_v): left and right, respectively for T equal to 1.75s.

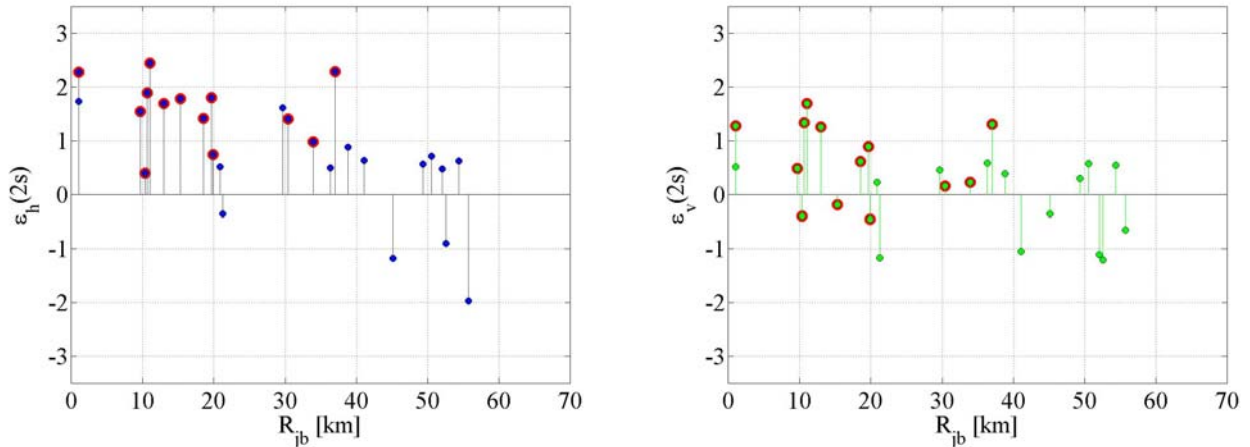


Figure 87. Epsilon values of $Sa(T)$ for geometrical mean of the horizontal components (ε_h) and vertical components (ε_v): left and right, respectively for T equal to 2.00s.

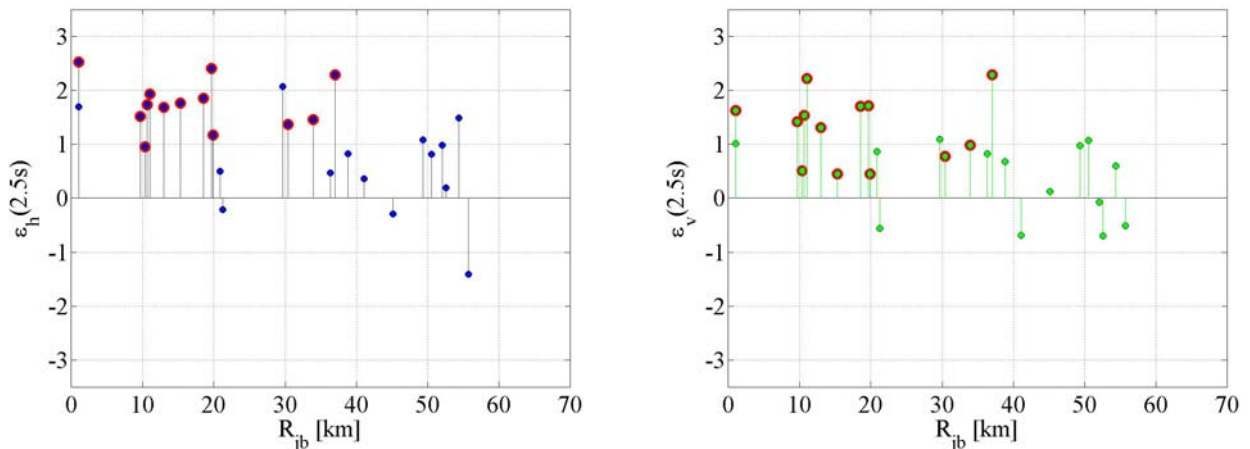


Figure 88. Epsilon values of $Sa(T)$ for geometrical mean of the horizontal components (ε_h) and vertical components (ε_v): left and right, respectively for T equal to 2.50s.

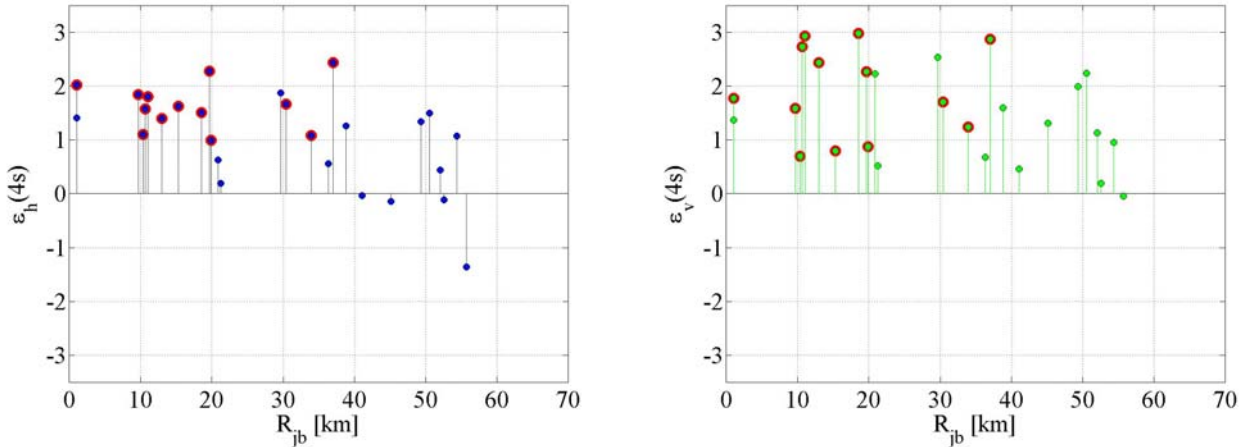


Figure 89. Epsilon values of $Sa(T)$ for geometrical mean of the horizontal components (ε_h) and vertical components (ε_v): left and right, respectively for T equal to 4.00s.

8. Comparison of data with Sabetta and Pugliese (1996) and Iervolino et al. (2010) GMPE predictions, I_A and I_D

The comparison of the registered data with the predictions of GMPEs is made also in term of integral parameters of ground motion. Figure 90 show the comparison of the registered data with the mean predictions and the $\pm\sigma$ error bands of Arias intensity (I_A) and Cosenza and Manfredi index (I_D), respectively.

Both these attenuation relationship are valid within 100km and are computed as function of the epicentral distance (R_{epi}); thus, in this case no distance conversion was necessary. It is worth to note that I_A in Figure 90 is expressed in cm^2/s^3 , so normalized by the constant factor $\pi/2g$ respect to the values in Table A1 to A3, evaluated according to Equation (3) and expressed in cm/s. The GMPE employed for I_A is the one by Sabetta and Pugliese (1996), while for I_D Iervolino et al. (2010a) GMPE was considered. Both the GMPEs considered provide the prediction of the highest horizontal component; so, in this case, the registered data refer to the maximum between the two registered horizontal components shown in Table A2 and A3.

$$I_A = \frac{\pi}{2 \cdot g} \int_0^{t_e} a^2(t) dt \quad (3)$$

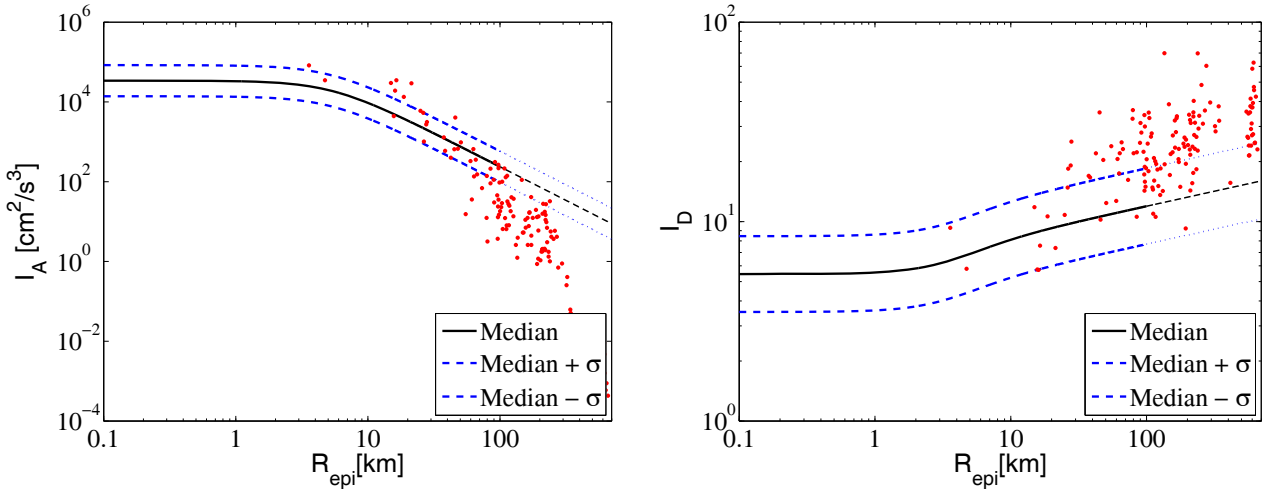


Figure 90. Comparison of the maximum horizontal component of the registered data with the median and $\pm\sigma$ predictions according to Sabetta and Pugliese (1996) and Iervolino et al. (2010a) GMPE predictions in terms of I_A and I_D , respectively.

9. Comparison with Italian hazard data

A preliminary comparison of the closest waveform registered MRN station ($R_{epi} = 3.6$ km) with Italian code prescription (CS. LL. PP., 2008) at the same site is shown in Figure 91. The N-S and E-W spectra at MRN are compared with code spectra computed for both soil classes A and D for two different return periods (Tr) equal to 475 and 2475 years.

For MRN station geographical coordinates, the hazard disaggregation (Iervolino et al, 2011) was computed for the PGA and Sa($T=1$ s) for the two Tr (475 and 2475 years) by means of REXEL v 3.3 (Iervolino et al., 2010b), as shown in Figure 92 and 93. PGA disaggregations shows single modal values for both considered Tr: modal magnitudes and distances range between 4.8 and 5.3, and 0-20km, respectively with slight differences depending on Tr. Conversely Sa($T=1$ s) disaggregation at Tr=475 yr seems to suggest a non negligible hazard contribution of more distant (from 50 to 100 km) and stronger (around 6.3 M) second design earthquake. As usually expected such second modal value contribution decreases increasing considered return period and for Tr=2475yr, a single design earthquake can be identified with about 20 km distance and 5.8 magnitude.

Similarly to the case of MRN station, in the following recorded waveforms are compared with design code spectra¹ for the other twenty-six stations with R_{epi} lower than 70 km (see Table 1).

¹ Lower differences are expected for design spectra in close sites thus for all the considered stations, design spectra are replaced by the spectra computed for Mirandola.

Before drawing conclusions from these comparisons, the following should be noted. A probabilistic hazard map, which is at the basis of the code spectra employed in the figures, hardly can be validated by the occurrence of a single earthquake, mainly for the following reasons.

(1) If the map refers to ground motion, which is exceeded on average every 475 yr, at least 5000 yr of records in each site of the map have to be observed to obtain a reliable statistic (e.g., based on 10 observations) of ground motion the map refers for comparison with the predicted values.

(2) This is the most important reason: the ground motion provided by probabilistic hazard assessment averages ground motions from different sources; it is therefore expected that, when an earthquake occurs, the ground motion at the source (e.g., in the epicenter) location is larger than that from the hazard map.

On the other hand, it seems that earthquake magnitude and location are consistent with the ranges considered by the national hazard assessment (i.e., Stucchi et al., 2011), and ground motion values are in general agreement with GMPEs. Therefore, in the opinion of the authors, this kind of earthquake cannot be claimed as not contemplated by that hazard assessment.

Having specified that the spectral comparison provided cannot be used to validate the official hazard map, it should be noted that recorded spectra do not exceed code spectra² anywhere close to the source, except in the epicentral location where, as discussed above at bullet (2), ground motion is naturally expected to be larger with respect to that predicted by an hazard assessment.

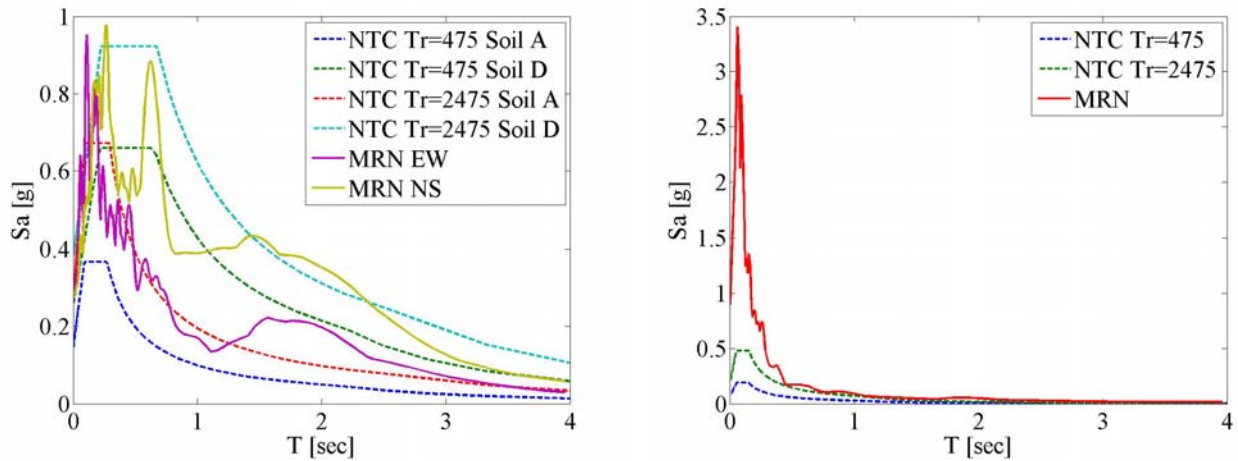


Figure 91. Comparison of the horizontal code spectra for soil classes A and D (on the right) and vertical code spectra (on the left) computed at MRN station (lat 42.87, long 11.06), Mirandola, and the spectra of the waveform registered at MRN station.

² In fact, code spectra are uniform hazard spectra (UHS) basically, and it is known that UHSs are not representative of any specific ground motion spectrum, being in fact, “envelopes” of spectra of ground motions corresponding to all magnitude and source-to-site distances considered as possible in the hazard evaluation.

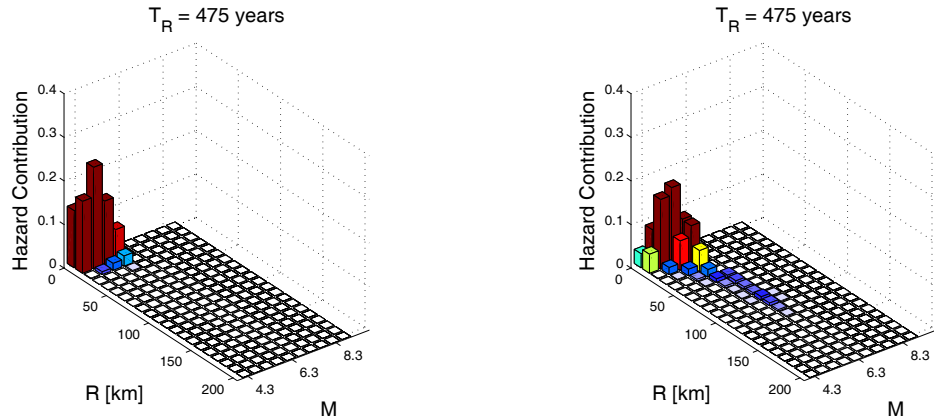


Figure 92. Disaggregation PGA and Sa(1 s) hazard with Tr 475 yr in Mirandola.

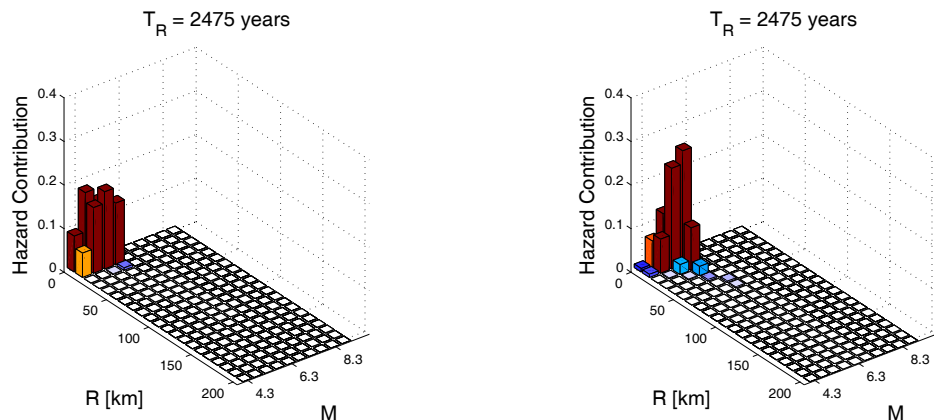


Figure 93. Disaggregation PGA and Sa(1 s) hazard with Tr 2475 yr in Mirandola

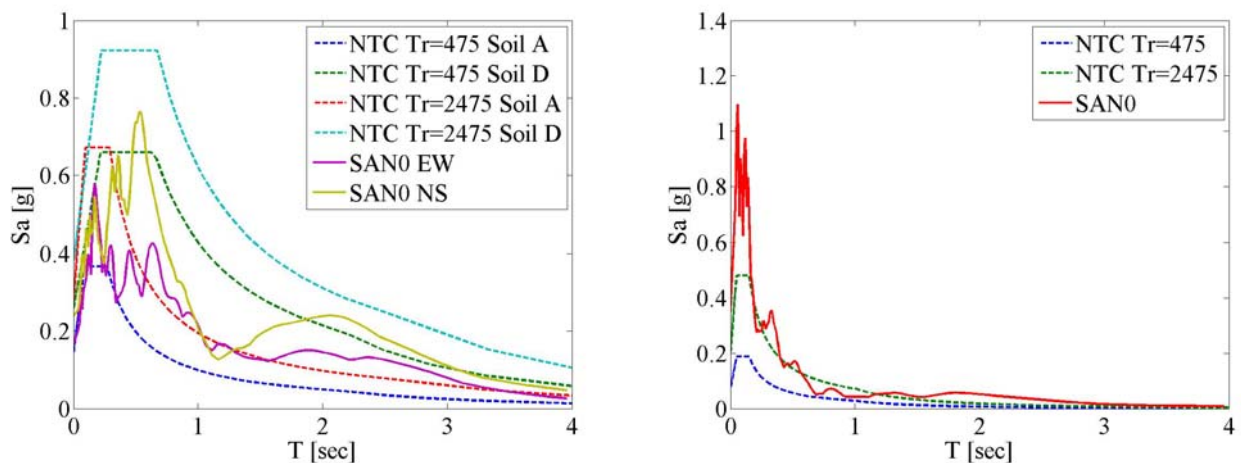


Figure 94. Comparison of the horizontal code spectra for soil classes A and D (on the right) and vertical code spectra (on the left) and the spectra of the waveform registered at SAN0 station.

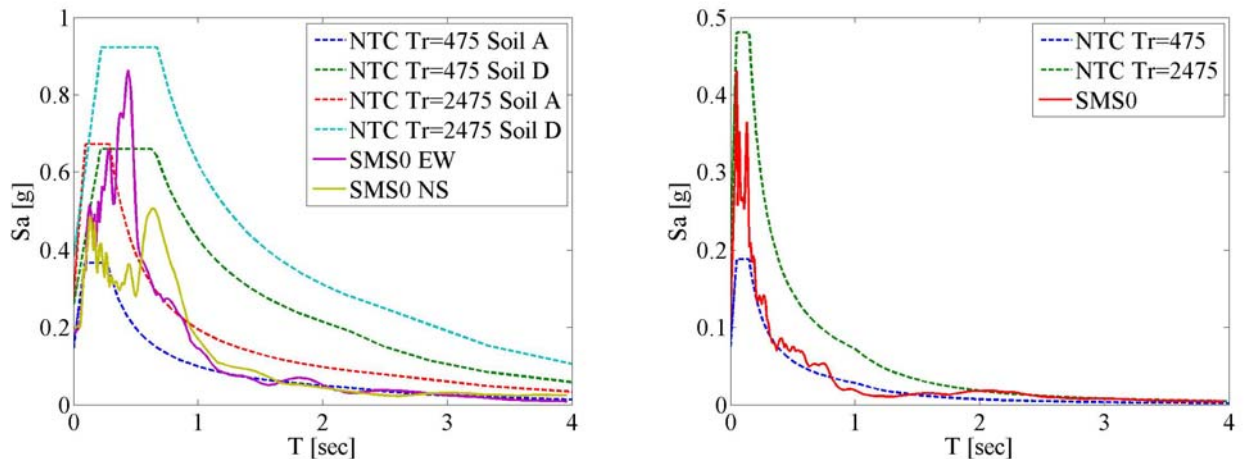


Figure 95. Comparison of the horizontal code spectra for soil classes A and D (on the right) and vertical code spectra (on the left) and the spectra of the waveform registered at SMS0 station.

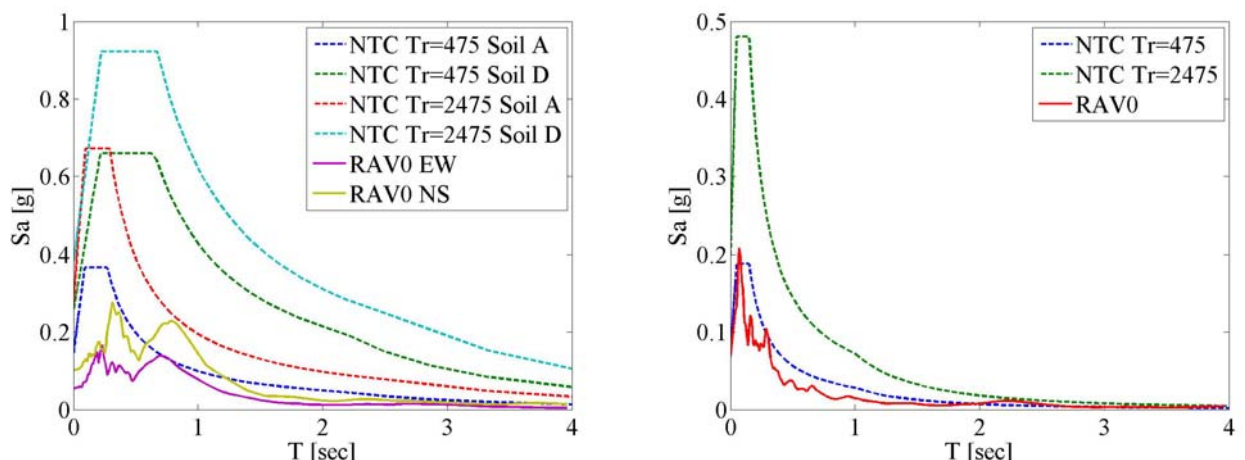


Figure 96. Comparison of the horizontal code spectra for soil classes A and D (on the right) and vertical code spectra (on the left) and the spectra of the waveform registered at RAV0 station.

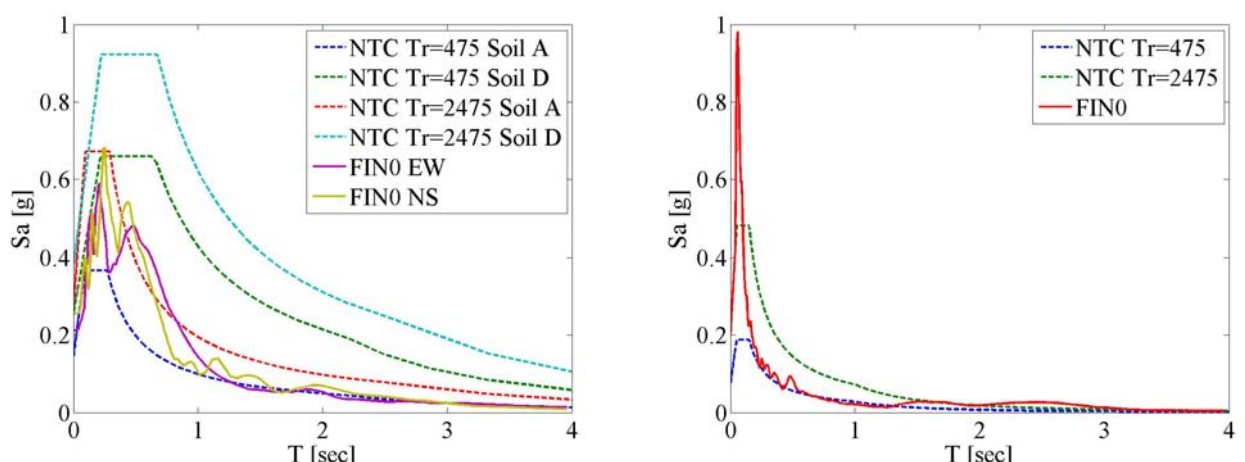


Figure 97. Comparison of the horizontal code spectra for soil classes A and D (on the right) and vertical code spectra (on the left) and the spectra of the waveform registered at FIN0 station.

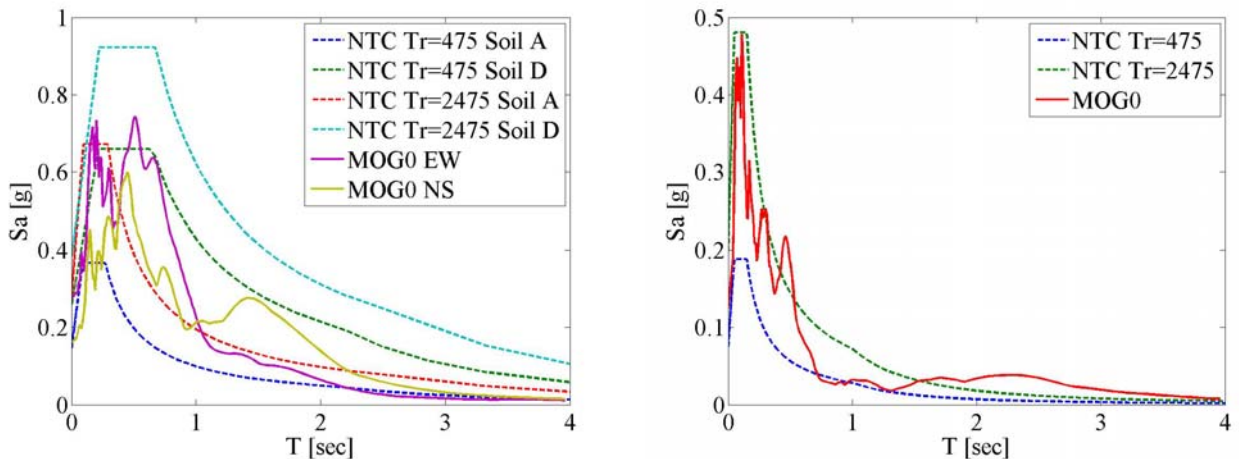


Figure 98. Comparison of the horizontal code spectra for soil classes A and D (on the right) and vertical code spectra (on the left) and the spectra of the waveform registered at MOG0 station.

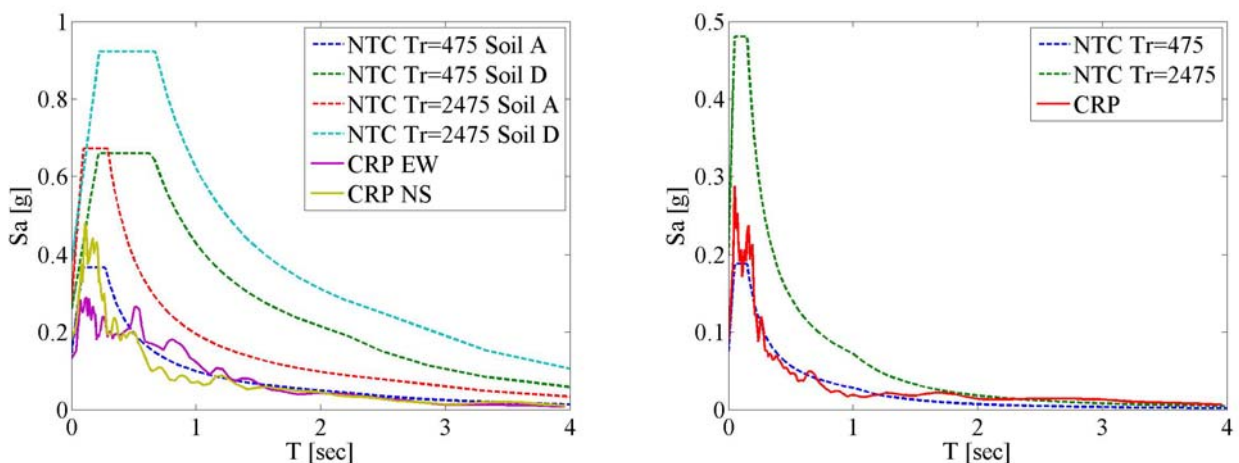


Figure 99. Comparison of the horizontal code spectra for soil classes A and D (on the right) and vertical code spectra (on the left) and the spectra of the waveform registered at CRP station.

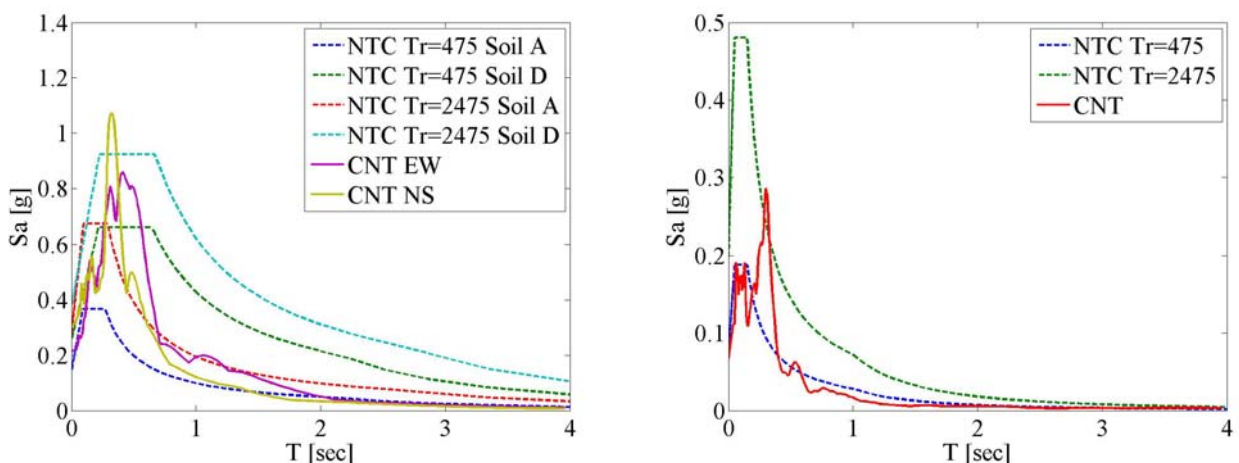


Figure 100 Comparison of the horizontal code spectra for soil classes A and D (on the right) and vertical code spectra (on the left) and the spectra of the waveform registered at CNT station.

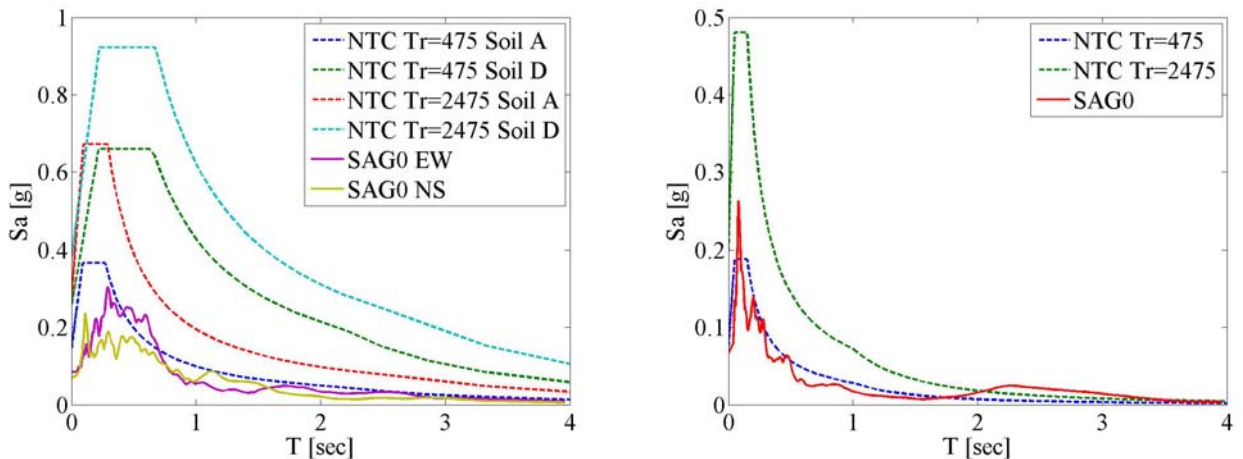


Figure 101 Comparison of the horizontal code spectra for soil classes A and D (on the right) and vertical code spectra (on the left) and the spectra of the waveform registered at SAG0 station.

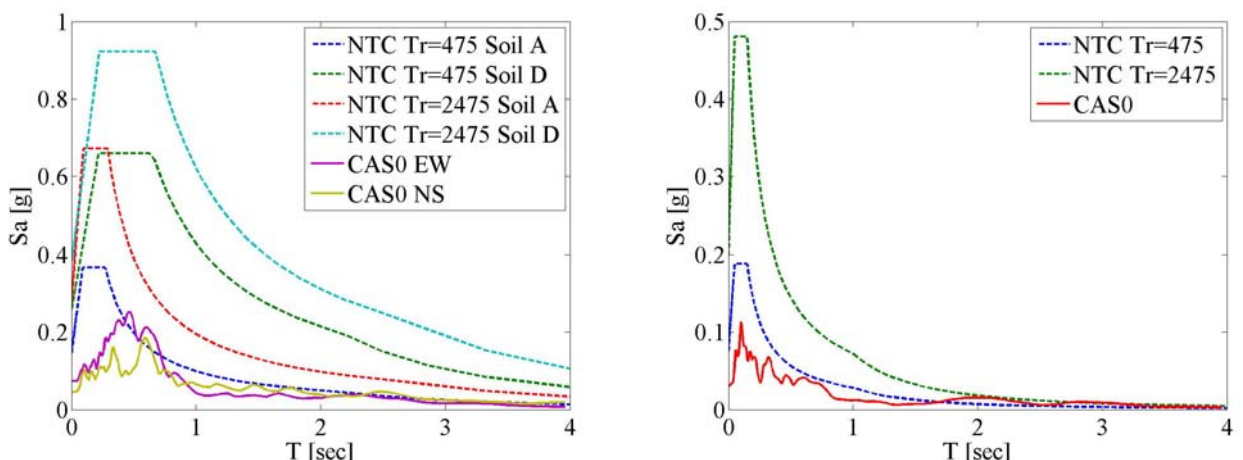


Figure 102 Comparison of the horizontal code spectra for soil classes A and D (on the right) and vertical code spectra (on the left) and the spectra of the waveform registered at CAS0 station.

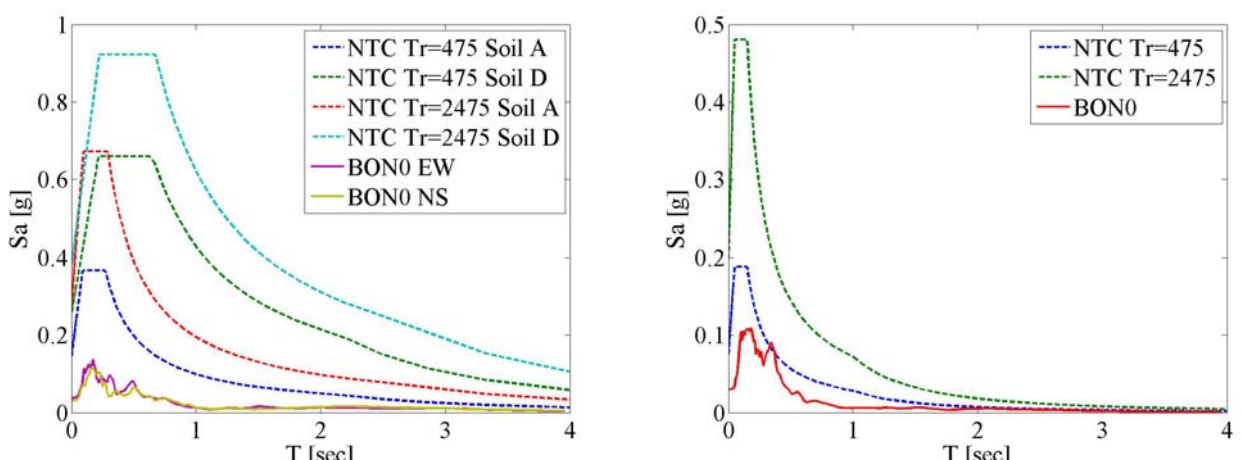


Figure 103 Comparison of the horizontal code spectra for soil classes A and D (on the right) and vertical code spectra (on the left) and the spectra of the waveform registered at BON0 station.

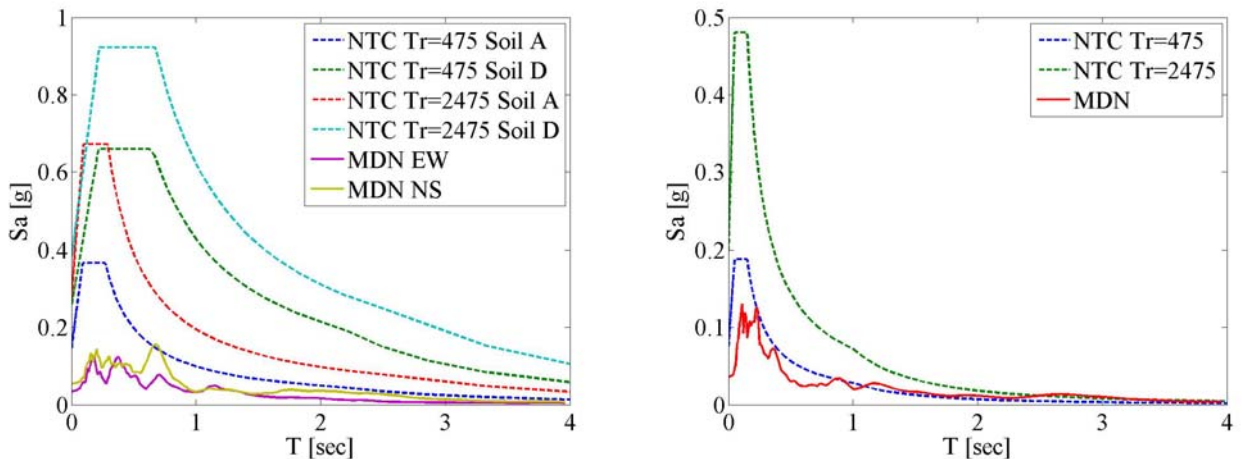


Figure 104 Comparison of the horizontal code spectra for soil classes A and D (on the right) and vertical code spectra (on the left) and the spectra of the waveform registered at MDN station.

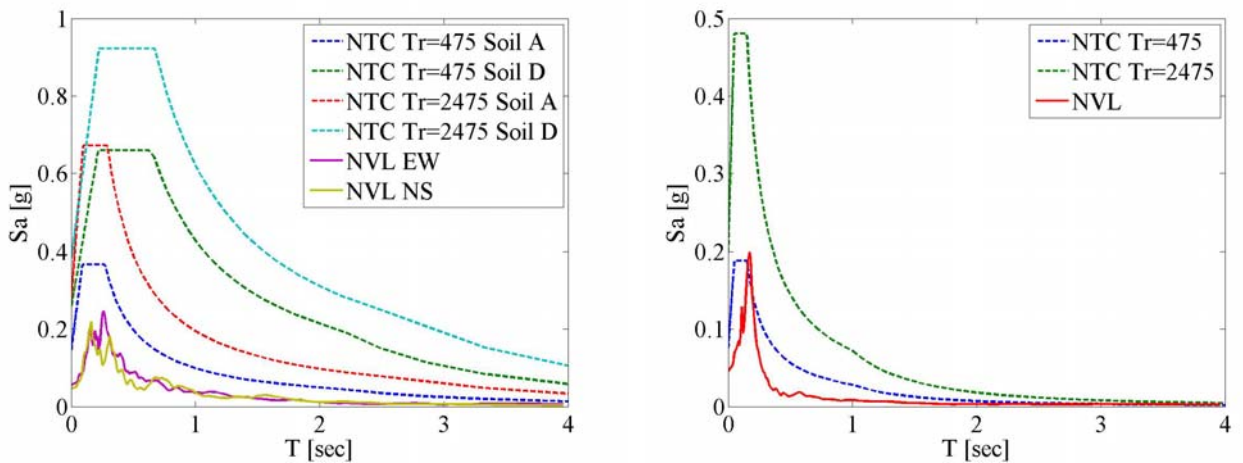


Figure 105 Comparison of the horizontal code spectra for soil classes A and D (on the right) and vertical code spectra (on the left) and the spectra of the waveform registered at NVL station.

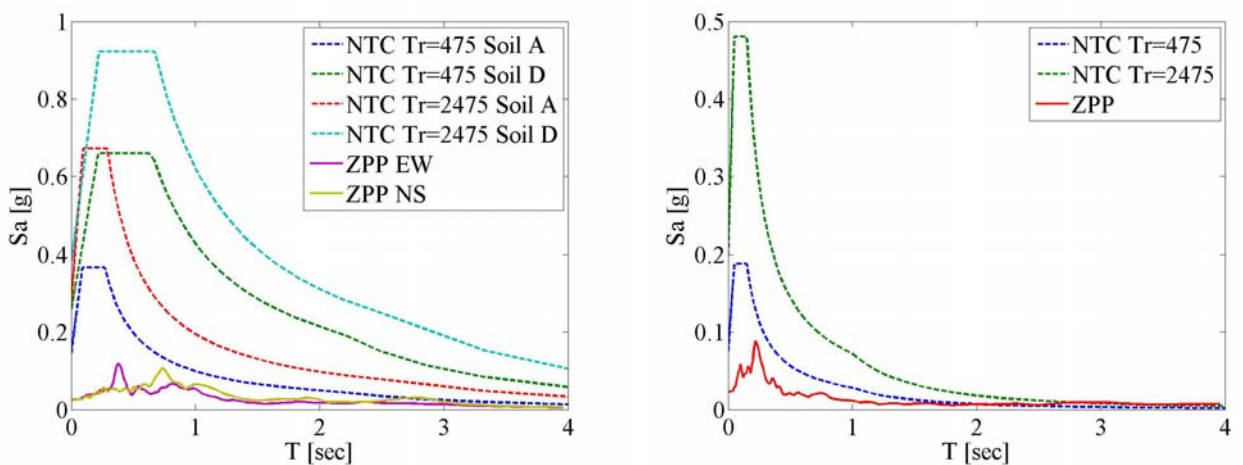


Figure 106 Comparison of the horizontal code spectra for soil classes A and D (on the right) and vertical code spectra (on the left) and the spectra of the waveform registered at ZPP station.

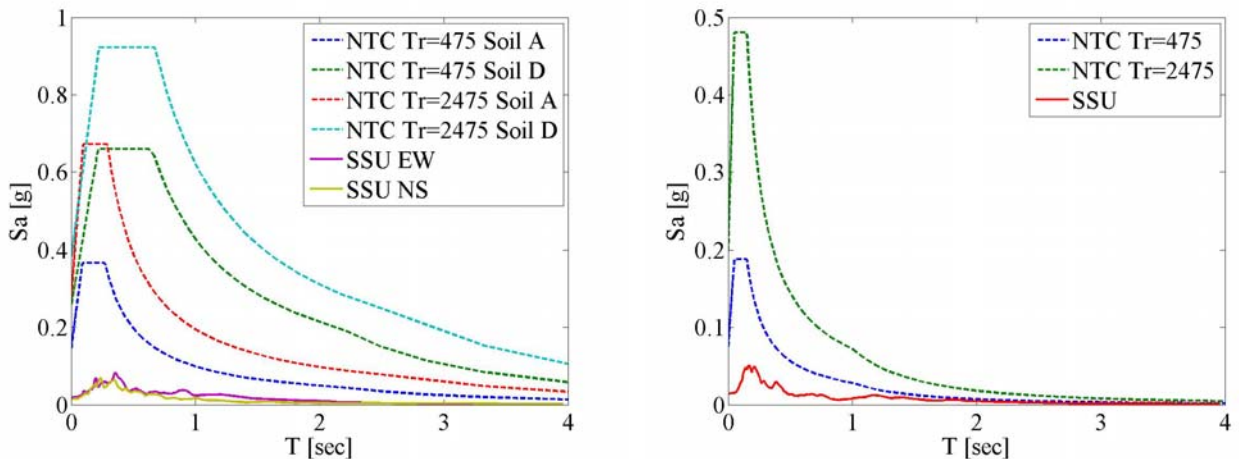


Figure 107 Comparison of the horizontal code spectra for soil classes A and D (on the right) and vertical code spectra (on the left) and the spectra of the waveform registered at SSU station.

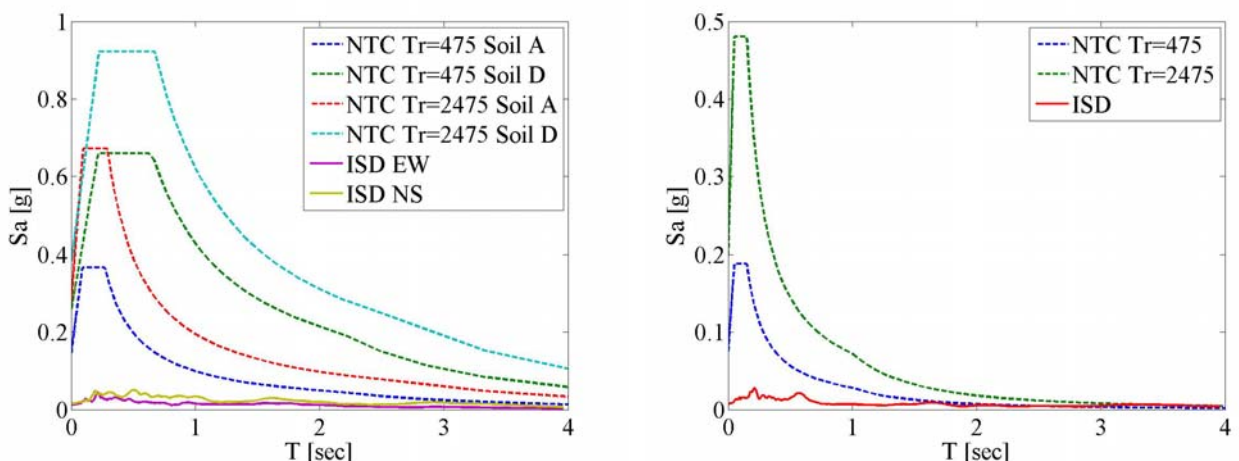


Figure 108 Comparison of the horizontal code spectra for soil classes A and D (on the right) and vertical code spectra (on the left) and the spectra of the waveform registered at ISD station.

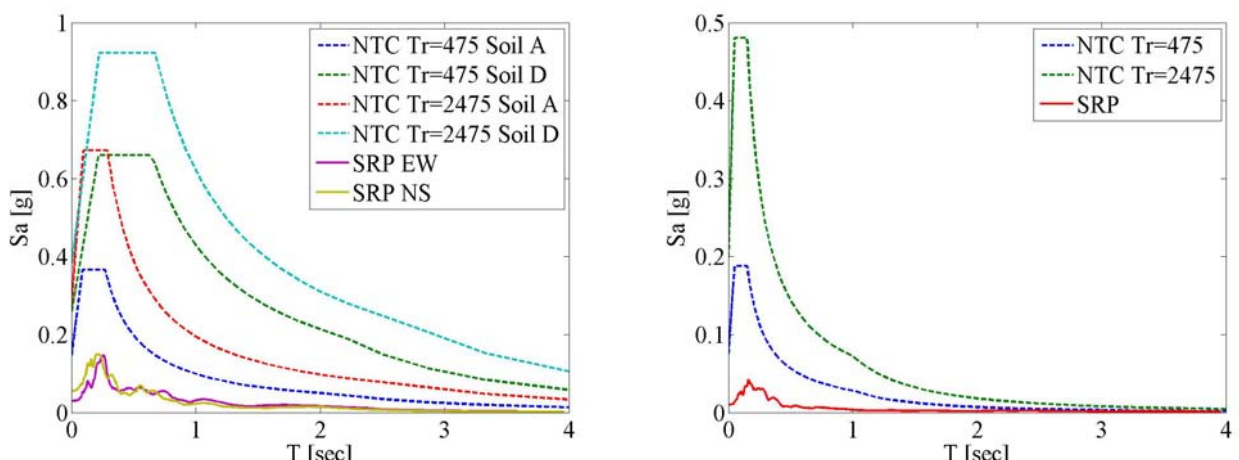


Figure 109 Comparison of the horizontal code spectra for soil classes A and D (on the right) and vertical code spectra (on the left) and the spectra of the waveform registered at SRP station.

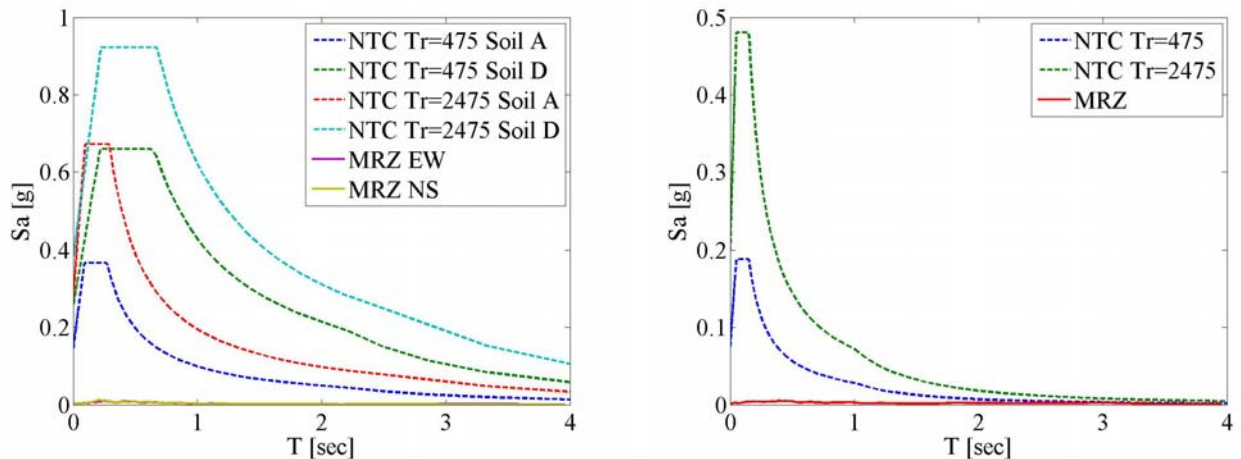


Figure 110 Comparison of the horizontal code spectra for soil classes A and D (on the right) and vertical code spectra (on the left) and the spectra of the waveform registered at MRZ station.

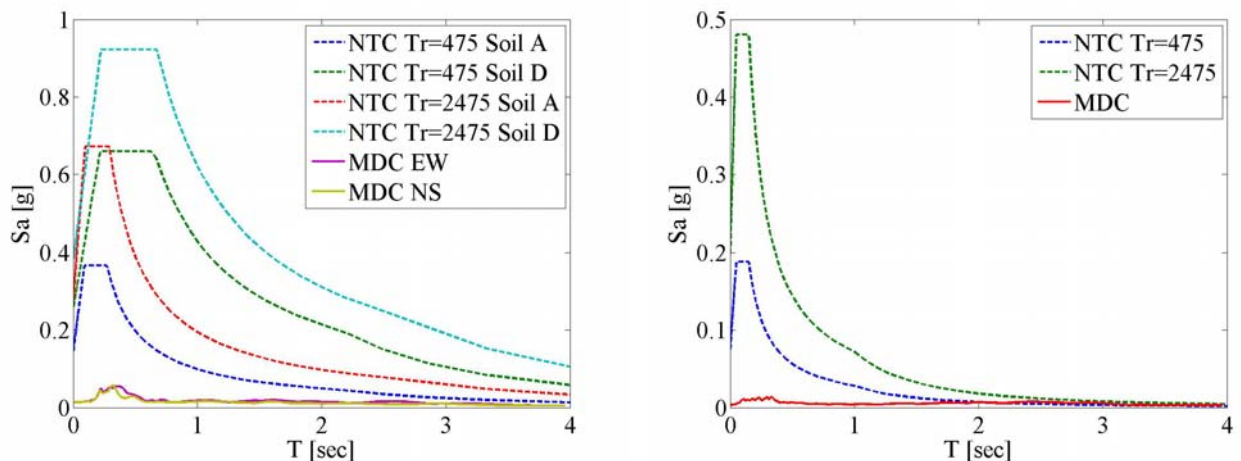


Figure 111 Comparison of the horizontal code spectra for soil classes A and D (on the right) and vertical code spectra (on the left) and the spectra of the waveform registered at MDC station.

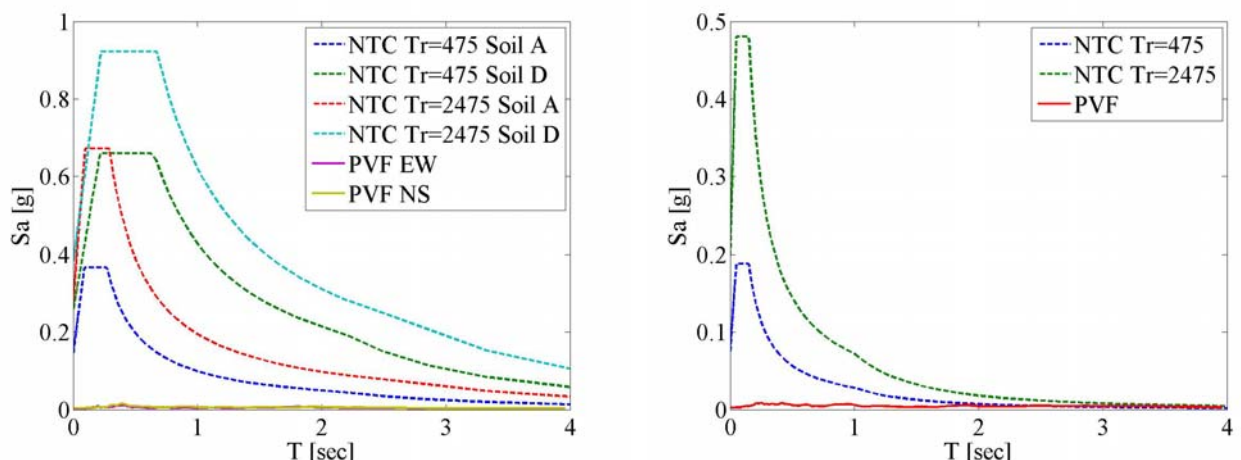


Figure 112 Comparison of the horizontal code spectra for soil classes A and D (on the right) and vertical code spectra (on the left) and the spectra of the waveform registered at PVF station.

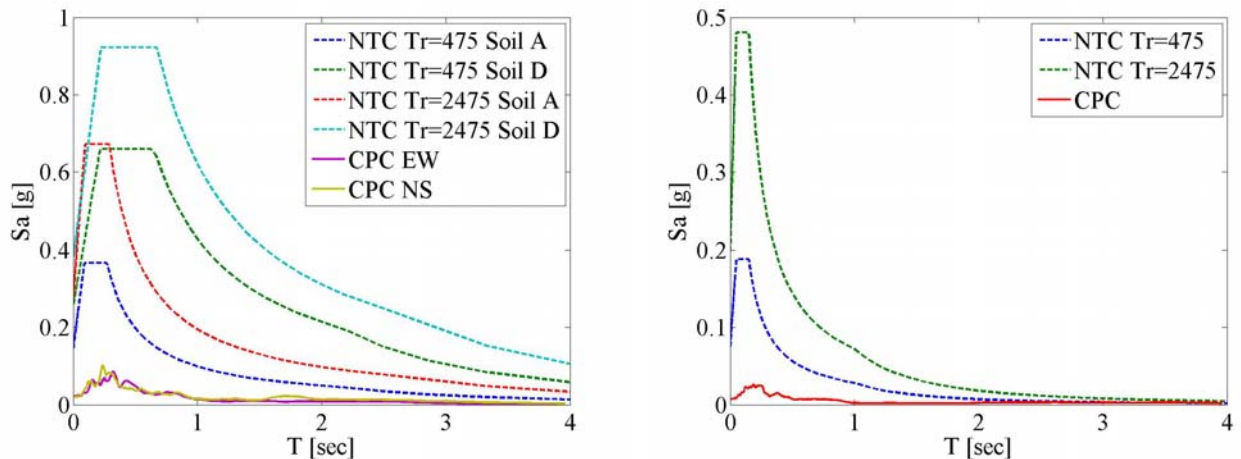


Figure 113 Comparison of the horizontal code spectra for soil classes A and D (on the right) and vertical code spectra (on the left) and the spectra of the waveform registered at CPC station.

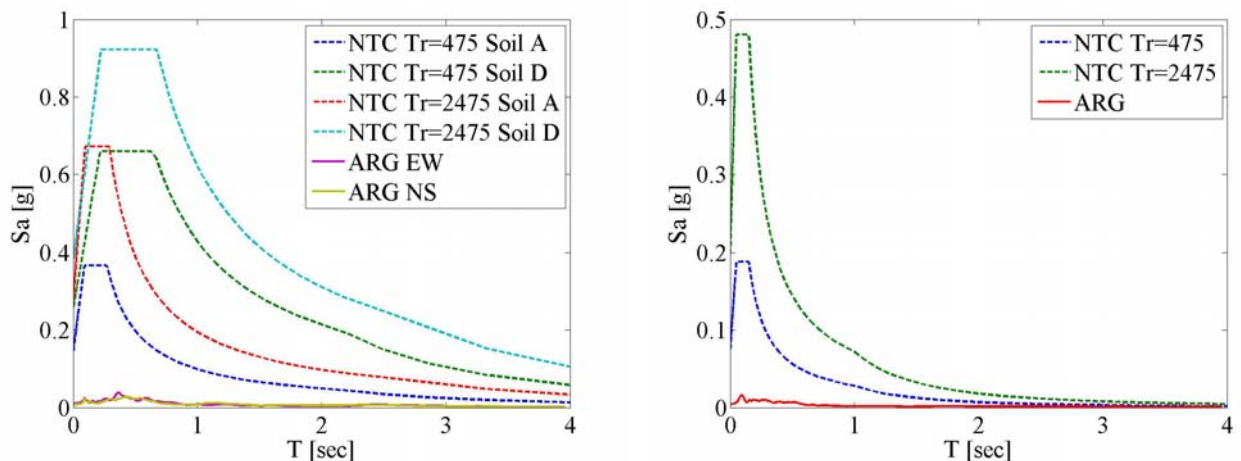


Figure 114. Comparison of the horizontal code spectra for soil classes A and D (on the right) and vertical code spectra (on the left) and the spectra of the waveform registered at ARG station.

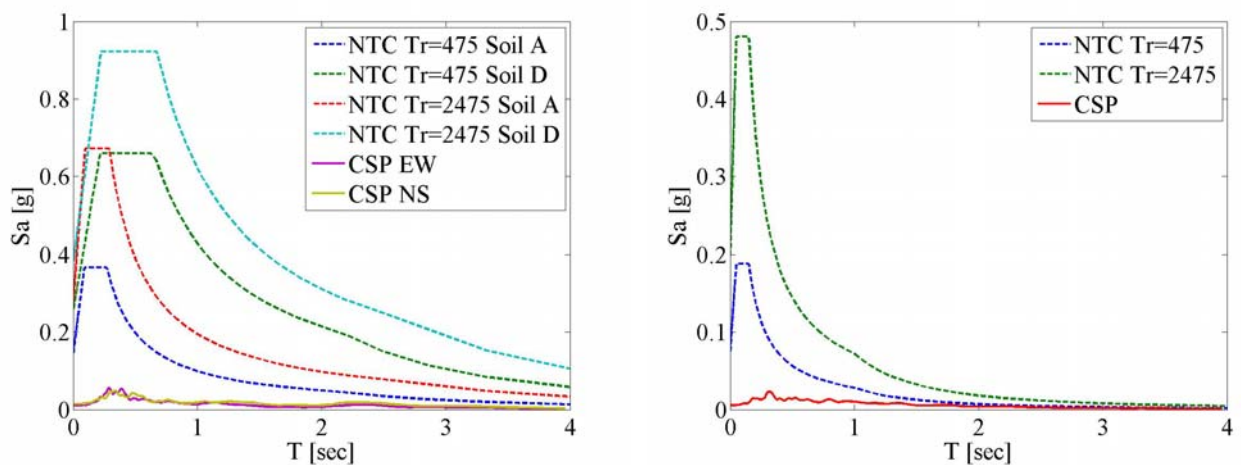


Figure 115 Comparison of the horizontal code spectra for soil classes A and D (on the right) and vertical code spectra (on the left) and the spectra of the waveform registered at CSP station.

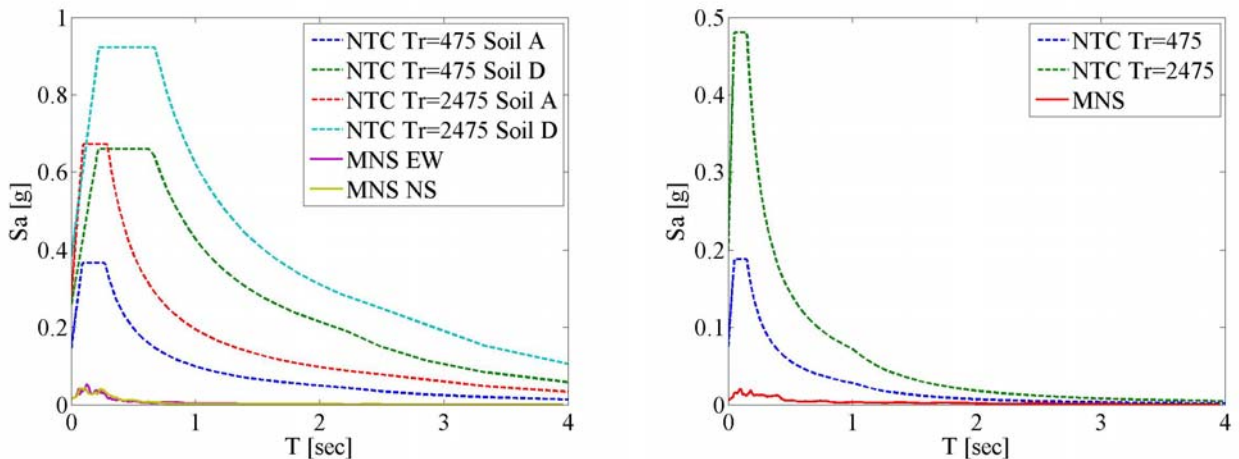


Figure 116 Comparison of the horizontal code spectra for soil classes A and D (on the right) and vertical code spectra (on the left) and the spectra of the waveform registered at MNS station.

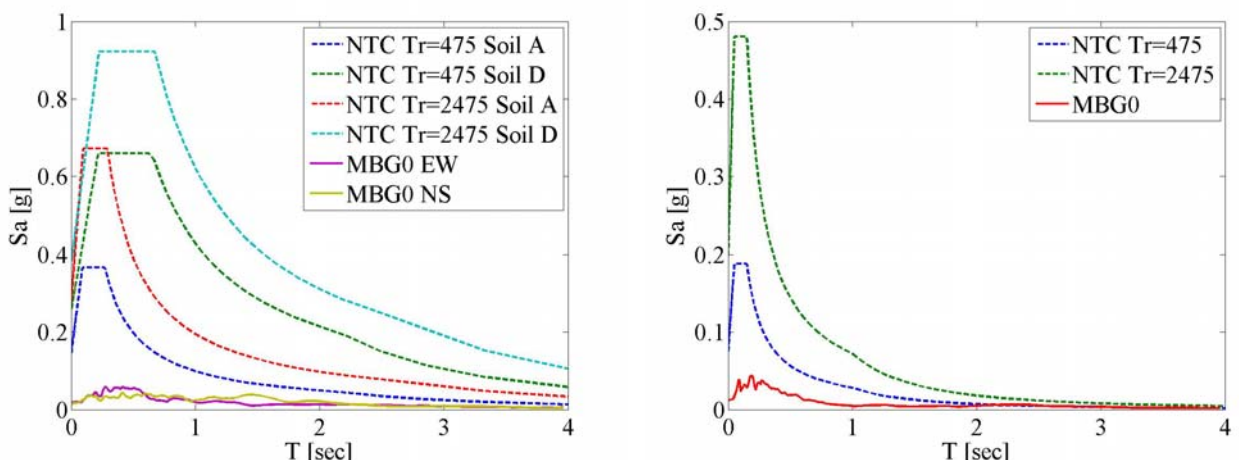


Figure 117 Comparison of the horizontal code spectra for soil classes A and D (on the right) and vertical code spectra (on the left) and the spectra of the waveform registered at MBG0 station.

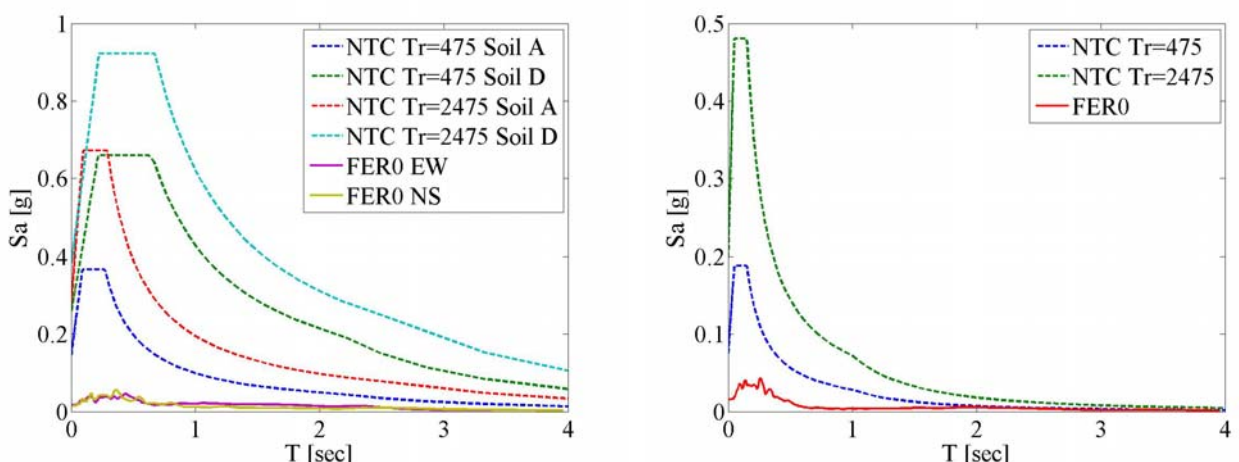


Figure 118 Comparison of the horizontal code spectra for soil classes A and D (on the right) and vertical code spectra (on the left) and the spectra of the waveform registered at FER0 station.

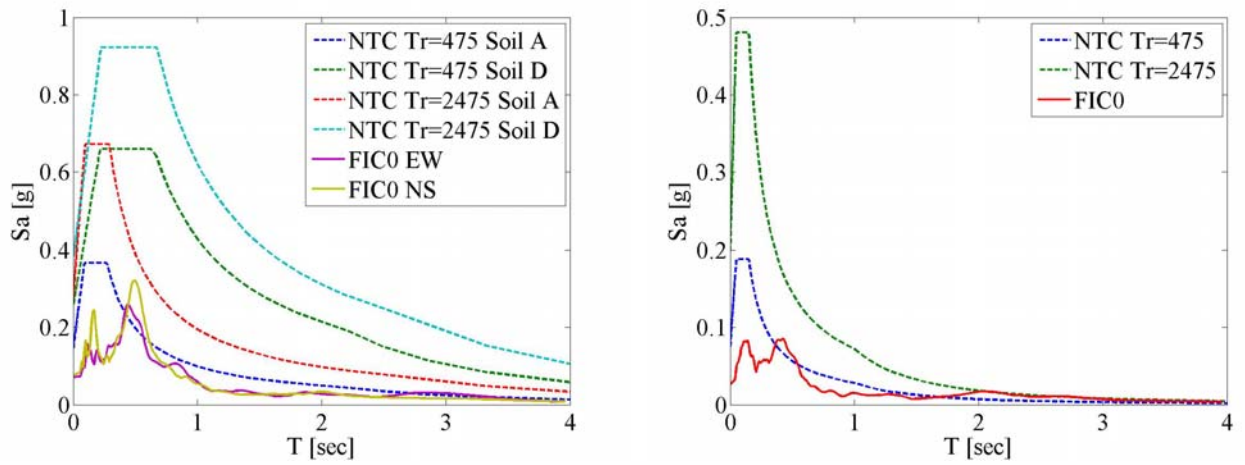


Figure 119 Comparison of the horizontal code spectra for soil classes A and D (on the right) and vertical code spectra (on the left) and the spectra of the waveform registered at FIC0 station.

Appendix

Table A1. Peak and integral parameters estimated on the uncorrected waveforms of the N-S component

Station Name	Comp	R _{epi}	PGA	PGV	PGD	I _A	I _D	Sd	Bd	H ₅₀
		[km]	[cm/s ²]	[cm/s]	[cm]	[cm/s]	[l]	[s]	[s]	[cm]
MRN	N	3.58	267.24	54.18	13.43	132.56	5.72	7.06	81.33	134.78
SAN0	N	4.73	234.05	26.26	8.72	55.72	5.66	6.79	42.37	79.91
SMS0	N	14.95	190.99	12.19	2.60	33.32	8.94	8.52	21.69	43.33
RAV0	N	15.69	100.39	7.63	1.82	7.06	5.75	12.83	27.83	26.05
FIN0	N	16.04	250.59	13.26	2.59	27.62	5.19	9.09	20.29	39.78
MOG0	N	16.43	157.34	21.22	5.10	40.48	7.57	6.56	25.34	77.14
CRP	N	18.69	177.97	7.04	1.32	21.33	10.62	13.13	24.23	23.11
CNT	N	21.34	298.17	14.70	2.38	44.38	6.32	5.77	16.32	37.87
SAG0	N	24.98	67.43	7.66	1.12	6.07	7.34	19.68	38.73	19.29
CAS0	N	26.25	43.80	5.54	1.76	5.76	14.82	19.41	63.56	19.95
BON0	N	26.52	28.92	1.91	0.80	1.63	18.42	19.38	51.07	5.35
MDN	N	27.61	53.53	4.01	0.83	4.38	12.76	31.15	50.43	14.93
NVL	N	28.00	45.35	2.65	0.53	4.84	25.19	15.21	42.24	10.13
ZPP	N	37.52	24.29	3.17	1.16	2.06	16.69	43.23	99.59	12.68
MBG0	N	38.37	15.28	2.29	0.62	0.77	13.81	49.34	108.61	8.90
FER0	N	42.36	14.28	1.27	0.43	0.64	21.99	32.53	84.51	4.12
SSU	N	45.10	14.31	1.01	0.18	0.81	35.27	26.09	68.20	3.69
FIC0	N	45.88	74.33	5.33	1.18	6.48	10.22	13.11	31.08	17.11
ISD	N	47.93	15.19	2.17	0.99	1.08	20.37	48.71	132.44	8.31
SRP	N	50.51	54.07	2.09	0.37	1.40	7.73	24.67	38.16	6.86
MRZ	N	55.03	3.03	0.21	0.12	0.02	23.87	33.23	66.04	0.88
MDC	N	59.79	13.52	1.59	0.47	0.44	12.69	76.38	126.96	4.60
PVF	N	61.17	3.71	0.61	0.30	0.06	15.89	57.66	85.87	2.05
CPC	N	62.90	19.72	1.92	0.55	1.06	17.45	27.08	89.30	6.37
ARG	N	63.48	7.23	0.80	0.24	0.20	22.02	99.55	173.31	2.77
CSP	N	65.55	14.39	2.07	0.64	0.57	11.94	44.76	79.69	5.40
MNS	N	67.04	14.70	0.45	0.08	0.25	23.12	17.16	46.61	1.02
VLM	N	73.06	5.06	0.97	0.31	0.11	14.09	35.42	95.83	3.88
PRT	N	79.03	1.87	0.17	0.06	0.02	32.77	38.22	60.66	0.77
TGG	N	79.39	5.86	0.23	0.11	0.08	36.23	34.97	79.41	0.83
BRM	N	80.27	1.29	0.18	0.07	0.01	14.00	64.26	107.63	0.45
ALF	N	84.60	16.23	1.26	0.35	0.33	9.95	74.67	121.88	3.87
FRE1	N	84.79	7.19	0.53	0.10	0.13	21.11	29.29	62.15	1.90
BRH	N	89.53	8.17	0.52	0.16	0.17	24.83	28.07	69.31	1.81
SMP	N	90.30	3.46	0.39	0.06	0.05	22.61	32.98	71.04	1.23
PTV	N	91.57	8.86	1.25	0.32	0.50	27.95	80.74	196.79	5.91
MDG	N	95.08	5.43	0.35	0.08	0.07	22.36	26.70	64.96	0.95
BSZ	N	96.04	1.33	0.16	0.08	0.01	17.23	33.15	56.70	0.62
PIT	N	96.44	2.42	0.20	0.05	0.02	26.16	34.35	62.34	0.74
MRR	N	96.65	3.64	0.29	0.07	0.02	14.13	32.01	54.06	0.86
GAI	N	97.07	12.57	0.87	0.11	0.28	16.08	18.98	64.68	2.13
PZS	N	97.21	3.43	0.65	0.18	0.06	15.85	22.66	67.15	3.09
SNZ1	N	97.21	8.47	0.72	0.21	0.26	26.39	108.08	205.37	3.23

Station Name	Comp	R _{epi}	PGA	PGV	PGD	I _A	I _D	Sd	Bd	H ₅₀
		[km]	[cm/s ²]	[cm/s]	[cm]	[cm/s]	[]	[s]	[s]	[cm]
CNF	N	98.29	2.92	0.44	0.12	0.02	11.65	32.99	60.61	1.84
MDT	N	99.15	8.28	0.62	0.10	0.15	18.53	29.05	63.46	1.94
BRB	N	100.18	2.58	0.29	0.07	0.02	20.53	33.55	63.98	1.29
FVZ	N	101.96	2.63	0.25	0.05	0.03	24.61	30.28	62.95	0.91
BGL	N	103.41	3.04	0.32	0.04	0.03	16.49	31.79	64.02	1.18
VGL	N	103.77	6.33	0.45	0.05	0.16	35.19	30.25	70.74	1.63
BGN	N	104.87	2.33	0.14	0.04	0.01	19.78	25.41	37.05	0.65
MLC	N	107.96	15.05	0.72	0.13	0.34	19.73	22.28	51.38	2.42
PNM	N	109.06	2.43	0.14	0.03	0.02	27.23	30.25	62.66	0.57
CST	N	110.40	9.01	0.99	0.24	0.16	11.44	29.61	90.06	2.75
PRM	N	111.60	1.72	0.26	0.05	0.01	14.41	43.81	87.04	0.84
DCM	N	112.10	2.53	0.34	0.06	0.01	8.90	26.11	56.22	1.10
MLD	N	113.33	9.58	0.71	0.14	0.23	20.82	27.90	61.28	2.28
AUL	N	113.70	4.94	0.34	0.05	0.04	16.06	21.92	70.29	1.51
CVT	N	115.80	4.09	0.23	0.06	0.03	20.07	32.49	51.01	0.82
RNC	N	116.66	2.81	0.38	0.07	0.01	7.61	18.12	52.67	1.40
RVR	N	117.68	3.30	0.30	0.07	0.03	19.43	78.61	190.60	1.31
STS	N	120.26	3.24	0.40	0.08	0.03	14.23	37.49	101.06	1.37
BDG	N	122.10	5.49	0.49	0.11	0.07	15.08	24.20	75.87	1.82
VRL	N	126.06	3.32	0.22	0.03	0.01	12.11	25.32	58.01	0.75
CES	N	126.76	3.58	0.57	0.19	0.06	16.81	74.00	135.25	1.69
LSP	N	131.86	1.33	0.11	0.03	0.00	14.25	33.80	54.85	0.41
SLS	N	135.23	0.01	0.00	0.00	0.00	69.83	255.77	284.65	0.00
BBN	N	135.98	0.74	0.18	0.07	0.00	18.45	45.76	67.98	0.65
FLP	N	146.20	8.84	0.31	0.04	0.17	38.75	28.98	60.86	0.62
SEL	N	148.69	1.88	0.16	0.03	0.01	17.12	33.00	59.91	0.62
SNM	N	150.68	0.86	0.14	0.09	0.00	21.82	63.46	80.71	0.51
BDT	N	155.58	2.29	0.27	0.05	0.02	18.16	37.19	68.59	0.92
TGL	N	156.27	2.24	0.17	0.02	0.01	17.47	26.67	61.88	0.61
MCR	N	161.40	2.55	0.15	0.03	0.02	32.13	39.12	74.85	0.47
APR	N	162.13	1.60	0.11	0.03	0.00	15.08	40.08	81.84	0.43
BRA	N	164.75	2.75	0.10	0.02	0.01	28.11	34.86	71.57	0.33
SNS	N	166.53	1.81	0.24	0.06	0.02	33.00	44.00	82.25	1.12
CTL	N	167.37	2.46	0.19	0.05	0.02	28.74	57.22	94.74	0.94
POR	N	172.01	3.36	0.56	0.21	0.05	18.11	84.70	145.63	1.87
LEC	N	172.59	1.05	0.10	0.03	0.00	23.14	28.24	60.27	0.47
RNS	N	172.64	1.88	0.13	0.03	0.01	15.71	39.58	60.55	0.50
GNV	N	177.09	2.82	0.20	0.03	0.01	13.23	30.80	66.12	0.67
MOV	N	186.89	4.08	0.21	0.05	0.03	23.25	28.92	68.29	0.77
PSR	N	190.35	2.66	0.22	0.06	0.02	21.95	35.51	66.11	0.66
CLA	N	190.79	0.65	0.06	0.02	0.00	23.69	29.65	50.96	0.20
PTL	N	194.32	0.96	0.13	0.03	0.00	9.24	29.50	36.49	0.40
OVD	N	194.96	2.35	0.24	0.04	0.01	10.51	29.63	67.12	0.82
SPI	N	195.60	2.77	0.19	0.05	0.02	25.77	38.44	74.89	0.63
UMB	N	202.02	0.52	0.09	0.02	0.00	22.26	65.40	285.69	0.26
PRAD	N	205.70	0.82	0.08	0.03	0.00	26.73	47.51	89.78	0.24
GBB	N	208.21	0.89	0.10	0.03	0.00	22.96	64.62	143.15	0.30

Station Name	Comp	R _{epi}	PGA	PGV	PGD	I _A	I _D	Sd	Bd	H ₅₀
		[km]	[cm/s ²]	[cm/s]	[cm]	[cm/s]	[]	[s]	[s]	[cm]
FDS	N	209.03	0.92	0.11	0.03	0.00	15.90	56.87	119.13	0.36
MAJ	N	209.86	2.25	0.32	0.09	0.03	21.62	37.54	72.87	1.21
SAS	N	210.13	1.28	0.14	0.03	0.00	9.64	37.87	61.24	0.52
GBP	N	211.74	2.22	0.53	0.19	0.04	21.42	82.78	155.14	1.61
AVS	N	217.41	0.96	0.14	0.03	0.00	15.58	30.36	52.64	0.42
GEDE	N	218.16	2.64	0.31	0.10	0.03	21.72	53.49	187.78	0.87
GEPF	N	220.50	0.83	0.13	0.05	0.00	17.54	55.16	148.43	0.47
TLM2	N	221.11	1.49	0.11	0.02	0.01	35.30	54.26	119.34	0.33
GESC	N	221.12	2.44	0.19	0.04	0.02	28.26	48.86	99.90	0.67
CESC	N	222.66	1.48	0.08	0.02	0.01	40.26	51.22	97.47	0.30
CVF	N	224.22	2.18	0.14	0.02	0.01	27.16	26.70	57.66	0.50
VINO	N	226.75	1.49	0.20	0.07	0.01	23.18	49.35	160.58	0.67
DST2	N	227.09	1.08	0.12	0.05	0.00	20.18	43.61	134.78	0.32
SDV	N	232.87	0.73	0.10	0.04	0.00	16.36	44.98	121.39	0.26
MOGG	N	233.13	0.70	0.07	0.02	0.00	26.57	54.93	116.11	0.27
RST	N	238.37	0.63	0.05	0.02	0.00	22.70	51.86	88.90	0.19
STOL	N	238.45	3.43	0.14	0.02	0.05	69.73	47.95	97.09	0.33
DRN	N	241.68	1.29	0.10	0.02	0.01	29.27	38.37	69.98	0.41
AUP	N	244.42	1.21	0.10	0.03	0.00	21.78	44.67	66.91	0.40
CLF	N	253.91	0.73	0.10	0.03	0.01	48.39	90.61	192.86	0.47
MCT	N	260.32	1.02	0.19	0.07	0.01	30.57	54.66	75.98	0.67
TNS	N	269.15	1.23	0.17	0.04	0.01	18.82	44.82	77.57	0.55
SPM	N	275.58	0.32	0.04	0.01	0.00	41.11	99.79	226.51	0.13
RQT	N	294.57	0.54	0.04	0.01	0.00	39.56	77.13	160.61	0.16
PCB	N	319.13	0.23	0.04	0.02	0.00	28.53	117.21	239.57	0.13
MSC	N	322.65	0.27	0.05	0.02	0.00	28.33	133.56	244.03	0.16
PLS	N	340.12	0.06	0.02	0.01	0.00	37.81	175.35	436.05	0.05
SPD	N	342.51	0.13	0.01	0.00	0.00	32.03	30.90	39.14	0.05
CDM	N	414.49	0.08	0.01	0.00	0.00	11.92	34.49	39.74	0.02
MND	N	543.83	0.03	0.00	0.00	0.00	35.58	34.60	67.92	0.00
SSB3	N	552.94	0.02	0.00	0.00	0.00	18.99	34.89	54.73	0.01
RSF3	N	560.40	0.02	0.00	0.00	0.00	26.29	39.06	55.46	0.01
MNT3	N	563.27	0.03	0.00	0.00	0.00	34.83	39.24	56.79	0.01
LIO3	N	566.77	0.01	0.00	0.00	0.00	16.24	40.08	55.94	0.01
NSC3	N	568.32	0.03	0.00	0.00	0.00	24.08	37.90	56.65	0.01
AND3	N	571.93	0.03	0.00	0.00	0.00	21.49	39.72	56.29	0.01
CLT3	N	578.20	0.18	0.01	0.00	0.00	22.27	29.27	54.54	0.02
SNR3	N	582.22	0.03	0.00	0.00	0.00	37.88	40.37	56.69	0.01
CMP3	N	584.26	0.04	0.00	0.00	0.00	38.83	42.41	59.34	0.01
RDM3	N	587.86	0.06	0.00	0.00	0.00	29.13	40.49	49.09	0.02
CSG3	N	589.03	0.02	0.00	0.00	0.00	24.05	42.77	58.24	0.01
COL3	N	593.87	0.03	0.00	0.00	0.00	31.06	42.53	59.20	0.01
VDS3	N	594.07	0.04	0.00	0.00	0.00	37.44	41.27	58.10	0.01
SFL3	N	597.90	0.03	0.00	0.00	0.00	21.66	44.93	59.50	0.01
PST3	N	601.03	0.02	0.00	0.00	0.00	39.17	43.16	60.78	0.00
SCL3	N	602.74	0.04	0.00	0.00	0.00	37.38	39.99	59.90	0.01
BEL3	N	607.70	0.01	0.00	0.00	0.00	39.33	42.78	60.33	0.01

Station Name	Comp	R _{epi}	PGA	PGV	PGD	I _A	I _D	Sd	Bd	H ₅₀
		[km]	[cm/s ²]	[cm/s]	[cm]	[cm/s]	[]	[s]	[s]	[cm]
AVG3	N	608.39	0.01	0.00	0.00	0.00	27.46	45.30	60.91	0.01
VDP3	N	614.14	0.05	0.00	0.00	0.00	62.65	52.23	61.47	0.01
CGG3	N	617.27	0.03	0.00	0.00	0.00	47.31	45.50	60.88	0.01
SRN3	N	619.03	0.02	0.00	0.00	0.00	45.62	45.57	62.69	0.01
STN3	N	625.22	0.01	0.00	0.00	0.00	24.71	45.66	63.06	0.01
PGN3	N	629.26	0.01	0.00	0.00	0.00	24.89	48.92	63.73	0.01
MRN3	N	638.89	0.01	0.00	0.00	0.00	32.72	48.41	65.90	0.00
VGG3	N	656.23	0.01	0.00	0.00	0.00	23.01	52.54	68.60	0.01

Table A2. Peak and integral parameters estimated on the uncorrected waveforms of the E-W component

Station Name	Comp	R _{epi}	PGA	PGV	PGD	I _A	I _D	Sd	Bd	H ₅₀
		[km]	[cm/s ²]	[cm/s]	[cm]	[cm/s]	[]	[s]	[s]	[cm]
MRN	E	3.58	255.78	20.70	7.02	78.86	9.30	7.95	79.50	67.72
SAN0	E	4.73	162.81	21.07	5.57	31.83	5.80	6.81	42.59	57.54
SMS0	E	14.95	178.18	14.21	2.63	47.93	11.82	6.14	18.90	42.88
RAV0	E	15.69	54.03	6.49	0.93	3.21	5.72	14.71	51.44	14.61
FIN0	E	16.04	207.38	16.20	2.25	30.81	5.73	9.08	21.55	39.45
MOGO	E	16.43	270.91	24.59	2.75	55.65	5.22	7.36	17.30	62.67
CRP	E	18.69	130.25	8.08	1.39	16.80	9.96	12.95	27.78	28.35
CNT	E	21.34	211.12	18.83	2.70	46.91	7.37	4.30	15.71	56.59
SAG0	E	24.98	83.31	6.67	1.09	9.60	10.80	18.45	31.13	20.71
CAS0	E	26.25	72.61	5.46	1.38	8.53	13.42	18.36	34.83	18.60
BONO	E	26.52	36.29	2.36	0.62	1.61	11.76	18.87	46.38	5.73
MDN	E	27.61	33.36	2.79	0.54	2.85	19.12	30.93	70.20	10.43
NVL	E	28.00	55.09	2.63	0.46	5.02	21.61	15.78	35.16	10.47
ZPP	E	37.52	24.33	2.80	0.78	1.85	16.95	51.82	95.75	9.39
MBG0	E	38.37	18.77	1.91	0.56	0.96	16.66	48.49	110.26	5.99
FER0	E	42.36	16.58	1.93	0.61	0.62	12.02	30.82	79.13	6.11
SSU	E	45.10	18.49	1.47	0.27	1.04	24.06	23.55	71.36	6.62
FIC0	E	45.88	69.69	6.19	1.36	5.44	7.88	14.97	38.72	16.76
ISD	E	47.93	11.87	1.37	0.39	0.49	19.04	68.86	147.86	4.82
SRP	E	50.51	29.27	2.67	0.61	1.55	12.38	22.13	73.75	8.53
MRZ	E	55.03	2.58	0.25	0.14	0.02	19.61	32.06	66.69	0.79
MDC	E	59.79	13.56	2.02	0.64	0.53	11.98	69.57	128.67	5.69
PVF	E	61.17	2.73	0.47	0.20	0.04	20.61	72.36	87.59	1.74
CPC	E	62.90	21.48	2.04	0.32	0.93	13.22	34.34	111.44	4.65
ARG	E	63.48	10.44	0.69	0.23	0.22	18.83	105.69	156.40	2.46
CSP	E	65.55	10.43	1.08	0.39	0.45	24.93	36.80	100.82	4.06
MNS	E	67.04	14.85	0.46	0.07	0.21	19.38	17.90	45.76	0.99
VLM	E	73.06	4.37	0.91	0.30	0.10	16.18	34.05	96.14	3.36
PRT	E	79.03	2.24	0.23	0.05	0.02	24.00	33.10	60.33	0.81
TGG	E	79.39	13.12	0.52	0.10	0.22	20.39	22.00	67.10	1.16
BRM	E	80.27	0.80	0.14	0.06	0.00	22.01	63.38	121.88	0.55
ALF	E	84.60	11.73	1.71	0.35	0.34	10.58	107.55	149.68	3.77
FRE1	E	84.79	8.17	0.50	0.11	0.15	22.25	25.97	59.95	2.11
BRH	E	89.53	12.54	0.60	0.16	0.18	14.77	28.21	63.26	1.77
SMP	E	90.30	3.10	0.21	0.03	0.03	31.25	34.01	71.76	0.75

Station Name	Comp	R_{epi}	PGA	PGV	PGD	IA	ID	Sd	Bd	H₅₀
		[km]	[cm/s ²]	[cm/s]	[cm]	[cm/s]	[]	[s]	[s]	[cm]
PTV	E	91.57	11.47	1.23	0.33	0.50	22.13	80.00	157.88	5.27
MDG	E	95.08	7.98	0.44	0.08	0.07	13.02	28.58	60.40	1.15
BSZ	E	96.04	0.99	0.21	0.06	0.00	11.55	39.47	56.17	0.55
PIT	E	96.44	2.14	0.16	0.03	0.02	34.22	35.03	61.46	0.61
MRR	E	96.65	5.64	0.30	0.08	0.04	14.28	31.23	52.44	1.05
GAI	E	97.07	14.46	0.97	0.10	0.42	18.81	18.19	51.34	2.61
PZS	E	97.21	4.00	0.66	0.17	0.06	13.54	21.65	65.24	2.95
SNZ1	E	97.21	9.47	0.77	0.19	0.35	29.95	98.88	186.14	3.12
CNF	E	98.29	2.11	0.28	0.08	0.01	14.96	33.31	64.41	1.25
MDT	E	99.15	9.14	0.54	0.13	0.10	12.86	30.43	70.65	1.51
BRB	E	100.18	3.82	0.36	0.06	0.03	13.16	34.97	62.74	1.27
FVZ	E	101.96	4.14	0.25	0.07	0.04	22.21	26.83	59.89	0.94
BGL	E	103.41	4.49	0.36	0.05	0.05	17.89	30.02	62.40	1.44
VGL	E	103.77	0.14	0.01	0.00	0.00	33.12	30.98	98.57	0.03
BGN	E	104.87	1.30	0.12	0.03	0.01	33.03	26.69	38.47	0.47
MLC	E	107.96	11.66	0.59	0.08	0.30	26.64	23.15	60.16	1.85
PNM	E	109.06	2.86	0.15	0.03	0.02	27.67	32.72	62.90	0.52
CST	E	110.40	10.48	0.83	0.22	0.21	14.83	36.19	85.93	3.50
PRM	E	111.60	2.05	0.20	0.07	0.01	14.46	43.28	86.36	0.65
DCM	E	112.10	2.16	0.34	0.06	0.01	10.95	25.07	56.78	1.22
MLD	E	113.33	9.15	0.55	0.12	0.16	20.22	28.00	62.65	1.92
AUL	E	113.70	5.02	0.48	0.10	0.05	13.22	28.51	74.72	1.91
CVT	E	115.80	5.68	0.40	0.08	0.04	12.10	30.26	50.46	1.10
RNC	E	116.66	1.59	0.32	0.09	0.01	10.56	26.47	53.26	1.20
RVR	E	117.68	4.01	0.52	0.10	0.04	11.94	83.20	187.73	1.50
STS	E	120.26	2.57	0.25	0.08	0.02	18.24	39.51	100.24	0.77
BDG	E	122.10	5.82	0.44	0.06	0.06	14.33	26.35	80.86	1.58
VRL	E	126.06	3.51	0.28	0.03	0.02	13.58	25.74	58.04	0.92
CES	E	126.76	3.44	0.59	0.19	0.06	18.47	74.10	130.33	2.01
LSP	E	131.86	1.70	0.14	0.04	0.00	10.79	30.79	54.75	0.49
SLS	E	135.23	1.01	0.12	0.03	0.00	10.05	16.98	84.92	0.47
BBN	E	135.98	0.98	0.21	0.08	0.01	19.38	35.68	67.93	0.80
FLP	E	146.20	8.46	0.34	0.05	0.18	38.28	32.30	72.32	0.73
SEL	E	148.69	2.09	0.22	0.04	0.01	11.52	31.21	58.06	0.67
SNM	E	150.68	1.34	0.26	0.13	0.01	15.39	47.97	80.94	0.80
BDT	E	155.58	1.68	0.19	0.07	0.01	22.26	44.86	69.65	0.82
TGL	E	156.27	1.78	0.15	0.03	0.01	27.01	32.69	62.21	0.65
MCR	E	161.40	1.92	0.14	0.06	0.01	30.00	41.90	74.60	0.48
APR	E	162.13	1.03	0.09	0.02	0.00	23.48	43.35	97.21	0.33
BRA	E	164.75	2.40	0.12	0.02	0.01	25.84	38.96	72.10	0.37
SNS	E	166.53	2.30	0.30	0.11	0.03	24.20	51.33	82.74	1.34
CTL	E	167.37	2.20	0.23	0.06	0.03	33.76	60.00	95.68	0.91
POR	E	172.01	3.28	0.61	0.24	0.07	20.56	60.37	144.04	1.83
LEC	E	172.59	1.19	0.12	0.04	0.00	17.74	31.63	59.16	0.50
RNS	E	172.64	1.97	0.11	0.02	0.01	19.87	36.73	61.07	0.51
GNV	E	177.09	3.52	0.24	0.06	0.02	14.93	32.52	62.55	0.85
MOV	E	186.89	2.94	0.13	0.04	0.02	24.59	32.20	68.93	0.54

Station Name	Comp	R_{epi}	PGA	PGV	PGD	IA	ID	Sd	Bd	H₅₀
		[km]	[cm/s ²]	[cm/s]	[cm]	[cm/s]	[]	[s]	[s]	[cm]
PSR	E	190.35	2.16	0.19	0.09	0.02	26.39	43.98	67.04	0.67
CLA	E	190.79	0.60	0.06	0.02	0.00	15.39	33.99	50.94	0.22
PTL	E	194.32	0.82	0.15	0.04	0.00	9.24	31.66	37.09	0.39
OVD	E	194.96	1.50	0.17	0.03	0.01	19.49	40.78	68.97	0.59
SPI	E	195.60	2.81	0.21	0.09	0.02	20.35	40.13	74.61	0.61
UMB	E	202.02	0.47	0.08	0.02	0.00	24.19	70.01	291.35	0.28
PRAD	E	205.70	0.77	0.06	0.02	0.00	34.34	47.15	88.98	0.22
GBB	E	208.21	0.98	0.09	0.04	0.00	20.88	68.00	134.59	0.32
FDS	E	209.03	0.66	0.08	0.03	0.00	32.34	60.27	120.03	0.39
MAJ	E	209.86	1.94	0.28	0.09	0.02	21.43	43.43	72.97	0.95
SAS	E	210.13	1.27	0.11	0.02	0.00	14.30	42.30	62.41	0.32
GBP	E	211.74	1.88	0.48	0.24	0.04	31.19	82.03	154.52	1.45
AVS	E	217.41	1.08	0.12	0.05	0.00	15.23	30.87	52.93	0.41
GEDE	E	218.16	2.17	0.28	0.07	0.02	23.73	66.74	187.85	0.95
GEPF	E	220.50	0.94	0.14	0.05	0.00	12.60	50.40	144.46	0.44
TLM2	E	221.11	2.25	0.19	0.04	0.02	25.85	42.18	111.72	0.59
GESC	E	221.12	2.13	0.20	0.06	0.02	33.63	48.45	100.49	0.77
CESC	E	222.66	3.25	0.24	0.05	0.04	34.20	44.51	95.98	0.81
CVF	E	224.22	2.47	0.17	0.04	0.02	23.31	26.26	55.76	0.55
VINO	E	226.75	1.82	0.22	0.07	0.01	17.39	52.11	132.35	0.66
DST2	E	227.09	1.03	0.09	0.02	0.00	31.31	46.41	123.45	0.34
SDV	E	232.87	0.76	0.10	0.03	0.00	18.30	54.60	126.38	0.21
MOGG	E	233.13	0.93	0.10	0.04	0.00	18.91	59.68	113.34	0.28
RST	E	238.37	0.66	0.07	0.03	0.00	20.70	47.20	87.30	0.23
STOL	E	238.45	2.97	0.16	0.03	0.04	50.85	49.12	94.48	0.35
DRN	E	241.68	1.56	0.12	0.03	0.01	29.06	34.16	69.80	0.44
AUP	E	244.42	1.42	0.09	0.03	0.01	33.95	45.15	66.96	0.36
CLF	E	253.91	0.86	0.15	0.03	0.01	28.10	87.38	198.08	0.56
MCT	E	260.32	1.28	0.14	0.04	0.01	30.96	51.91	75.87	0.64
TNS	E	269.15	0.90	0.13	0.03	0.01	36.05	47.01	77.89	0.59
SPM	E	275.58	0.36	0.03	0.01	0.00	60.39	88.59	205.59	0.14
RQT	E	294.57	0.41	0.06	0.02	0.00	31.96	86.38	194.35	0.22
PCB	E	319.13	0.20	0.04	0.01	0.00	30.05	111.49	239.67	0.14
MSC	E	322.65	0.31	0.05	0.02	0.00	23.52	118.73	234.57	0.17
PLS	E	340.12	0.09	0.03	0.01	0.00	22.06	180.05	429.37	0.06
SPD	E	342.51	0.16	0.01	0.00	0.00	18.95	32.15	38.65	0.05
CDM	E	414.49	0.09	0.01	0.00	0.00	15.64	33.57	39.75	0.02
MND	E	543.83	0.03	0.00	0.00	0.00	23.03	33.77	67.88	0.01
SSB3	E	552.94	0.02	0.00	0.00	0.00	26.62	36.20	54.74	0.01
RSF3	E	560.40	0.02	0.00	0.00	0.00	17.74	38.25	55.46	0.01
MNT3	E	563.27	0.02	0.00	0.00	0.00	27.85	40.93	56.78	0.00
LIO3	E	566.77	0.01	0.00	0.00	0.00	21.43	40.44	56.01	0.01
NSC3	E	568.32	0.02	0.00	0.00	0.00	22.87	40.25	56.46	0.01
AND3	E	571.93	0.03	0.00	0.00	0.00	20.88	41.09	56.38	0.02
CLT3	E	578.20	0.14	0.01	0.00	0.00	35.29	33.02	49.26	0.02
SNR3	E	582.22	0.02	0.00	0.00	0.00	21.85	41.53	58.17	0.01
CMP3	E	584.26	0.03	0.00	0.00	0.00	41.36	42.59	59.41	0.01

Station Name	Comp	R_{epi}	PGA	PGV	PGD	IA	ID	Sd	Bd	H₅₀
		[km]	[cm/s ²]	[cm/s]	[cm]	[cm/s]	[]	[s]	[s]	[cm]
RDM3	E	587.86	0.04	0.00	0.00	0.00	27.05	42.27	57.44	0.02
CSG3	E	589.03	0.03	0.01	0.00	0.00	20.92	50.83	58.31	0.02
COL3	E	593.87	0.04	0.00	0.00	0.00	30.83	40.73	59.26	0.01
VDS3	E	594.07	0.04	0.00	0.00	0.00	29.67	42.75	59.19	0.01
SFL3	E	597.90	0.02	0.00	0.00	0.00	27.08	47.22	59.49	0.01
PST3	E	601.03	0.03	0.00	0.00	0.00	58.38	41.95	60.67	0.00
SCL3	E	602.74	0.02	0.00	0.00	0.00	28.64	42.58	60.08	0.01
BEL3	E	607.70	0.03	0.00	0.00	0.00	24.02	43.34	60.72	0.01
AVG3	E	608.39	0.02	0.00	0.00	0.00	19.74	44.62	60.90	0.01
VDP3	E	614.14	0.03	0.00	0.00	0.00	53.54	52.89	61.48	0.01
CGG3	E	617.27	0.06	0.00	0.00	0.00	28.90	42.48	53.64	0.01
SRN3	E	619.03	0.02	0.00	0.00	0.00	32.88	47.16	62.69	0.01
STN3	E	625.22	0.01	0.00	0.00	0.00	23.39	47.05	63.09	0.00
PGN3	E	629.26	0.01	0.00	0.00	0.00	19.77	48.38	63.83	0.00
MRN3	E	638.89	0.02	0.00	0.00	0.00	42.29	48.17	65.87	0.00
VGG3	E	656.23	0.01	0.00	0.00	0.00	16.44	53.40	68.59	0.00

Table A3. Peak and integral parameters estimated on the uncorrected waveforms of the Z component.

Station Name	Comp	R_{epi}	PGA	PGV	PGD	IA	ID	Sd	Bd	H₅₀
		[km]	[cm/s ²]	[cm/s]	[cm]	[cm/s]	[]	[s]	[s]	[cm]
MRN	Z	3.58	882.80	19.00	2.24	289.90	10.80	5.37	9.67	25.67
SAN0	Z	4.73	343.01	7.51	2.15	42.19	10.23	4.53	10.63	20.06
SMS0	Z	14.95	105.09	2.75	0.57	9.58	20.70	6.56	21.11	7.19
RAV0	Z	15.69	66.76	1.51	0.45	2.37	14.71	9.21	15.96	3.85
FIN0	Z	16.04	196.27	3.00	0.85	32.06	33.99	5.62	19.72	8.78
MOGO	Z	16.43	122.33	4.05	1.49	15.86	19.98	9.13	22.89	13.02
CRP	Z	18.69	86.55	2.63	0.60	7.22	19.85	10.91	33.39	7.43
CNT	Z	21.34	65.40	2.54	0.37	5.02	18.87	9.24	25.04	5.39
SAG0	Z	24.98	65.90	1.78	0.53	3.41	18.14	15.43	46.39	5.15
CAS0	Z	26.25	29.55	1.17	0.36	1.08	19.56	31.10	64.88	4.69
BON0	Z	26.52	29.30	1.28	0.19	1.54	25.68	14.09	39.28	2.89
MDN	Z	27.61	35.25	1.64	0.34	1.77	19.08	19.29	79.15	6.50
NVL	Z	28.00	44.97	1.22	0.24	2.61	29.69	13.67	33.85	2.26
ZPP	Z	37.52	22.91	1.14	0.61	0.66	15.64	58.67	81.24	3.31
MBG0	Z	38.37	12.08	0.59	0.18	0.33	28.92	65.76	159.97	2.06
FER0	Z	42.36	15.16	0.71	0.16	0.31	18.12	27.26	70.96	1.73
SSU	Z	45.10	13.77	0.73	0.15	0.29	18.13	24.81	50.34	2.71
FIC0	Z	45.88	25.70	1.57	0.40	1.25	19.35	19.36	50.19	5.17
ISD	Z	47.93	7.46	0.69	0.31	0.18	21.50	81.87	148.36	2.35
SRP	Z	50.51	10.06	0.37	0.11	0.27	45.12	25.31	105.43	1.15
MRZ	Z	55.03	1.46	0.25	0.12	0.01	17.70	45.15	66.90	0.71
MDC	Z	59.79	3.46	0.70	0.32	0.08	20.74	98.02	176.70	1.71
PVF	Z	61.17	2.58	0.70	0.27	0.04	12.84	68.92	88.48	1.47
CPC	Z	62.90	7.18	0.34	0.19	0.13	32.04	48.81	99.66	1.03
ARG	Z	63.48	4.04	0.18	0.08	0.03	28.07	120.63	167.77	0.70
CSP	Z	65.55	5.68	0.58	0.16	0.13	23.73	48.93	120.65	2.37
MNS	Z	67.04	4.73	0.36	0.08	0.07	23.85	22.25	62.08	0.94

Station Name	Comp	R_{epi}	PGA	PGV	PGD	IA	ID	Sd	Bd	H₅₀
		[km]	[cm/s ²]	[cm/s]	[cm]	[cm/s]	[]	[s]	[s]	[cm]
VLM	Z	73.06	2.09	0.36	0.15	0.03	26.37	62.08	121.01	1.34
PRT	Z	79.03	2.78	0.16	0.06	0.01	19.26	34.21	60.59	0.64
TGG	Z	79.39	12.41	0.47	0.04	0.23	24.37	21.09	53.77	1.05
BRM	Z	80.27	1.02	0.13	0.06	0.00	18.12	61.26	115.48	0.45
ALF	Z	84.60	3.93	0.29	0.16	0.06	32.43	93.54	202.25	0.76
FRE1	Z	84.79	2.82	0.24	0.08	0.02	20.37	38.80	65.31	0.87
BRH	Z	89.53	3.42	0.29	0.11	0.05	29.75	38.71	84.19	1.39
SMP	Z	90.30	2.40	0.12	0.05	0.01	26.09	34.44	69.76	0.57
PTV	Z	91.57	8.08	0.42	0.22	0.18	32.21	98.49	176.95	1.37
MDG	Z	95.08	2.40	0.17	0.07	0.02	32.08	42.44	103.21	0.64
BSZ	Z	96.04	1.02	0.18	0.08	0.00	16.66	40.63	57.50	0.53
PIT	Z	96.44	1.18	0.14	0.05	0.01	24.10	39.84	62.76	0.54
MRR	Z	96.65	2.19	0.21	0.07	0.01	15.10	38.79	55.58	0.77
GAI	Z	97.07	8.91	0.38	0.07	0.16	30.57	22.85	59.79	1.19
PZS	Z	97.21	2.15	0.42	0.12	0.02	14.07	34.17	69.00	1.63
SNZ1	Z	97.21	3.13	0.34	0.16	0.05	28.01	151.21	212.25	1.11
CNF	Z	98.29	1.44	0.22	0.04	0.01	17.56	37.48	66.28	0.97
MDT	Z	99.15	5.30	0.34	0.09	0.05	18.01	39.91	67.25	1.05
BRB	Z	100.18	1.77	0.23	0.06	0.02	25.43	44.61	64.86	0.89
FVZ	Z	101.96	3.02	0.28	0.06	0.02	13.76	29.41	61.47	1.10
BGL	Z	103.41	2.96	0.16	0.04	0.02	21.22	33.05	59.91	0.73
VGL	Z	103.77	3.93	0.27	0.07	0.04	22.35	31.98	64.83	0.99
BGN	Z	104.87	1.39	0.12	0.03	0.01	19.83	28.33	38.50	0.51
MLC	Z	107.96	6.39	0.35	0.07	0.08	22.41	25.70	78.09	1.27
PNM	Z	109.06	1.33	0.09	0.02	0.01	28.03	35.50	63.23	0.35
CST	Z	110.40	3.40	0.29	0.13	0.04	25.51	57.66	107.94	1.05
PRM	Z	111.60	1.85	0.29	0.08	0.01	10.58	60.47	87.13	0.69
DCM	Z	112.10	1.45	0.17	0.06	0.01	15.43	36.31	58.97	0.62
MLD	Z	113.33	5.93	0.26	0.10	0.05	20.27	40.16	63.40	0.97
AUL	Z	113.70	1.55	0.20	0.05	0.01	18.68	38.75	75.71	0.75
CVT	Z	115.80	0.01	0.00	0.00	0.00	16.37	58.83	62.99	0.00
RNC	Z	116.66	1.48	0.31	0.09	0.01	8.05	35.68	53.56	0.87
RVR	Z	117.68	2.14	0.21	0.05	0.02	27.30	121.47	186.53	1.04
STS	Z	120.26	1.64	0.20	0.06	0.01	25.21	64.65	113.63	0.80
BDG	Z	122.10	2.17	0.16	0.03	0.01	23.21	43.75	107.27	0.60
VRL	Z	126.06	2.66	0.20	0.03	0.01	13.46	30.68	59.47	0.73
CES	Z	126.76	1.14	0.21	0.09	0.01	21.29	94.88	135.95	0.51
LSP	Z	131.86	0.95	0.09	0.02	0.00	20.91	36.38	55.89	0.40
SLS	Z	135.23	1.53	0.13	0.02	0.00	13.21	39.97	84.64	0.39
BBN	Z	135.98	1.29	0.26	0.07	0.01	13.70	38.56	67.92	0.83
FLP	Z	146.20	2.81	0.13	0.03	0.02	31.32	34.73	81.09	0.49
SEL	Z	148.69	1.44	0.15	0.03	0.01	16.42	35.36	60.44	0.61
SNM	Z	150.68	0.54	0.15	0.06	0.00	21.02	66.16	80.94	0.41
BDT	Z	155.58	1.03	0.13	0.04	0.00	22.88	49.17	70.02	0.40
TGL	Z	156.27	1.45	0.12	0.04	0.00	15.99	39.60	61.92	0.49
MCR	Z	161.40	0.89	0.08	0.02	0.00	34.55	50.94	76.27	0.34
APR	Z	162.13	0.85	0.11	0.02	0.00	24.59	44.58	120.47	0.37

Station Name	Comp	R _{epi} [km]	PGA [cm/s ²]	PGV [cm/s]	PGD [cm]	IA [cm/s]	ID [s]	Sd [s]	Bd [s]	H ₅₀ [cm]
BRA	Z	164.75	1.18	0.11	0.03	0.01	25.66	41.52	73.47	0.43
SNS	Z	166.53	0.86	0.17	0.05	0.01	26.39	57.80	85.44	0.62
CTL	Z	167.37	1.02	0.08	0.02	0.00	33.70	64.40	98.96	0.29
POR	Z	172.01	1.53	0.22	0.10	0.02	28.72	76.30	169.92	0.75
LEC	Z	172.59	0.83	0.10	0.03	0.00	18.59	41.24	61.13	0.48
RNS	Z	172.64	1.19	0.11	0.02	0.00	16.73	41.50	61.44	0.41
GNV	Z	177.09	2.37	0.22	0.04	0.01	10.51	33.60	62.89	0.63
MOV	Z	186.89	2.50	0.18	0.04	0.01	16.10	31.29	69.56	0.68
PSR	Z	190.35	0.92	0.10	0.04	0.00	27.08	53.59	70.38	0.31
CLA	Z	190.79	0.51	0.05	0.02	0.00	19.24	36.00	50.99	0.17
PTL	Z	194.32	0.58	0.08	0.03	0.00	10.66	32.71	38.46	0.33
OVD	Z	194.96	0.89	0.09	0.02	0.00	24.58	47.10	69.52	0.33
SPI	Z	195.60	1.08	0.12	0.05	0.00	21.15	49.88	74.99	0.30
UMB	Z	202.02	0.27	0.04	0.02	0.00	27.93	76.28	192.50	0.13
PRAD	Z	205.70	0.76	0.06	0.03	0.00	25.66	49.67	90.31	0.22
GBB	Z	208.21	0.47	0.06	0.02	0.00	27.91	72.96	159.89	0.23
FDS	Z	209.03	0.55	0.08	0.03	0.00	22.50	59.74	120.61	0.26
MAJ	Z	209.86	1.40	0.18	0.06	0.01	19.76	45.02	72.82	0.67
SAS	Z	210.13	0.72	0.07	0.01	0.00	11.95	46.53	63.52	0.21
GBP	Z	211.74	1.39	0.26	0.08	0.01	24.24	80.32	156.87	1.10
AVS	Z	217.41	0.78	0.11	0.03	0.00	13.31	34.60	52.94	0.34
GEDE	Z	218.16	1.10	0.12	0.05	0.01	28.14	125.78	187.90	0.36
GEPF	Z	220.50	0.56	0.12	0.05	0.00	16.39	66.61	175.64	0.33
TLM2	Z	221.11	0.67	0.06	0.02	0.00	31.29	59.52	122.29	0.20
GESC	Z	221.12	1.16	0.11	0.05	0.01	27.25	55.33	102.80	0.36
CESC	Z	222.66	2.95	0.22	0.04	0.02	20.91	44.28	106.45	0.73
CVF	Z	224.22	1.45	0.10	0.02	0.01	30.53	44.52	59.64	0.30
VINO	Z	226.75	1.49	0.17	0.06	0.01	22.62	57.60	124.28	0.57
DST2	Z	227.09	0.79	0.07	0.02	0.00	24.87	70.23	170.74	0.24
SDV	Z	232.87	0.51	0.04	0.02	0.00	32.61	70.76	173.62	0.18
MOGG	Z	233.13	0.53	0.07	0.02	0.00	21.72	63.73	120.88	0.26
RST	Z	238.37	0.53	0.05	0.02	0.00	25.94	56.35	88.74	0.18
STOL	Z	238.45	1.04	0.07	0.02	0.01	45.63	48.86	103.49	0.18
DRN	Z	241.68	0.76	0.08	0.02	0.00	30.40	45.73	69.97	0.27
AUP	Z	244.42	0.60	0.06	0.01	0.00	24.07	50.86	66.92	0.23
CLF	Z	253.91	0.43	0.05	0.01	0.00	52.99	80.21	196.85	0.21
MCT	Z	260.32	0.47	0.07	0.03	0.00	38.44	61.62	75.99	0.32
TNS	Z	269.15	0.63	0.08	0.02	0.00	28.92	62.12	77.88	0.26
SPM	Z	275.58	0.13	0.03	0.01	0.00	38.36	116.65	329.71	0.09
RQT	Z	294.57	0.25	0.04	0.02	0.00	32.49	102.90	206.62	0.14
PCB	Z	319.13	0.09	0.03	0.02	0.00	27.76	125.19	240.28	0.07
MSC	Z	322.65	0.13	0.04	0.02	0.00	28.08	123.76	234.82	0.10
PLS	Z	340.12	0.05	0.02	0.01	0.00	33.20	175.66	423.58	0.05
SPD	Z	342.51	0.11	0.01	0.00	0.00	33.48	34.27	39.71	0.04
CDM	Z	414.49	0.13	0.01	0.00	0.00	19.19	34.96	40.04	0.03
MND	Z	543.83	0.05	0.00	0.00	0.00	23.70	33.15	66.59	0.01
SSB3	Z	552.94	0.02	0.00	0.00	0.00	12.36	38.14	54.62	0.01

Station Name	Comp	R_{epi} [km]	PGA [cm/s ²]	PGV [cm/s]	PGD [cm]	IA [cm/s]	ID [l]	Sd [s]	Bd [s]	H₅₀ [cm]
RSF3	Z	560.40	0.02	0.00	0.00	0.00	14.38	42.13	55.32	0.01
MNT3	Z	563.27	0.01	0.00	0.00	0.00	13.61	42.17	56.82	0.00
LIO3	Z	566.77	0.01	0.00	0.00	0.00	7.86	41.20	55.98	0.01
NSC3	Z	568.32	0.01	0.00	0.00	0.00	16.81	42.26	56.61	0.01
AND3	Z	571.93	0.03	0.00	0.00	0.00	18.67	39.89	55.59	0.01
CLT3	Z	578.20	0.07	0.00	0.00	0.00	24.84	34.47	56.42	0.01
SNR3	Z	582.22	0.01	0.00	0.00	0.00	13.14	42.85	58.24	0.00
CMP3	Z	584.26	0.01	0.00	0.00	0.00	22.65	42.06	59.38	0.00
RDM3	Z	587.86	0.02	0.00	0.00	0.00	16.83	42.45	58.00	0.01
CSG3	Z	589.03	0.01	0.00	0.00	0.00	18.74	44.57	58.25	0.01
COL3	Z	593.87	0.02	0.00	0.00	0.00	17.22	42.61	59.18	0.01
VDS3	Z	594.07	0.02	0.00	0.00	0.00	22.32	43.03	59.20	0.01
SFL3	Z	597.90	0.01	0.00	0.00	0.00	20.23	45.75	59.49	0.01
PST3	Z	601.03	0.01	0.00	0.00	0.00	29.59	46.49	60.73	0.00
SCL3	Z	602.74	0.01	0.00	0.00	0.00	22.21	43.45	60.09	0.00
BEL3	Z	607.70	0.02	0.00	0.00	0.00	14.60	45.76	60.54	0.01
AVG3	Z	608.39	0.01	0.00	0.00	0.00	15.02	46.54	60.88	0.01
VDP3	Z	614.14	0.01	0.00	0.00	0.00	24.35	53.85	61.50	0.00
CGG3	Z	617.27	0.01	0.00	0.00	0.00	21.43	47.86	62.22	0.00
SRN3	Z	619.03	0.01	0.00	0.00	0.00	12.70	48.41	62.64	0.00
STN3	Z	625.22	0.01	0.00	0.00	0.00	16.84	50.08	63.10	0.00
PGN3	Z	629.26	0.01	0.00	0.00	0.00	24.84	48.33	63.83	0.00
MRN3	Z	638.89	0.01	0.00	0.00	0.00	21.14	53.37	65.94	0.00
VGG3	Z	656.23	0.01	0.00	0.00	0.00	20.00	53.67	68.58	0.00

References

- Bindi D, Pacor F, Luzi L, Puglia R, Massa M, Ameri G, Paolucci R, 2011. Ground motion prediction equations derived from the Italian strong motion database, *Bulletin of Earthquake Engineering*, 9(6), 1899-1920.
- Chioccarelli E, De Luca F, Iervolino I. (2012), Preliminary study of Emilia (May 20th 2012) earthquake ground motion records V2.1, available at <http://www.reluis.it>.
- Comité Européen de Normalisation (CEN), 2004. Eurocode 8 – Design of Structures for earthquake resistance – Part 1: General rules, seismic actions and rules for buildings. EN 1998-1, CEN, Brussels.
- Cosenza E, Manfredi G, Ramasco R, 1993: The Use of Damage Functionals in Earthquake Engineering: A Comparison between Different Methods. *Earthquake Engineering and Structural Dynamics*, 22 (10), 855-868.
- CS.LL.PP; DM 14 Gennaio 2008: Norme tecniche per le costruzioni. *Gazzetta Ufficiale della Repubblica Italiana*, 29. 4/2/2008 (In Italian).
- Gruppo di Lavoro (2004) Redazione della Mappa di Pericolosità Simica Prevista dall'Ordinanza PCM 3274 del 20 Marzo 2003, Rapporto conclusivo per il Dipartimento della Protezione Civile, INGV, Milano-Roma, 65pp. (in Italian)

Iervolino I., Giorgio M., Galasso C., Manfredi G., 2010a. Conditional hazard maps for secondary intensity measures, Bulletin of Seismological Society of America, 100(6), 3312-3319.

Iervolino I., Galasso C., Cosenza C., 2010b. REXEL :computer aided record selection fro code based seismic structural analysis, Bulletinf of Earthquake Engineering, 8, 339-362.

Iervolino I, Chioccarelli E, Convertito V, 2011. Engineering design earthquakes from multimodal hazard disaggregation. Soil Dynamics and Earthquake Engineering, 31, 1212-1231.

INGV Comunicato: aggiornamento del 27/06/2012 ore 05:45 UTC. Available at <http://www.ingv.it/primo-piano/comunicazione/2012/05200508/>

Joyner WB, Boore DM, 1981. Peak horizontal acceleration and velocity from strong-motion records including records from the1979 Imperial Valley, California, earthquake, Bulletin of Seismological Society of America 71, 2011–2038.

Massa M, Pacor F, Luzi L, Bindi D, Milana G, Sabetta F, 2009. The ITalian Accelerometric Archive (ITACA): processing of strong-motion data, Bulletin of Seismological Society of America 8(5), 1175–1187.

Mirandola Earthquake Working Group, 2012a (DPC, UNiCHieti, Uni Trieste, Regione Umbria) – Report 1 – (<http://www.protezionecivile.gov.it/jcms/it/ran.wp>)

Mirandola Earthquake Working Group, 2012b (DPC, UNiCHieti, Uni Trieste, Regione Umbria) – Report 2 – (<http://www.protezionecivile.gov.it/jcms/it/ran.wp>)

Pacor F, Paolucci R, Ameri G, Massa M, Puglia R, 2011. Italian strong motion records in ITACA: overview and record processing. Bulletin of Earthquake Engineering, 9(6), 1741.1759.

Sabetta F, Pugliese A, 1996: Estimation of Response Spectra and Simulation of Nonstationary Earthquake Ground Motion. Bulletin of the Seismological Society of America, 86, 337-352.